UNIVERSITY OF CALIFORNIA
RIVERSIDE

Assessment of Irrigation and Rainfall Effects on Soil Salinity in Selected Drip-Irrigated Orchards in San Joaquin Valley, CA

A Dissertation submitted in partial satisfaction
of the requirements for the degree of

Doctor of Philosophy

in

Environmental Sciences

by

Sarah Awad Helalia

March 2021

Dissertation Committee:
Dr. Jiří Šimůnek, Chairperson
Dr. Todd Skaggs
Dr. Ray Anderson
Dr. Amir Haghverdi

The Dissertation of Sarah Awad Helalia is approved:

_____

_____

_____

_____

Committee Chairperson

University of California, Riverside

Acknowledgments

I want to express my deep gratitude to my supervisors, **Jiří Šimůnek** and **Todd Skaggs**, for their academic and professional support. I am thankful for all the effort and time I received from them. Thanks to my qualifying exam members and professors, **Ray Anderson, Robert Graham, Laosheng Wu,** and **Darrel Jenerette.** Thanks to my dissertation committee, Drs. **Jiří Šimůnek, Todd Skaggs, Ray Anderson,** and **Amir Haghverdi.** Thanks to my collaborators, mentors, and colleagues at UC Riverside and the USDA Salinity Laboratory in Riverside. My brothers, **Ahmed** and **Yousef Awad Helalia**, thanks for all the support. My mother, father, and husband, no words are enough to express my gratitude.

ABSTRACT OF THE DISSERTATION

Assessment of Irrigation and Rainfall Effects on Soil Salinity
in Selected Drip-Irrigated Orchards in San Joaquin Valley, CA

by

Sarah Awad Helalia

Doctor of Philosophy, Graduate Program in Environmental Sciences
University of California, Riverside, March 2021
Dr. Jiří Šimůnek, Chairperson

Preventing an accumulation of harmful salts in the root zone (RZ) of crops is necessary for sustaining irrigated agriculture in arid and semi-arid regions. Climate change may impact future maintenance of the RZ salt balance due to changing temperatures and evapotranspiration, altered precipitation patterns, and related shifts to alternative, lower quality irrigation waters. In this study, experimental field data, including soil water contents, electrical conductivities, spatial root distributions, and soil physical and chemical properties, were collected to assess salinity trends under different environmental and management conditions in almond and pistachio orchards at five locations in San Joaquin Valley (SJV), California, in 2017-2019. Diverse seasonal soil salinity trends were obtained for the eastern and western geo-hydrological regions of SJV and almond and pistachio orchards. The experimental data were then used to carry out numerical analyses with the one-dimensional HYDRUS-1D model to quantify water and solute transport in almond and pistachio trees' RZs. The model was successfully calibrated and validated using soil water content

and electrical conductivity measurements at two experimental sites during 2017-2018 and 2019. Simulated soil water contents and evapotranspiration at these two sites showed good agreement with the measured data. Salinity patterns in the RZ were also described successfully by the HYDRUS-1D simulations. There were uncertainties in simulated trends at the other locations due to, for example, the presence of a duripan, solution chemistry effects on soil hydraulic properties, or functional errors with the GS3 soil sensors in some depths. Finally, additional simulations were carried out to predict future soil salinity accumulation and leaching trends for selected future climate (rainfall) and irrigation (the use of surface (less saline) and ground (more saline) waters) scenarios. Future rainfall trends were predicted using two climate models (CSM4_mid-range precipitations and CNRM_CM5_wetter precipitations) (CalAdapt, 2018). The simulated results of future salinity trends under different regional, geological, irrigation, and climate conditions in SJV can be used to design different salinity management options in the future.

Keywords: root zone soil salinity, almond, pistachio, San Joaquin Valley, rainfall, irrigation, HYDRUS-1D, climate change

Table of Contents

List of Figures

List of Tables

Chapter 1 Introduction

1.1. Motivation and Background

Irrigation and Soil Salinity Problems

Salts accumulate in the root zone either due to natural factors (primary salinization) or due to irrigation (secondary salinization) (Podmore, 2009). Soil salinity can be mainly attributed to climate conditions and the availability and management of irrigation water (Askri et al., 2010). Shortage of freshwater resources, inefficient irrigation practices, and inadequate drainage/leaching contributes to soil salinity problems. The saline water use for irrigation is one of the main factors in the soil salt buildup. However, waters of salinities higher than crop tolerance thresholds have been used for years under the right conditions and management techniques in many countries worldwide (Skaggs et al., 2006; and Haj-Amor et al., 2016). The two most common water quality factors that influence infiltration are the irrigation water salinity and its sodium content relative to the calcium and magnesium content (Hoffman, 2010).

The San Joaquin Valley (SJV), located in the southern portion of California's Central Valley, is one of the USA's most productive farming areas. However, continuous salt buildup in the soils (Figure 1.1) and groundwater limits its productivity and sustainability (Schoups et al., 2005). Early irrigation in the SJV, CA, started at the end of the 19th century. Groundwater pumping started in the 1920s (Schoups et al. 2005). The recent alteration of irrigation resources to more saline groundwaters is likely the main factor. However, drip irrigation in recent decades also played a vital role in SJV soil salinization (Tindula *et al*., 2013). Drip irrigation became a source of a continuous increase in the salinity-impacted zones (Machado and Serralheiro, 2017).

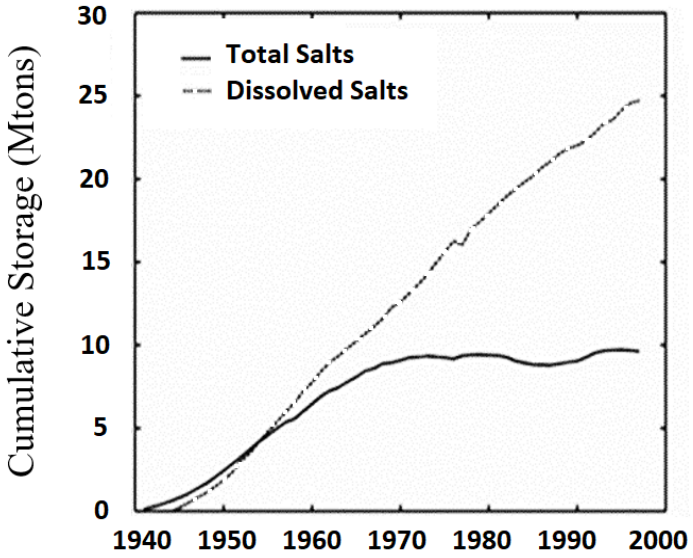

(Schoups *et al.*, 2005)

Figure 1.1. Soil salts in the San Joaquin Valley during the years 1940 – 2000.

Approximately 113 thousand acres in SJV have been retired (permanently removed from irrigation) due to regional drainage problems (high salinity, shallow groundwater). Even more land retirement is anticipated in the future (Schneider *et al.*, 2006). Vast areas of SJV almond and pistachio orchards were retired because of the excessive accumulation of salts in the tree root zones (Brown *et al.*, 2016).

Future Climate Change and Restrictions on Surface Water Supplies

The annual variability of heavy rains and corresponding droughts dramatically increased over the past few decades and severely impacted California's agriculturally productive regions (Ashraf, 2018). The severity of the recent drought has been unprecedented in modern times (Blomquist, 2016). In the Spring of 2015, the Sierra Nevada snowpack measurements (the primary surface water resource for CA) were only 6 percent of the average annual values (Blomquist, 2016). Reductions in rainfall would lead to dramatic shifts in long-term soil salinity trends (Suweis *et al.*,

2010). The latest droughts resulted in dramatic increases in groundwater extraction for irrigation. A Sustainable Groundwater Management Act (SGMA) in 2014 was passed in CA due to five years of drought (Hanak et al., 2019). The development of management practices that would address water use's highest priorities is needed (Hanak et al., 2019). Climate change will make it harder to manage the available water resources (AghaKouchak et al., 2014; Underwood et al., 2018). Management actions to address climate change impacts on water resources should not be postponed (Underwood et al., 2018).

Modern Irrigation and Salinity

Root zone soil salinity in California agricultural lands was recently surveyed and mapped (Figure 2.1) by Scudiero et al. (2017), who indicated that 0.78 million acres of farmland in the western SJV were salt-affected (i.e., ECe > 4 dS/m). The existing impacts of limited water resources in California should be optimized for each crop use of water, such as almond. Recommendations on agricultural water allocations are needed for different California crops (Fulton et al., 2019). Tree nut farmers in CA are committed to improving the efficiency of water use due to an increase in the competition for water resources (Bellvert et al., 2018). Recently, most almond orchards have been irrigated using micro-irrigation systems, which results in a highly non-uniform salt distribution. However, there is limited information on the almond response to non-uniform distributions of salinity in the RZs (Brown et al., 2016). The dynamics of water use and salinity in the soils are crucial management factors, which influence the productivity and long-term sustainability of almonds, pistachios, and other trees and crops (Phogat et al., 2018). Monitoring changes in soil salinity is necessary to manage properly salt-affected soils (Haghverdi et al., 2018).

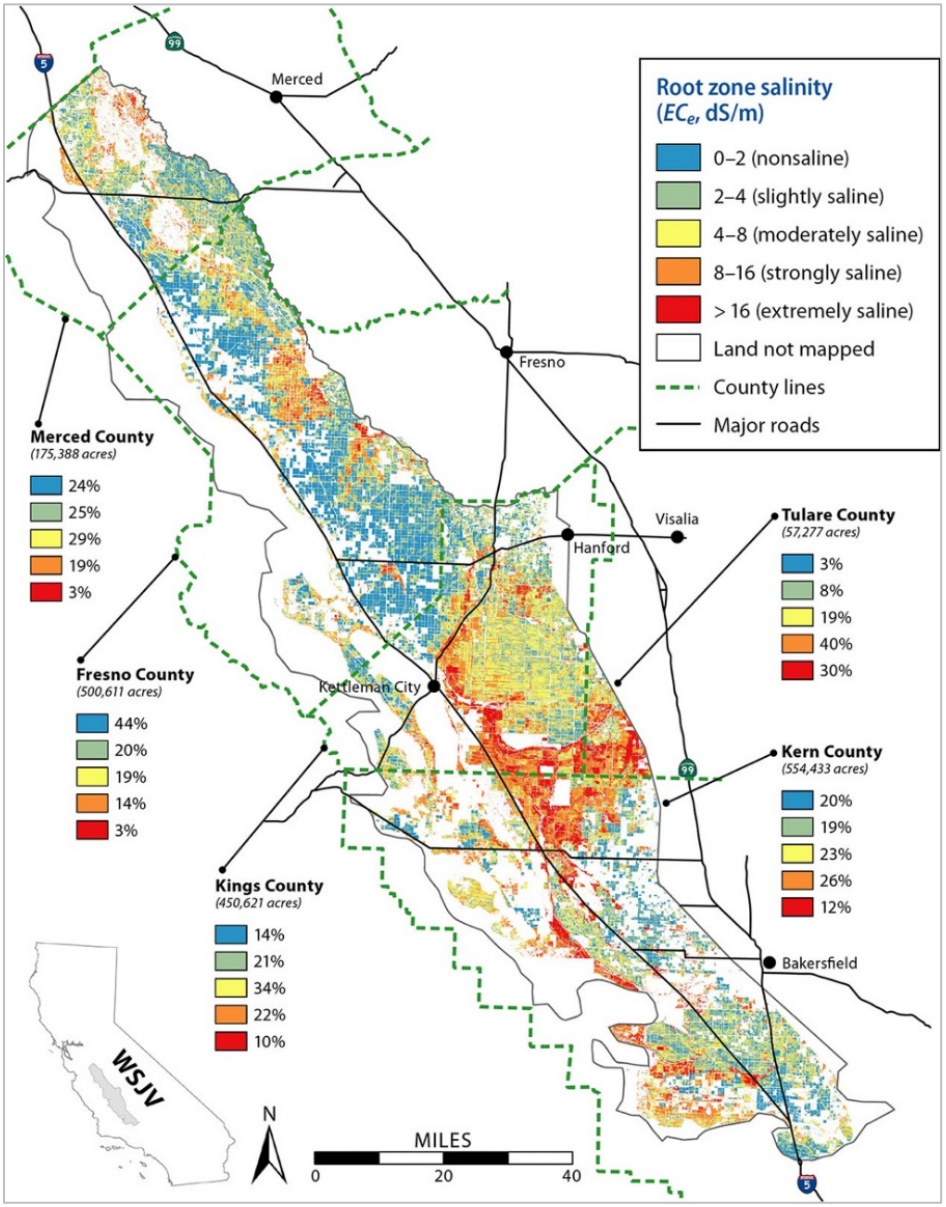

Figure 1.2. Soil salinity distribution in California (Scudiero et al., 2017).

Studying the reasons for soil salinity and its effects on the crops is still an on-going critical concern of research (Phogat et al., 2013; Nethaji Mariappan et al., 2014; Mehdi-Tonsi et al., 2017; Minhas, 2020; Phogat et al., 2020a, 2020b), including in the SJV, CA (Scudiero et al., 2017). Salinity inventory is needed to develop informed water and salinity management decisions (Scudiero et al., 2014).

Addressing long-occurring water and soil quality problems in irrigated agriculture requires new analytical tools to improve our predictive capabilities (Jury et al., 2011). Accurate methods and strategies to describe salinity patterns and their changes over time and space are required to develop sustainable agricultural practices (Schoups et al., 2005; Brown et al., 2016). Future studies should focus on using decision-oriented models (Lobell et al., 2010; Rasouli et al., 2013; Bellvert, 2018). Despite their one-dimensional nature, these models need few parameter adjustments, which allows direct analysis of the processes and hydro-climatic fluctuations in the study of long-term salinity trends. Modeling can explain the effects of irrigation practices on the temporal and spatial soil water and soil salts distributions (Šimůnek et al., 2008).

The HYDRUS-1D model (Šimůnek *et al*., 2008) was used in many studies to assess problems associated with soil salinity, including those involving drip irrigation, through one- and two-dimensional analyses (Kaledhonkar and Keshari, 2006; Goncalves *et al*., 2006; Suarez 2006; Corwin *et al*., 2007; Kaledhonkar *et al*., 2012; Gonçalves *et al*., 2011; Rasouli *et al*., 2013; Zeng *et al*., 2014; Li *et al*. 2015; Haj-Amor *et al*., 2016; Ramos *et al*., 2019). HYDRUS-1D is widely acknowledged as a powerful tool for analyzing soil salinity (e.g., Gonçalves *et al*., 2011). For example, HYDRUS-1D was used to investigate the effects of soil water dynamics, soil salinization, and groundwater salinity (Li *et al*., 2015). HYDRUS-1D was also used to clarify the impact of different water salinities and irrigation practices on soil salinity (Haj-Amor *et al*., 2016).

1.2. Research Objectives

This research has several major objectives: i) to determine the future contribution of seasonal winter rainfall to root zone solute transport, ii) to provide transient assessments of salinity problems associated with the planned future use of irrigation waters of increased salinity in SJV, CA, and iii) to assess the impact of the long-term use of drip irrigation in two different geological regions of SJV planted with almond and pistachio. This research combines measured (2017-2019) and generated (2020-2045) meteorological data for two geological and hydrological regions of the San Joaquin Valley, CA, USA. The regions and orchards were chosen to examine the seasonal accumulation of soil salinity in rootzones with a wide range of variable initial and boundary conditions. Orchards are described in detail in Chapter 2 (the Methods section). The research analysis did not rely on specific empirical salt models (Oosterbaan, 1990; Dirksen *et al*., 1993; Raes Dirk, 2002; Suarez, 2012; Domínguez, 2011). Instead, the HYDRUS-1D model (Šimůnek *et al*., 2008, 2016) that numerically simulates the one-dimensional movement of soil water, solutes, and energy in soils was used. The model was used to determine the effects of irrigation water salinity and rainfall patterns on root zone salinity. Root water uptake and transpiration were considered.

The proposed research addresses two hypotheses. 1. Seasonal rainfall events during wet and dry seasons and irrigation with saline water impact the long-term accumulation of salts and the solute dynamics in almond and pistachio trees' root zone. These complex processes are continuously changing. 2. The future use of saline groundwater under variable rainfall patterns will significantly impact salt leaching and the need for soil amendments in the drip-irrigated almond and pistachio orchards.

1.3. References

AghaKouchak, A., Cheng, L., Mazdiyasni, O., and Farahmand, A., 2014. Global warming and changes in risk of concurrent climate extremes: Insights from the 2014 California drought. *Geophysical Research Letters*, 41(24), 8847–8852.

Ashraf, A., 2018. Assessing the Resilience of Desert and Southern California Farming Systems to Water Scarcity. UC Riverside UC Riverside Electronic Theses and Dissertations. UC Riverside.

Askri, B., Bouhlila, R., and Job, J., 2010. Development and application of a conceptual hydrologic model to predict soil salinity within modern Tunisian oases. *J. Hydrol*. 380, 45–61.

Bellvert, J., Adeline, K., Baram, S., Pierce, L., Sanden, B.L., and Smart, D.R., 2018. Monitoring Crop Evapotranspiration and Crop Coefficients Over an Almond and Pistachio Orchard Throughout Remote Sensing. *Remote Sensing*, 10 (12).

Blomquist, B., 2016. Implementing California's Sustainable Groundwater Management Act *(SGMA)*. Ostrom Workshop Colloquium Presentation, February 29, 2016. https://ostromworkshop.indiana.edu/pdf/seriespapers/2016s_c/Blomquist%20paper.pdf

Brown, P., 2016. Improving nitrate and salinity management strategies for almond grown under micro-irrigation. Ongoing project 2016-2018, UC Davis, CA. https://www.cdfa.ca.gov/is/docs/15-0523-SA_Brown.pdf.

Cal-Adapt. Data: Extended Drought Scenarios, LOCA Downscaled Climate Projections, VIC generated climate variables forced by LOCA (Scripps Institution of Oceanography), Gridded Historical Observed Meteorological and Hydrological Data (University of Colorado, Boulder). https://caladapt.org/tools/extendeddrought/#year=wateryear&lat=36.15625&lng=-120.21875&boundary=locagrid&scenario=late_century&units=imperial.

Corwin, D.L., Rhoades, J.D., Šimůnek, J., 2007. Leaching requirements for soil salinity control: steady state versus transient models. *Agric. Water Manage*., 90, 165–180.

Dirksen, C., Kool, J.B., Koorevaar, P., and Van Genuchten, M.Th., 1993. HYSWASOR—simulation model of hysteretic water and solute transport in the root zone. In Water flow and solute transport in soils (pp. 99-122). Springer Berlin Heidelberg.

Domínguez, A., Tarjuelo, J.M., De Juan, J.A., López-Mata, E., Breidy, J., and Karam, F., 2011. Deficit irrigation under water stress and salinity conditions: The MOPECO-Salt Model. *Agricultural water management*, *98* (9), 1451-1461.

Fulton, J., Norton, M., Shilling F.,2019. Water-indexed benefits and impacts of California almonds. *Ecological Indicators*, 96, 711-717.

Gonçalves, M.C., Martins, J.C., Prazeres, A., Castanheira, N.L., Pereira, L.S., Ramos, T.B., and Šimůnek, J., 2011. Field evaluation of a multicomponent solute transport model in soils irrigated with saline waters, *J. of Hydrology* 407, 129–144.

Gonçalves, M.C., Šimůnek, J., Ramos, T.B., Martins, J.C., Neves, M.J., Pires, F.P., 2006. Multi-component solute transport in soil lysimeters irrigated with waters of different quality. *Water Resour. Res.*, 42, 1–17.

Haghverdi, A., Wu., L., Hartin, J., and Ahiablame L., 2018. Soil Salinity. Parksandrecbusiness.com/articles/2018/11/soil-salinity.

Haj-Amor, Z., Ibrahimi, M.K., Feki, N., Lhomme, J.P., and Bouri, S., 2016. Soil salinization and irrigation management of date palms in a Saharan environment. *Environmental monitoring and assessment*, 188 (8), 497.

Hanak E., Escriva-Bou, A., Gray, B., Green, S., Harter, T., Jezdimirovic, J., Lund, J., Medellin-Azuara, J., Moyle, P., and Seavy, N., 2019. Water and the future of the San Joaquin Valley. *EPIC*, Public Policy Institute of California.

Hoffman, G.J., 2010. Salt Tolerance of Crops in the Southern Sacramento-San Joaquin Delta Final Report. California Environmental Protection Agency State Water Resources Control Board Division of Water Rights.*Hydrology and Hydromechanics*, 50, 3-19.

Jury, W.A., Or, D., Pachepsky, Y., Vereecken, H., Hopmans, J.W., Ahuja, L.R., Clothier, B.E. 2011. Kirkham's Legacy and Contemporary Challenges in Soil Physics Research. *Agronomy Publications*. Iowa state university. https://lib.dr.iastate.edu/agron_pubs.

Kaledhonkar, M.J., and Keshari, A.K., 2006. Modeling the effects of saline water use in agriculture. *J. of Irrig. and Drain.*, 55, 177 -190.

Kaledhonkar, M.J., Sharma, D.R., Tyagi, N.K., Ashwani, K., Van Der Zee, S.E.A.T.M., 2012. Modeling for conjunctive use irrigation planning in sodic groundwater areas. Agricultural Water Management, 107, 14 -22.

Li, H., Yi, J., Zhang, J., Zhao, Y., Si, B., Hill, R. L., Cui, L., and Liu, X., 2015. Modeling soil water and salt dynamics and its effects on root water uptake in Heihe arid wetland, Gansu, China. Water (Switzerland), 7 (5), 2382–2401.

Lobell, D.B., Lesch, S.M., Corwin, D.L., Ulmer, M.G., Anderson, K.A., Potts, D.J., Doolittle, J.A., Matos, M.R., and Baltes, M.J., 2010. Regional-scale assessment of soil salinity in the Red River Valley using multi-year MODIS EVI and NDVI. Journal of Environmental Quality, 39 (1), 35-41.

Machado, R.A., and Serralheiro, R.P., 2017. Soil Salinity: Effect on Vegetable Crop Growth. Management Practices to Prevent and Mitigate Soil Salinization. Horticulture, 3,30. doi:10.3390.

Mehdi-Tonsi, H., Chelli-Chaabouni, A., Mahjoub-Boujnah, D., Boukhris, M., 2017. Long-term field response of pistachio to irrigation water salinity, Agricultural Water Management, 185, 1.

Minhas P.S., Ramos, T.B., Ben-Gal, A., and Pereira, L.S., 2020. Coping with Salinity in Irrigated Agriculture: Crop Evapotranspiration and Water Management Issues. *Agric. Water Manag. J.*, 227, 105832.

Nethaji Mariappan, V.E., Selvaraj, T., and Vadivel, N., 2014. Soil Salinity Perspectives, Approaches, and Strategies. J. of Advanced Research in Civil and Environmental Engineering, 1, 33-39.

Oosterbaan, R.J., and Senna, M.A., 1990. Using SALTMOD to predict drainage and salinity in the Nile Delta. Using SALTMOD to predict drainage and salinity in the Nile Delta., pp.63-74.

Phogat V., Mallants, D., Cox, J., Simunek, J., Oliver, D.P., Pitt, T., and Petrie, P.R., 2020b. The impact of long-term recycled water irrigation on crop yield and soil chemical properties. Agric. Water Manag., 237, 106167.

Phogat V., Pitt, T., Cox, J.W., Simunek, J., and Skewes, M.A., 2018. Soil water and salinity dynamics under sprinkler irrigated almond exposed to varied salinity stress at different growth stages. Agriculture Water Manag., 201, 70 -82.

Phogat, V., Mallants, D., Cox, J., Simunek, J., Oliver, D.P., and Awad, J., 2020a. Management of soil salinity associated with the irrigation of protected crops. Agric. Water Manag. 227, 105845.

Phogat, V., Skewes, M.A., Mahadevan, M., and Cox, J.W., 2013. Evaluation of soil-plant system response to pulsed drip irrigation of Almond tree under sustained stress conditions, Agric. Water Manage., 118, 1-11.

Podmore, C., 2009. Irrigation Salinity Causes and impacts. Prime Facts 937, 1-4.

Raes, D., 2002. A soil water and salt balance model, V.5 manual. Faculty of Agricultural and Applied Biological Sciences Institute for Land and Water Management Vital Decosterstraat 102, B-3000 LEUVEN, Belgium.

Ramos, T.B., Darouich, H., Šimůnek, J., Gonçalves, M.C., Martins, J.C., 2019. Soil salinization in very high-density olive orchards grown in southern Portugal: Current risks and possible trends. *Agric. Water Manage.*, 217, 265–281.

Rasouli, F., Pouya, A.K., and Šimůnek, J., 2013. Modeling the effects of saline water use in wheat-cultivated lands using the UNSATCHEM model. *Irrigation Science*, 31 (5), 1009-1024.

Schneider, R., Adams, L., Betancourt, P., Brizard, A., Cabaldon, C., Hart, K., Mulholland, S., and Odenweller, D., 2006. Salinity in the Central Valey. Report byRegioal water control board, Central Valley Region, CA, USA.

Schoups, G., Hopmans, J.W., Young, C.A., Vrugt, J.A., Wallender, W.W., Tanji, K.K., and Panday, S., 2005. Sustainability of irrigated agriculture in the San Joaquin Valley, California. *Proceedings of the National Academy of Sciences*, 102 (43), 15352-15356.

Scudiero, E., Corwin D., Anderson R., Yemoto, K., Clary, W., Wang, Z., and Skaggs, T., 2017. Remote sensing is a viable tool for mapping soil salinity in agricultural lands. *California Agriculture*, 1-8.

Scudiero, E., Skaggs, T.H., Corwin, D.L., 2014. Regional-scale soil salinity assessment using Landsat ETM + canopy reflectance. *Remote Sensing of Environment,* 169, 335- 343.

Šimůnek, J., van Genuchten, M.Th., and Šejna, M., 2008. Development and applications of the HYDRUS and STANMOD software packages, and related codes, *Vadose Zone J*., doi:10.2136/VZJ2007.0077, *Special Issue "Vadose Zone Modeling," 7*(2), 587-600.

Šimůnek, J., van Genuchten, M.Th., Šejna, M., 2016. Recent Developments and Applications of the HYDRUS Computer Software Packages. *Vadose Zone Journal* 15, 7.

Skaggs, T.H., Shouse, P.J., and Poss, J.A., 2006. Irrigating Forage Crops with Saline Waters. 2. Modeling Root Uptake and Drainage, *Vadose Zone J.,* 5, 824-837.

Suarez, D.L., 2012. Modeling transient root zone salinity (SWS Model). In: Wallender, W.W. and Tanji, K.K. (eds.) Agricultural Salinity Assessment and Management: Chapter 28. *ASCE Manual and Reports on Engineering Practice* No. 71 (2nd Edition). ASCE, Reston, VA., pp. 855-897.

Suarez, D.L., Wood, J.D., Lesch, S.M., 2006. Effect of SAR on water infiltration under a sequential rain–irrigation management system. Agric. *Water Manage*. 86, 150–164.

Suweis, S., Rinaldo, A., Van der Zee, S.E.A.T.M., Daly, E., Maritan, A., and Porporato, A., 2010. Stochastic modeling of soil salinity. *Geophysical Research Letters*, *37* (7), 07404. doi: 10.1029/ 2010GL042495.

Tindula, G.N., Orang, M.N., and Snyder, R.L., 2013. Survey of Irrigation Methods in California in 2010. *ASCE J. of Irrigation and Drainage Engineering* 139, 233-238.

Underwood, E.C., Hollander, A.D., Flint, L.E., Flint, A.L., and Safford, H.D., 2018. Climate change impacts on hydrological services in southern California. *Environ. Res. Lett.,* 13 (2), 124019.

Zeng, W., Xu, C., Wu, J., and Huang, J., 2014. Soil salt leaching under different irrigation regimes: HYDRUS-1D modelling and analysis. *Journal of Arid Land*, *6* (1), 44-58.

Chapter 2 Seasonal Salinity in the Root Zones of Selected Drip-Irrigated Orchards of San Joaquin Valley, CA

Abstract

Soil salinity increases when growers are forced to use higher saline irrigation waters due to water shortages. To manage the effects of salinity on perennial crops, it is necessary to estimate the impact of irrigation water on soil properties and conditions for crop growth. Therefore, in this study, we monitored root zone salinity in five almond and pistachio orchards in eastern and western San Joaquin Valley (SJV), California (CA). Volumetric soil water contents and bulk electrical conductivities were measured at four root-zone depths. Evapotranspiration measured by eddy covariance was assessed in relation to three criteria. The first is seasonal precipitation and irrigation patterns, including the temporal distribution of rains, irrigation events, and irrigation water salinity. The second is soil chemistry, including the initial sodium adsorption ratio (*SAR*) and soil solute electrical conductivity (*ECe*)**.** The third criterion is soil's physical properties, including soil type, hydraulic conductivity, and bulk density. We found that salinity was well controlled at the eastern sites. Leaching of salts at the western sites was not as successful. The western sites have finer textured soils and poorer quality irrigation water; measured actual *ET* was about 90% of modeled crop *ET*. Across the three western sites, the annual average apparent leaching fraction ranged from 11 to 28%. Although the eastern sites showed evidence of sodicity problems and related reductions in soil hydraulic conductivity, overall salinity was controlled, and crop performance appeared maximal, with measured *ET* matching almost exactly modeled crop *ET* each year. Apparent leaching fractions in the eastern sites were approximately 20%.

2.1. Introduction

Competition for scarce water resources is increasing in many parts of the world, and consequently, water availability for irrigation is decreasing. Farmers are necessarily learning to be more efficient water managers. Many growers are now using micro or drip irrigation and other technologies to conserve water. However, drip systems create complicated, multidimensional "onion shell" patterns of water and salt movement in the soil, and uncertainties exist regarding the long-term use of drip irrigation due to the redistribution of salts in the rootzones (RZs) (Tindula *et al*., 2013). Root zone soil salinity affects crop water uptake, transpiration, and growth directly due to both osmotic and ion toxicity effects and indirectly through altering soil properties and processes such as infiltration (Minhas, 2020). Soil hydraulic properties, including available soil water within the effective root zone, are needed to estimate optimum irrigation schedules (Haghverdi *et al*., 2015).

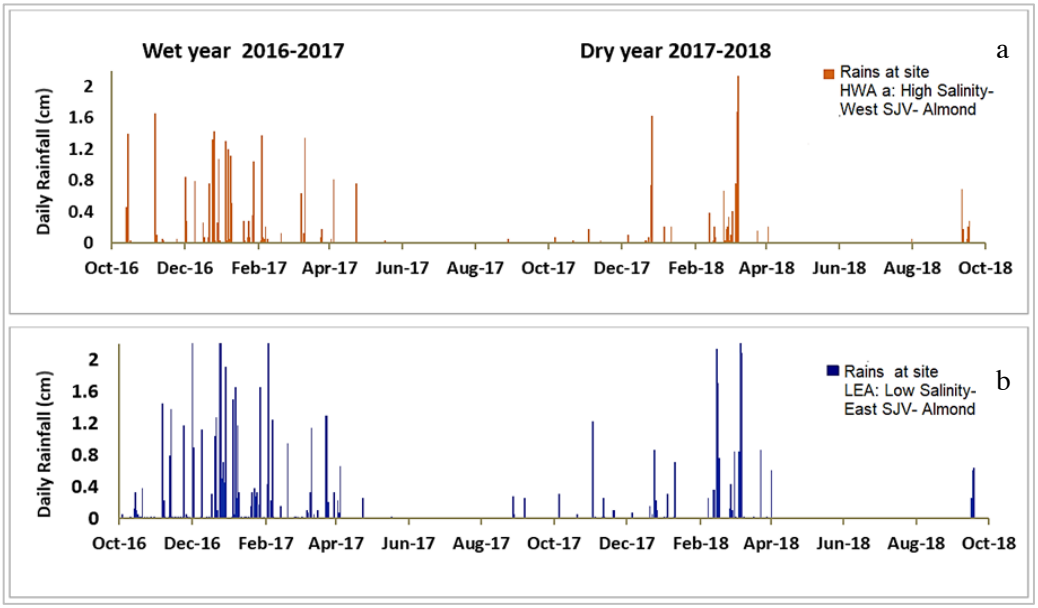

Figure 2.1. Two consecutive rain seasons in the western (a) and eastern (b) SJV.

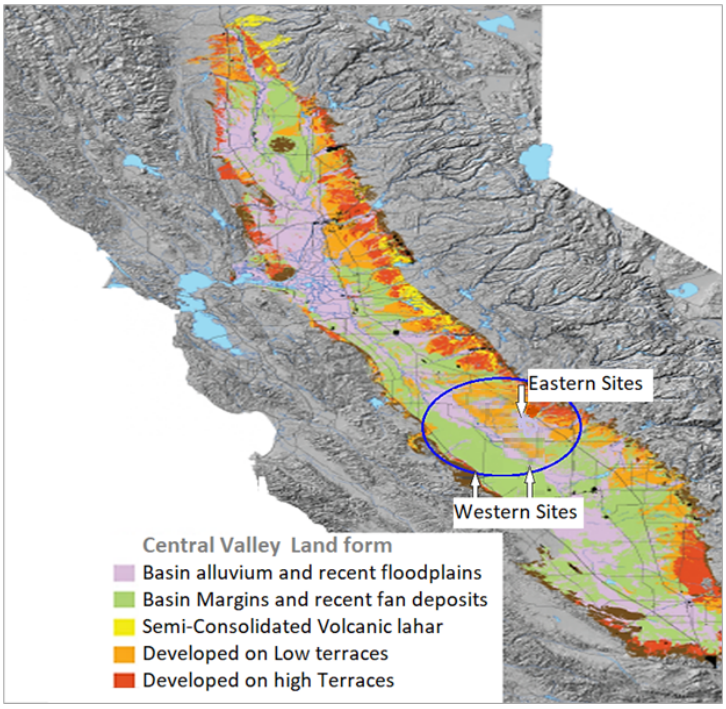

Figure 2.2. Soil Geology of SJV Parent Material (Turk and Graham, 2012).

San Joaquin Valley (SJV), California, is one of the most productive agricultural regions in the world and a prime example of evolving patterns of agricultural water availability and irrigation management. Annual rainfall in SJV is not enough to sustain cultivated agriculture (USGS, 1999). Eighty-five percent of rain occurs between November and April. Precipitation can vary significantly from year-to-year, as illustrated, for example, by the relatively wet water year 2017 and the relatively dry year 2018 (Figures 2.1.a and 2.1.b). Hence, the highly productive SJV relies on irrigation on a massive scale, which is possible because of an extensive statewide water distribution system that brings water from the northern part of the state and the Sierra Nevada mountains to the east (Carle, 2016).

Beyond water and water availability, a second key to understanding SJV agriculture is soil geology. The SJV floor is formed primarily by alluvial and lacustrine plains (Chang and Silva, 2014). Parent material lithology determines the physical and mineralogical nature of the soil, as

shown in (Figure 2.2). The western SJV consists of alluvial and lacustrine deposits, from which much of the Valley soils are derived. These soils of marine origin are mostly high in natural salts and trace elements such as boron and selenium (Quinn and Michael, 1994). Groundwater in west SJV tends to be more saline than in the east, where unconfined aquifers contain coarser, cleaner sands and better-quality water (Quin, 2014). The poor drainage conditions in western SJV impact crop production adversely (SJVDIP, 1998; Gaines, 1998; He *et al*., 2017).

In recent years, SJV has seen a significant shift from annual to perennial crops and from furrow and flood irrigation to drip and micro-irrigation. Agriculture in SJV has a long history, but the trend towards perennial orchards and drip irrigation systems is relatively recent. Although tree nut farmers are committed to improving the efficiency of water used for food production (Bellvert et al., 2018), the impact of drip irrigation systems and perennial crops on long-term salinity and water management is not fully understood.

In this chapter, we aimed to observe the effect that drip irrigation systems, irrigation water quality, soil quality, and rain have on soil root zone salinity and on water and salt balances in commercial orchards. These data and observations are needed to develop models that can be used to assess the possible future use of lower quality saline groundwater for irrigation in dry years. The data will also help clarify the salinity and water dynamics that occur in salt-affected almond and pistachio orchards under drip irrigation.

2.2. Methods

2.2.1. Field Sites

Five commercial SJV orchards were chosen for monitoring and evaluating seasonal water and salinity balances under drip irrigation (Figure 2.3.). The network of field sites was part of a concurrent USDA-ARS study evaluating soil and water quality impacts on crop productivity. The

orchards had varying crop types (almond, pistachio), soil and water salinities (low, medium, high), and geographic location (east vs. west SJV). In Figure 2.3, the salinity designations low, medium, and high are informal descriptors indicating relative salinity levels at the sites. As a point of reference, USDA advises that salinity effects on crop yields are mostly negligible in the range EC_e = 0–2 dS/m, can restrict the yields of sensitive crops in the range 2 – 4 dS/m and will restrict the yields of most crops in the range 4 – 8 dS/m (U.S. Salinity Laboratory Staff, 1954). Almond is classified as a "sensitive" crop with reported Maas-Hoffman threshold and slope parameters of 1.5 dS/m and 19 % m/dS, respectively. Maas and Hoffman (1977) rated pistachio as "moderately sensitive" although subsequent studies found the threshold to be 8 – 10 dS/m and the slope around 10 % m/dS (Sanden and Ferguson, 2004; and Sanden *et al*., 1988). The trees in all five orchards were ten to fifteen years old.

The five orchards were all irrigated with dual drip line systems (one line on either side of the tree line). As detailed below, the installation of monitoring equipment for the current study occurred during the fall of 2016. In typical water years, SJV farmers generally have access to high-quality surface water for irrigation. The four years preceding the current study had been historically dry years. During the drought, surface water deliveries were sharply curtailed, and many growers turned to groundwater for irrigation, which typically is of lower quality (higher salinity). As our study got underway, our collaborators at the western sites believed their use of groundwater was beginning to salinize the soil and that the orchards were starting to show signs of distress. However, a historically wet 2017 winter replenished much of the State's water reservoirs, and surface water was generally available for irrigation at the field sites during our study. Groundwater depths at the western and eastern SJV sites were about 25 m (82.5 ft) and 79 m (260 ft), respectively (USGS data, 2014).

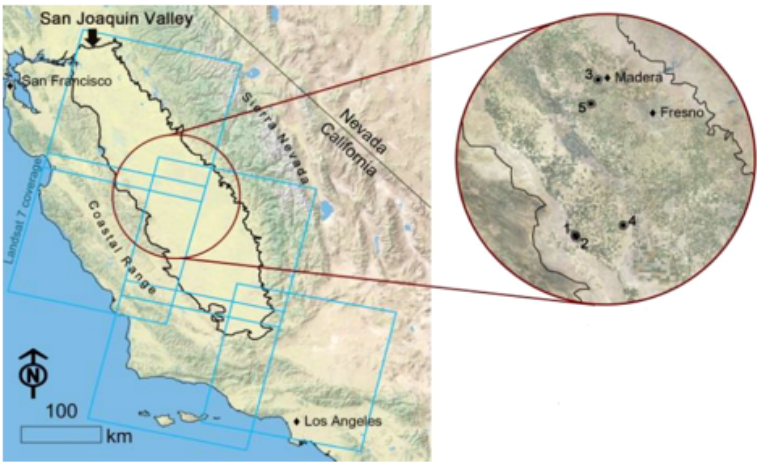

Key	Identifier	Initial Salinity* (dS/m)	Location**	Crop	Size (ha)
1	HWA	2.2 – 4.1 ("High")	West SJV	Almond	81
2	MWA	1.8 – 3.5 ("Medium")	West SJV	Almond	53
3	LEA	1.3 – 1.9 ("Low")	East SJV	Almond	16
4	HWP	2.3 – 4.7 ("High")	West SJV	Pistachio	63
5	LEP	1.1 – 2.1 ("Low")	East SJV	Pistachio	16

*Soil solution extract electrical conductivity, EC_e.
**SJV = San Joaquin Valley

Figure 2.3. Location of field sites in San Joaquin Valley, California.

2.2.2. Soil Properties

Concurrent with the instrument installation at the tower and outer sites, soil samples were collected for characterizing soil physical and chemical properties and root distributions (Figure 2.4). Samples were taken down to 1.2 m in 20 cm intervals. The following physical and chemical measurements were made on selected samples. Soil separate percentages were determined using the PARIO automated particle size analyzer (METER, 2020b), which uses the integral suspension pressure method to analyze particle settling. Bulk densities were determined from the oven-dry mass of undisturbed soil cores of known volume (Black, 1982). Saturated hydraulic conductivity was measured for each depth interval using the constant head method on samples repacked to the field bulk densities (Klute and Dirksen, 1986). Soluble cation concentrations of soil saturation

extracts were determined by ICP analysis. Saturation extract electrical conductivity (EC_e) and pH were measured using a conductivity/pH electrode calibrated against 0.01M and 0.001M KCl (Rayment and Higginson, 1992; Pratt *et al*., 2001). Cation exchange capacity (CEC) was determined by the ammonium acetate method (Chapman, 1965). Extracted cation solutions were analyzed for Ca, Mg, Na, and K. Roots were separated from the soil of each sample, and the mass of roots per sample was recorded. The measured masses were then used to construct normalized root density vs. depth curves for the sites.

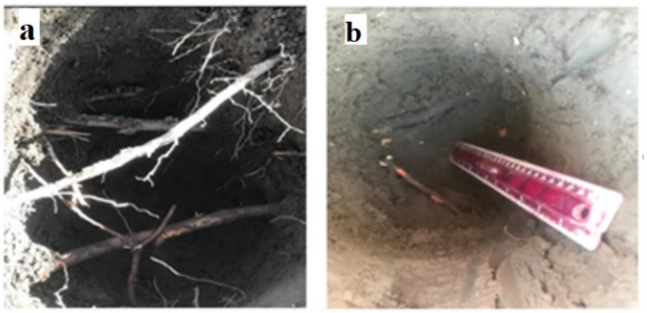

Figure 2.4. Excavations made at the relatively low salinity LEA site (a), and the relatively high salinity HWA site (b) for soil sampling and instrument installation.

2.2.3. Evaporation, Rainfall, and Irrigation

Evapotranspiration in the orchards was measured using eddy covariance. Eddy covariance instrumentation included sonic anemometers, infrared gas analyzers for CO_2 and H_2O, solar radiometers, and thermal heat flux plates. Evapotranspiration (ET_a) was determined from the eddy covariance data at 30 min interval datasets (Anderson,2016a; 2016b; 2016c; 2016d; 2016e). Modeled crop evapotranspiration (ET_c) was estimated from monthly crop coefficients from (SIMIS, 2016-2020) and (CIMIS regional data) for almond and pistachio, respectively. The daily reference evapotranspiration (ET_0) was available from nearly CIMIS weather stations (Stations #15, #80, and #205) (CIMIS, 2020). Tipping rain gauges were installed on the eddy covariance towers. Measured

rain was compared with rain reported at nearby CIMIS weather stations, and the amounts were similar. Irrigation water samples were collected periodically from drippers. Collected irrigation water samples were analyzed for Ca, Mg, Na, and K using ICP analysis. Solution electrical conductivity and pH were measured with a conductivity/pH electrode. A record of irrigation depth vs. time for each site was constructed based on emitter discharge rates, the spatial density of emitters in the orchards, reports from growers on the timing and duration of irrigations, and our adjustment and augmentation of those reports based on a review of soil moisture times series data and tipping rain gauge data.

2.2.4. Soil Moisture and Salinity Monitoring

The orchards were instrumented with Decagon GS3 sensors (METER Group Inc. USA), measuring bulk permittivity, temperature, and bulk electrical conductivity. Within each orchard, sensors were installed at three locations: a central "tower" location (so-called due to being co-located with an eddy covariance instrument tower) and two outlying locations referred to as "outer 1" and "outer 2." At the tower locations, four sensors were installed directly beneath a dripline at 25, 50, 75, and 100 cm depths, and two sensors were installed midway between the dual drip lines at 50 and 100 cm depths. Installations at the outer locations were the same except that only three sensors were installed at the 25, 75, and 100 cm depths at the drip position.

Soil-specific calibrations for the GS3 sensors were developed according to "Method A" of METER (2020a). A representative soil sample was collected from 25 cm at each site. In the lab, dry soil was packed in containers to the field bulk density, and a GS3 sensor was installed in the same manner as in the field. Water was added to the containers in steps. The soil container was weighed, and sensor readings were taken at each step. Soil volumetric water contents were calculated at each step from the soil dry bulk density and measured wet mass. The measurements

of dielectric permittivity versus the soil volumetric contents were plotted, and a quadratic calibration function for each site was fitted. Bulk electrical conductivity measured with the GS3 was converted to pore water electrical conductivity according to Hilhorst (2000),

$$EC_w = \frac{\varepsilon_p . EC_B}{\varepsilon_b - \varepsilon_{EC_B=0}} \quad (2.1)$$

where EC_w is the pore water electrical conductivity (dS/m), ε_p is the real portion of the dielectric permittivity of the soil pore water (unitless), EC_B is the bulk electrical conductivity (dS/m) measured directly by the GS3, ε_b is the real portion of the dielectric permittivity of the bulk soil (unitless), and $\varepsilon_{ECb=0}$ is the real portion of the dielectric permittivity of the soil when bulk EC is 0 (unitless). As recommended by Hilhorst (2000), we set $\varepsilon_{ECB=0} = 4.1$. The real part of the permittivity ε_p was calculated from (METER, 2020a),

$$\varepsilon_P = 80.3 - 0.37\ (T_{soil} - 20) \quad (2.2)$$

where T_{soil} is the soil temperature (in degrees Celsius) measured by the GS3.

2.3 Results and Discussion

2.3.1 Soil Properties

The measured soil characterization data are given in Appendix 2 (Tables A.2.1 through A2.5). Figure 2.5 and Table 2.1 summarize the soil textural properties of the five field sites. As expected from their geographic location, the east SJV sites generally have coarser textured soils than the west SJV sites. Sites HWA and LEP had the largest variability, with soil samples encompassing 5 and 6 textural classes, respectively. The HWP samples were relatively homogeneous with a clay texture (Table A2.4). Samples from site MWA had relatively high silt content (Table A2.2). The LEA site was also relatively uniform and mostly loam.

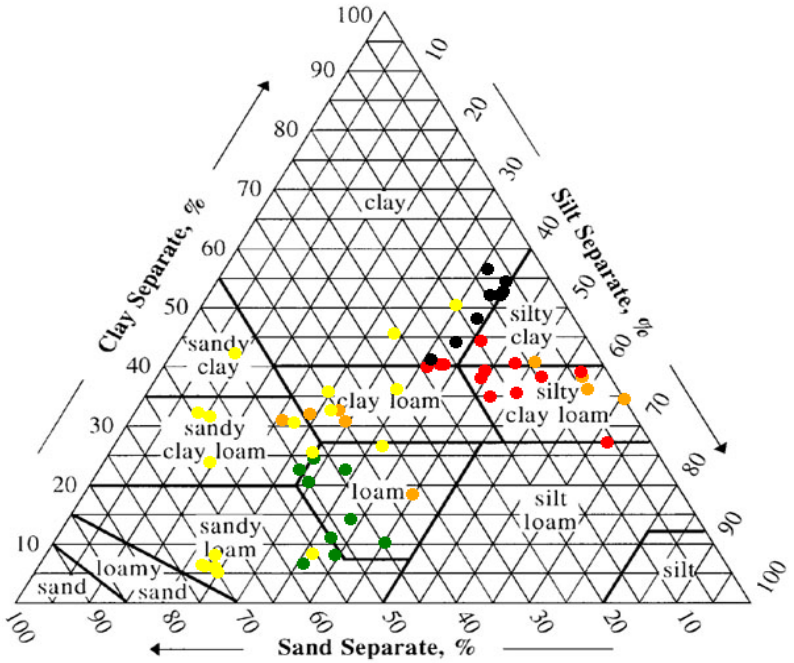

Figure 2.5. Soil separates percentages at the five sites: LEA (green dots), HWA (orange dots), MWA (red dots), LEP (yellow dots), and HWP (black dots). Chart made using https://www.nrcs.usda.gov/wps/portal/nrcs/detail/soils/survey/?cid=nrcs142p2_054167

Table 2.1. Soil textural classes of the studied sites

Key	Site	Texture Classes
1	HWA	Clay Loam, Loam, Silty Clay, Silty Clay Loam, Sandy Clay Loam
2	MWA	Silty Clay, Silty Clay Loam, Clay Loam,
3	LEA	Loam, Sandy Loam, Sandy Clay Loam
4	HWP	Clay
5	LEP	Sandy Loam, Sandy Clay Loam, Sandy Clay, Clay Loam, Clay

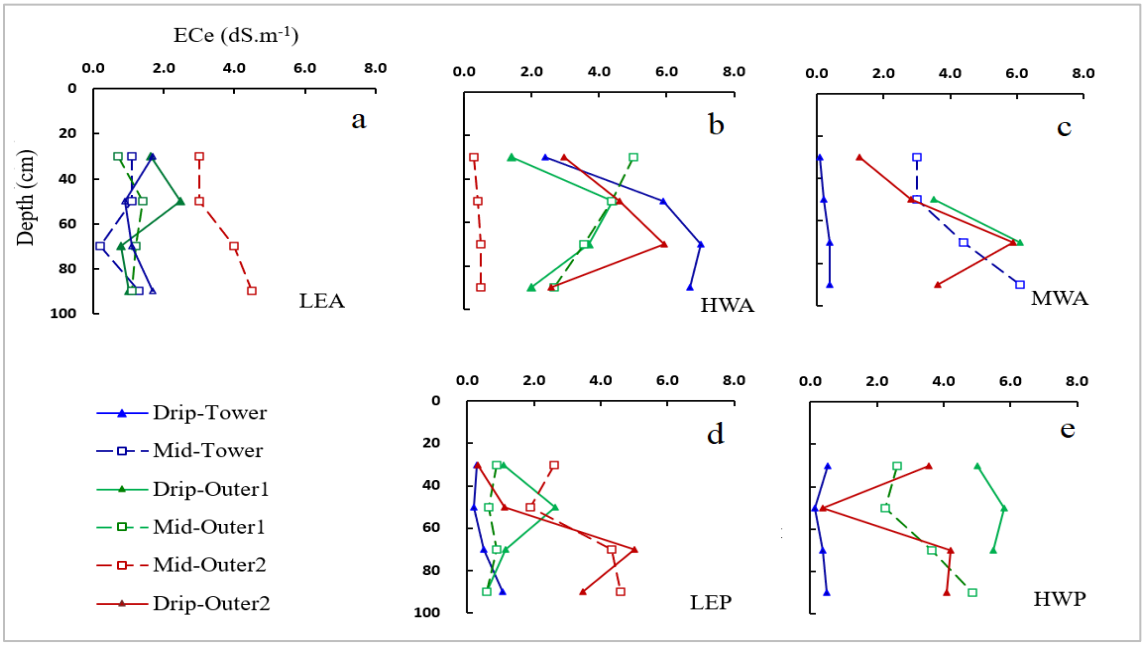

Figure 2.6. Electrical conductivity of soil saturation extract (EC_e) profiles at monitoring locations within the five study sites, fall 2016.

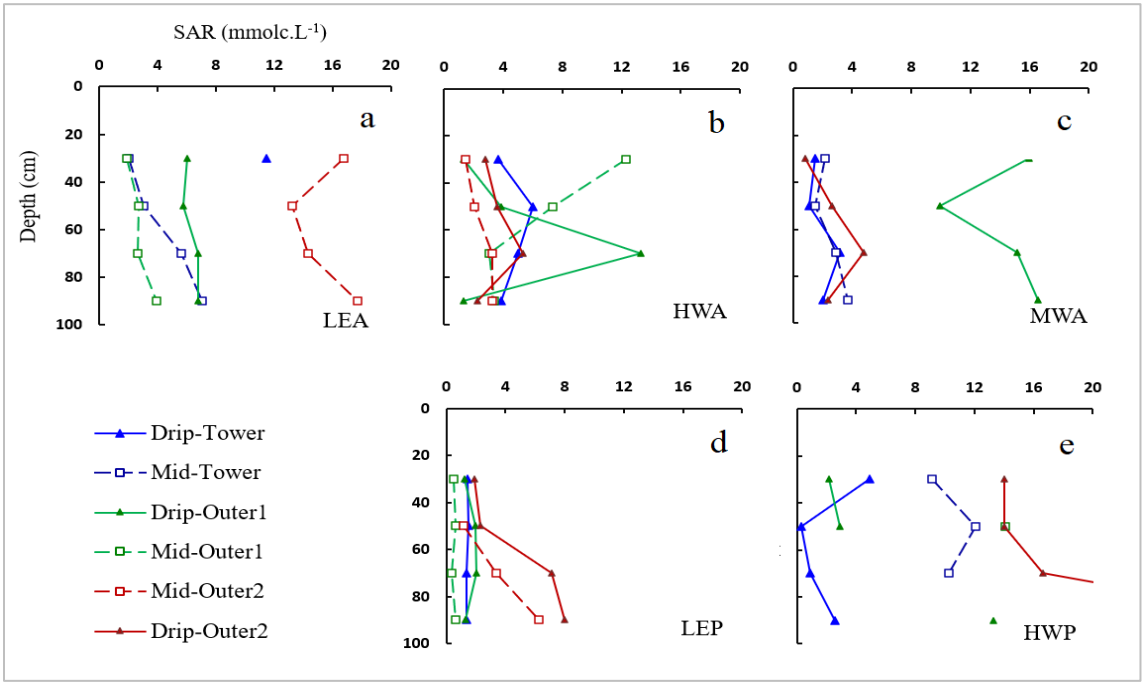

Figure 2.7. Sodium adsorption ratio (*SAR*) profiles at monitoring locations within the five study sites, fall 2016.

2.3.2 Initial Soil Salinity

The electrical conductivities (EC_e) of saturation extracts for the soil samples collected during fall 2016 are shown in Figure 2.6. Corresponding sodium adsorption ratios (*SAR*) are shown in Figure 2.6. Initial soil salinity at the pistachio sites (Figures 2.6de) was below the reported pistachio threshold of 8–10 dS/m. Many of the salinity profiles measured in the almond fields had depth-averaged values that exceeded the reported threshold of 1.5 dS/m, particularly at the finer textured, western sites HWA and MWA (Figures 2.6abc). At the HWA and MWA sites, salinity was highest, and saturated hydraulic conductivity lowest, at the middle depths, 40-100 cm (Figures 2.6bc; Tables A2.1 and A2.2). Fields LEA, MWA, and HWP all had locations where high sodium content in the soil profile suggests a possible sodicity hazard (Figures 2.7ace). On average, the coarser textured eastern sites had lower sodium content than the western sites.

2.3.3. Root Distribution

Figure 2.8 shows the measured root density profiles. The plotted values are the mass of the roots in a 20 cm soil sample divided by the total mass found at the location, i.e., the combined mass from the "drip" and "mid" excavations at each location within the field sites. For most of the sites and locations, the majority of the root mass was found between 20 and 60 cm. The eastern pistachio site LEP was an exception. Under the drip point at all three LEP locations, the peak root mass occurred within the 0-20 cm layer. Under the mid-points, significant root mass was found down to 100 cm. We speculate that the coarse soil texture at the LEP site results in lower rates of lateral water spread and consequently lower water availability and root mass near the surface beneath the mid-points. At the MWA and HWP sites, a relatively larger proportion of the root mass was found in the mid-point excavations compared to the drip point excavations (Figures 2.8ce).

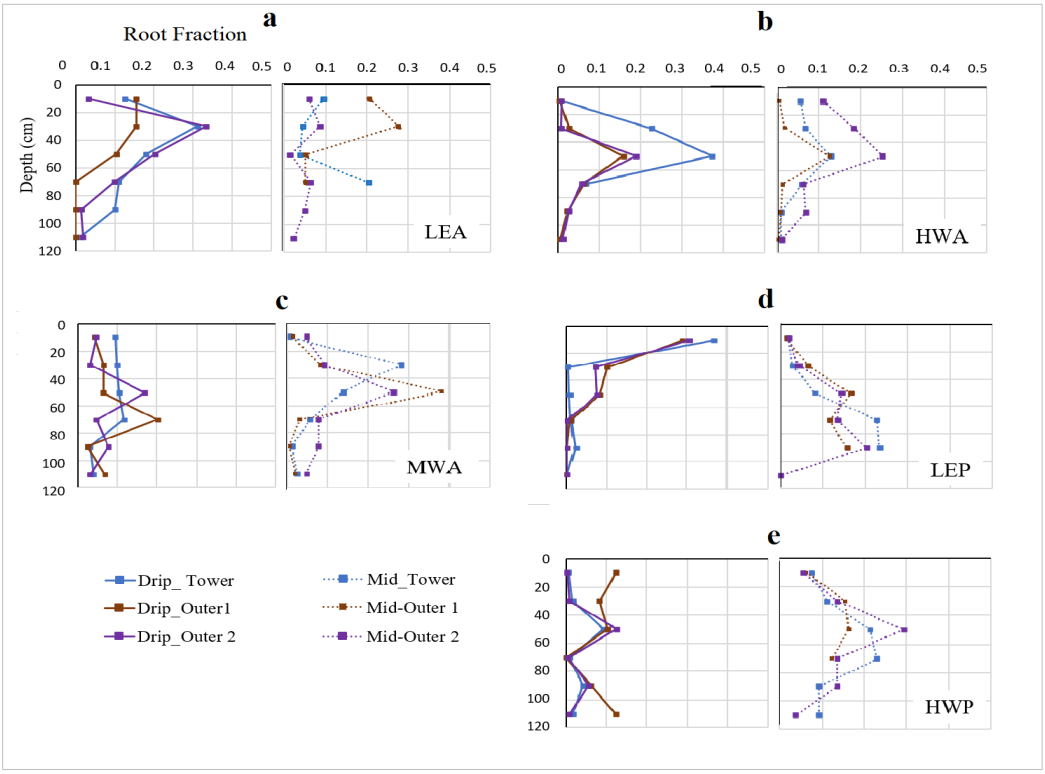

Figure 2.8. Fractions of the total roots under the drip and mid-measurement points.

The reason is not known. In general, one expects root growth and distributions to be affected by soil physical properties such as texture and porosity, chemical properties such as salinity and nutrient content, and management factors affecting soil water distributions and availability in the soil.

2.3.4. Evapotranspiration and Water Balances

Figure 2.9 shows an example of the collected rain, irrigation, and evapotranspiration data. The presented data are from field HWP, for water years 2017 and 2018. The water years 2017 and 2019 were similar to one another, and both were wetter than the relatively dry 2018 (Tables A2.7 to A.2.11). Irrigation water quality results are given in Figure 2.11 and Table A2.6.

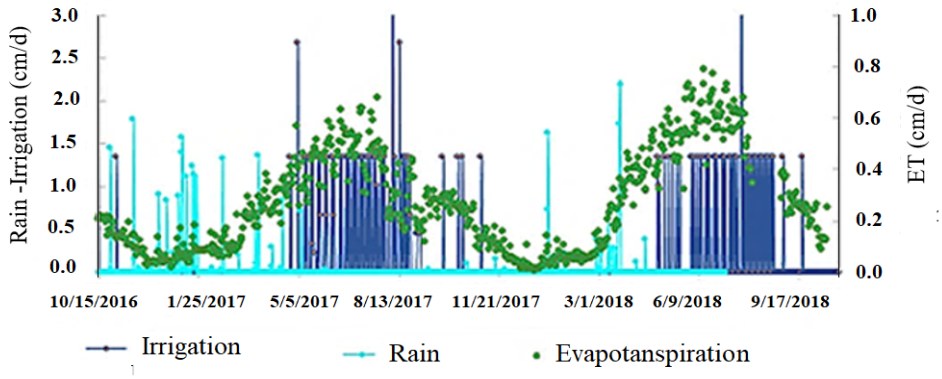

Figure 2.9. Example evapotranspiration, rainfall, and irrigation data measured at site HWP.

The lowest salinity irrigation waters were found at the eastern sites, where collected samples were generally less than 0.1 dS/m. Samples from the western sites ranged approximately from 0.25 to 0.9 dS/m.

A detailed accounting of the seasonal water balances for the five sites across all seasons and years is given in Tables A2.7 to A2.11. Note that due to the start date of the current study, values given for the first season, fall 2016, are only two months totals rather than three. The apparent leaching fractions included in the tables were calculated as:

$$LF = 1 - \left(\frac{ET_a}{(1+R)}\right) \tag{2.3}$$

where I, R, and ET_a are seasonal or annual totals of irrigation, rainfall, and measured ET, respectively. Thus, the LF calculation is based on an effective one-dimensional model of the soil and root zone and assumes the water stored in the soil at the beginning of the season is the same as at the end. Also, note that with this definition, LF will be negative if $ET_a > I + R$. Negative values were observed in some summer seasons.

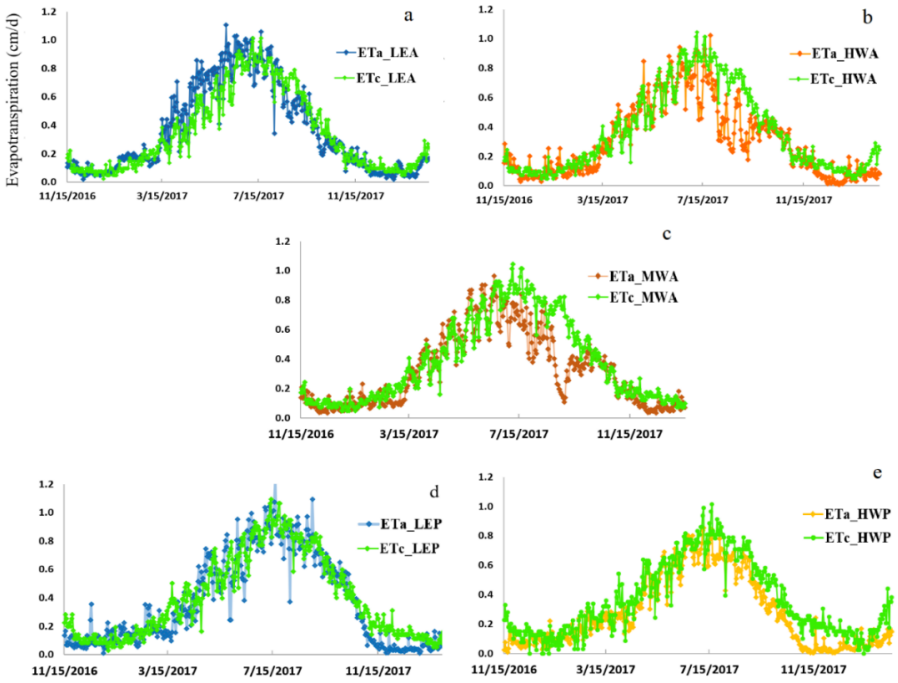

Figure 2.10. Measured evapotranspiration (ET_a) and modeled evapotranspiration (ET_c) at the eastern (a and c) and the western (b, c, and d) sites for the water year 2017.

Measured evapotranspiration, ET_a, matched modeled crop evapotranspiration, ET_c, relatively well at the low salinity eastern sites LEA and LEP (data for the water year 2017 shown in Figures 2.10a, d). However, at the western sites, ET_a was less than ET_c, especially at sites HWA and MWA (Figures 2.10bce). Almond harvest took place in mid-August, where some of the largest discrepancies between ET_a and ET_c occurred. From the data, it is not possible to determine if the *ET* discrepancies at the western sites were due to a relatively poor model ET_c estimate or if the western sites had reduced *ET* due to growth conditions, including higher soil and irrigation water salinities.

The low salinity sites in the east were very consistent with respect to the measured annual evapotranspiration. At the LEP eastern pistachio site, the ratio of measured and reference evapotranspiration, ET_a/ET_c, was 101, 99, and 104% for the water years 2017, 2018, and 2019,

respectively (Table A2.11). The corresponding values for the LEA eastern almond site were 106, 97, and 99%. The overall three-year average for both sites was 101%.

The ET_a/ET_c ratios at the salt-affected western sites were notably lower on average and exhibited greater interannual variability (Tables A2.7 -A2.11). The annual *ET* ratios at the western sites in 2017, 2018, and 2019 were: 92, 69, and 101 percent at HWP; 79, 92, and 97 percent at MWA; and 79, 90, and 93 percent at HWA. The three-year average values were 87 percent at HWP, 90 percent at MWA, and 87 percent at HWA.

The apparent equivalent leaching fractions at the sites varied with year and season (Tables A2.7 to A2.11). The most consistent site was LEP, where the annual leaching fractions were 25, 21, and 17%, with a three-year average value of 21%. Other sites were more variable. For example, site LEA had a similar average value of 19 percent, but with annual values of 29, 0, and 29 percent. Sites LEP (21 percent), LEA (19 percent), and HWA (18 percent) all had three-year averages near 20 percent. Site HWP had the highest apparent leaching fraction at 27%, whereas MWA had the lowest at 11%.

Inter-seasonal variations in leaching were high (Appendix 2, Tables A2.7 – A2.11). Winter is the rainy season, and a significant amount of leaching occurred, with apparent leaching fractions generally greater than or equal to 50%. Apparent leaching during the other seasons varied substantially, both across five field sites and year-to-year at individual sites.

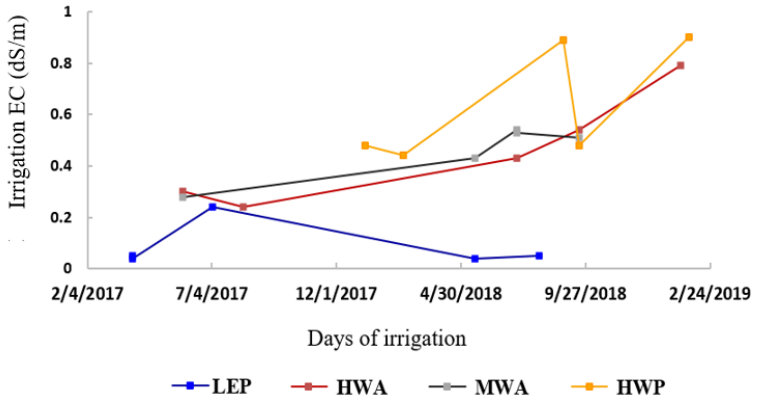

Figure 2.11. The measured electrical conductivity of irrigation water at four studied sites during 2017- 2019.

2.3.5. Soil Water and Salinity

Seasonal root zone salinity profiles for 2017–2019 are shown for the five study sites in Figures 2.12–2.16. Seasonal and annual trends are not easily identified from the plotted data. The plots in the top two rows of Figures 2.12 - 2.16 are for the tower locations, and because they contain an extra monitoring depth, they are a little easier to interpret; the discussion below focuses mainly on those plots.

Among the western field sites, HWA (Figure 2.12) and MWA (Figure 3.13) showed a general trend of increasing salinity between 2017 and 2019. Both sites relied on relatively saline irrigation water (Figure 2.11) and have medium-to-fine textured soils. The MWA site also had the lowest apparent average leaching fraction among the five sites at 11% (Table A2.8).

At the other western site HWP, root zone salinity remained relatively constant during the three years. However, some higher salinity readings were obtained at the shallowest depths at the mid-tower position in 2019 (Figure 2.15). Site HWP site had the highest average leaching fraction at 28% (Table A2.10).

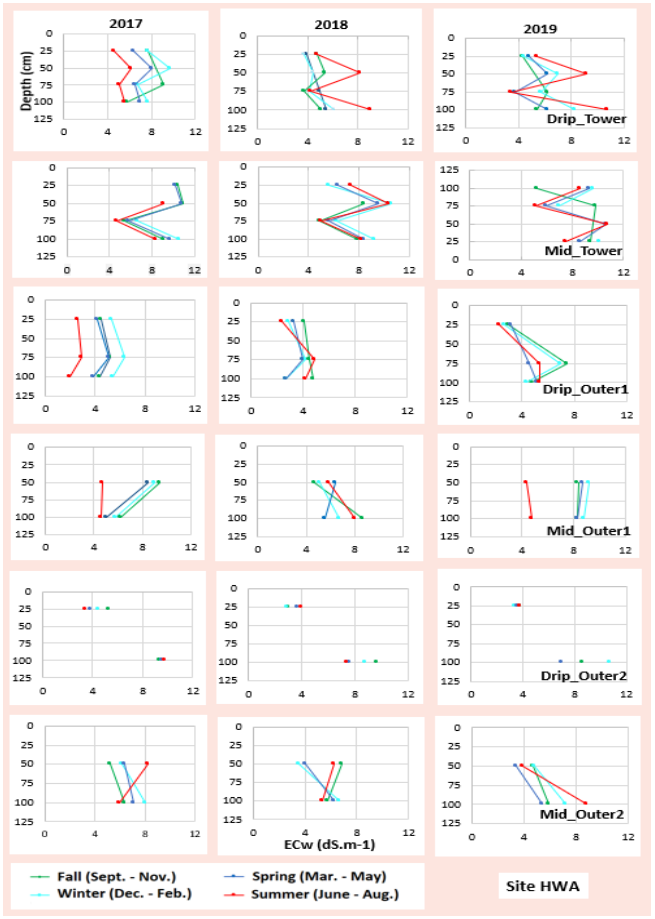

Figure 2.13. Seasonal average root zone soil water *EC* at six monitoring locations in the western almond site HWA.

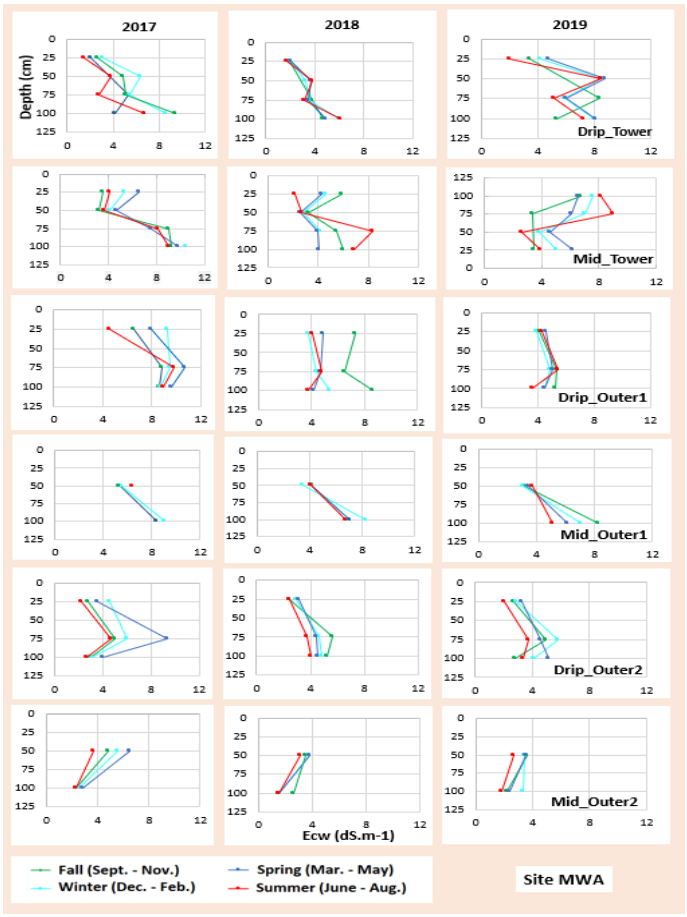

Figure 2.12. Seasonal average root zone soil water *EC* at six monitoring locations in the western almond site MWA.

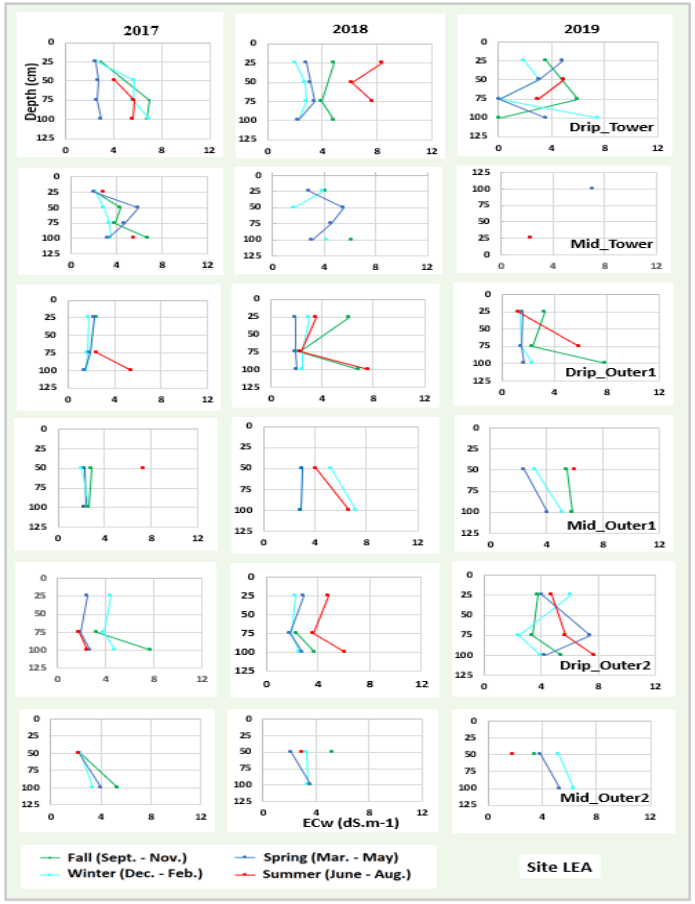

Figure 2.14. Seasonal average root zone soil water *EC* at six measuring locations in the eastern almond site LEA.

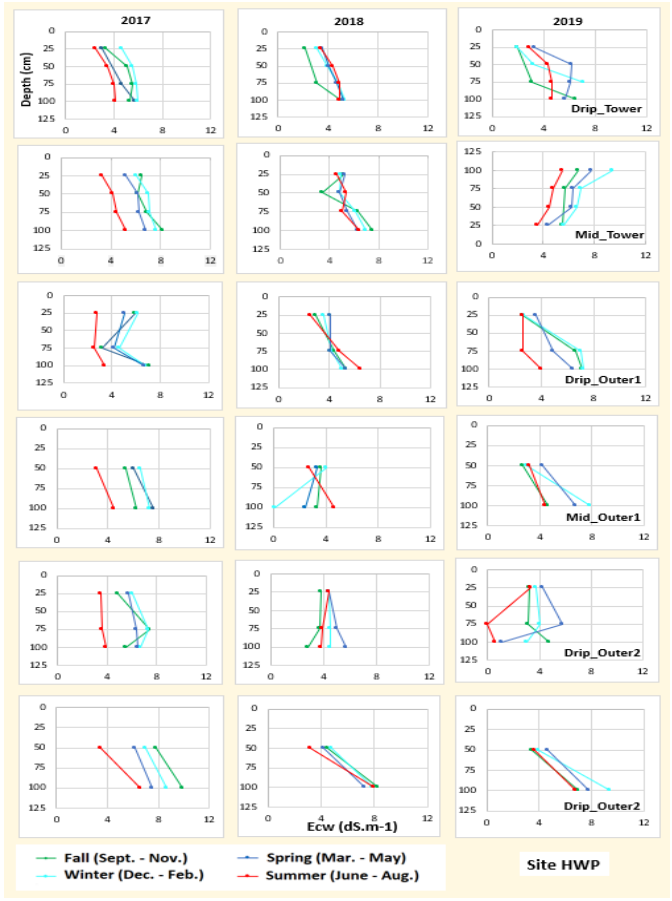

Figure 2.15. Seasonal average root zone soil water *EC* at six measuring locations in the western pistachio site HWP.

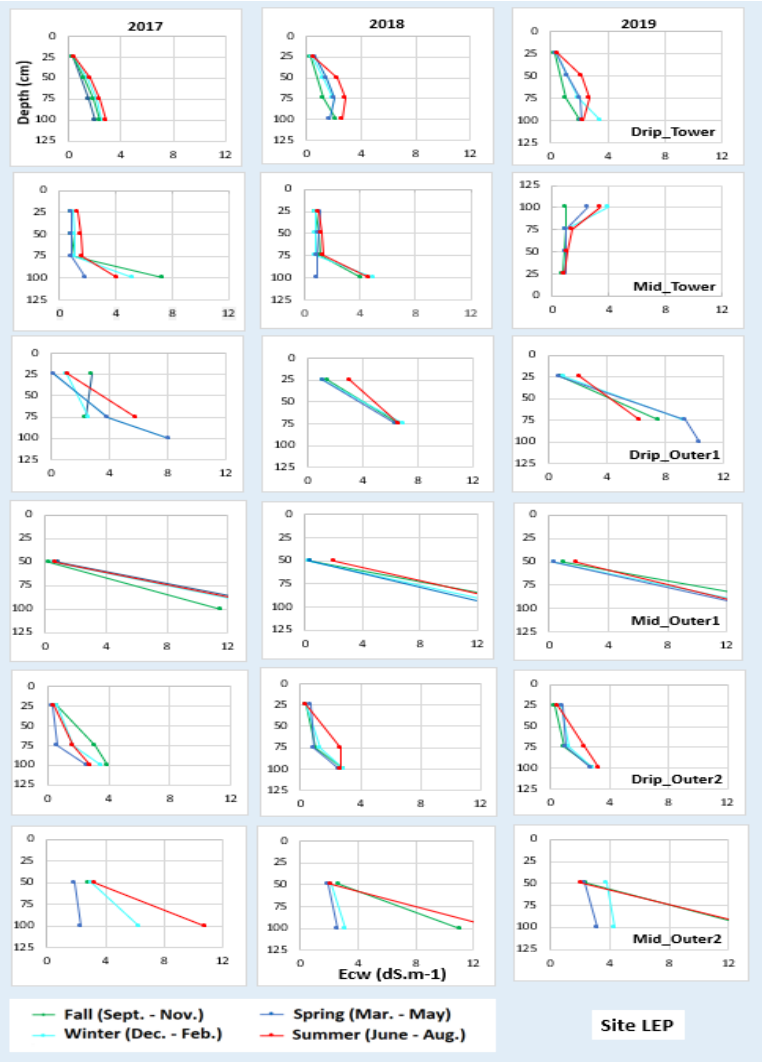

Figure 2.14. Seasonal average root zone soil water *EC* at six measuring locations in the eastern pistachio site LEP.

The western sites are in the rain shadow of the California Coast Ranges, and consequently, the eastern sites receive higher amounts of winter rains. The effect of winter rains at LEA and LEP can be seen in Figures 2.14 and 2.16 by noting that the highest salinities are obtained in the summer (red curves) but are reduced between growing seasons by fall and winter rain (blue curves).

2.4. Conclusions

As expected, the western sites had more significant salinity problems than the eastern sites. The western sites have finer textured soils and poorer quality irrigation water. Assuming the crop *ET* for the western sites was adequately modeled, the measured actual *ET* was about 90% of potential. While it is not possible to identify the cause of the ET reductions definitively, it is plausible that salinity was a contributing factor. Two of the western sites showed some evidence of increasing soil salinity levels throughout the study. The third western site appeared to maintain the level of salinity by imposing a relatively high apparent leaching fraction (28%). Across the three western sites, the annual average apparent leaching fraction ranged from 11 to 28%.

Although the eastern sites showed evidence of sodicity problems and related reductions in soil hydraulic conductivity, overall salinity was controlled, and crop performance appeared maximal, with measured *ET* matching modeled crop *ET* almost exactly each year. Apparent leaching fractions in the eastern sites were approximately 20%.

A more detailed assessment of salt transport mechanisms in the soil root zone and their impact on plant growth requires the use of process-based models, which is the subject of chapter 3.

2.5. References

Anderson, R.G., 2016-a. US-PSH USSL San Joaquin Valley Pistachio High, Dataset. https://doi.org/10.17190/AMF/1617719. https://doi.org/10.17190/AMF/1617719.

Anderson, R. G., 2016-b. AmeriFlux US-ASL USSL San Joaquin Valley Almond Low Salinity, Dataset. https://doi.org/10.17190/AMF/1617706.

Ray G. Anderson, R.G., 2016-c. AmeriFlux US-ASM USSL San Joaquin Valley Almond Medium Salinity, Dataset. https://doi.org/10.17190/AMF/1617709.

Anderson, R.G., 2016-d AmeriFlux US-ASH USSL San Joaquin Valley Almond High Salinity, Dataset. https://doi.org/10.17190/AMF/1634880.

Anderson, R.G., 2016_e. AmeriFlux US-PSL USSL San Joaquin Valley Pistachio Low. United States: N. p., 2020. Web. doi:10.17190/AMF/1617720.

Ayars, J.E., 2007. Adapting irrigated agriculture to saline environments. CAB Reviews: Perspectives in Agriculture, Veterinary Science, Nutrition, and Natural Resources 2, 13.

Bellvert, J., Adeline, K., Baram, S., Pierce, L., Sanden, B.L., and Smart, D.R., 2018. Monitoring Crop Evapotranspiration and Crop Coefficients Over an Almond and Pistachio Orchard Throughout Remote Sensing. *Remote Sensing*, 10 (12).

Ben-Hur, M., 2011. Water Use Efficiency in Agriculture: Opportunities for improvement. In: Glinski J., Lipiec J. (eds). Encyclopedia of Agrophysics. Encyclopedia of Earth Sciences Series. Springer, Dordrecht.

Bernstein, N., 2013. Plant roots, the hidden half. 4th edition. Ch. 36: Effects of Salinity on Root Growth. Edited by Emran Eshel, Tom Beeckman- Taylor and Francis Group, LLC.

Bernstein, N., Meiri, A., and Zilberstaine, M., 2004. Root Growth of Avocado (*Persea Americana Mill*) is more sensitive to salinity than shoot growth. *J. Am. Soc. Hortic. Sci.*. 129, 188- 192.

Black, G.R., 1982. Bulk density, in methods of Soil Analysis, Part I (C.A. Black, Ed._in_Chief), Am. Soc. Agron., Madison, WI.

Blomquist, B., 2016. Implementing California's Sustainable Groundwater Management Act (SGMA). Ostrom Workshop Colloquium Presentation, February 29. https://ostromworkshop.indiana.edu/pdf/seriespapers/2016s_c/Blomquist%20paper.pdf

Burt, C.M., and Ishell, B., 2005. Leaching of accumulated soil salinity under drip irrigation. *Trans. ASAE* 48, 2115 -2121.

Carter, M.R., and Ball, B.C., 1993. Soil Sampling and Methods of Analysis. Ch: 54. Soil Porosity, Ed., Canadian Society of Soil Science, Lewis Publisher.

Cecooli, G., Ramos, J.C., Ortega, L.I., Acosta, J.M., and Perreta, M.J., 2011. Salinity Induced anatomical and morphological changes in Chloris gayana Kunth roots. *Biocell* 35, 9-17.

Chang, A.C., and Brawer Silva, D., (eds.), 2014. Chapter 3: The San Joaquin Valley: Salinity and Drainage Problems and the Framework for a Response. *Salinity and Drainage in San Joaquin Valley, California: Science, Technology, and Policy*, Global Issues in Water Policy 5 ©Springer Science. DOI 10.1007/978-94-007-6851-2_3.

Chapman, H.D., 1965. Method of Soil Analysis, Part 2: Chemical and Microbiological Properties: Cation-exchange Capacity, pp. 891-900, in C.A. Black (ed.), Am. Soc. Agron., Madison, Wisconsin.

Cheeseman, J.M., 1988. Mechanisms of Salinity Tolerance in Plants. Annual Rev. *Plant Physiol*. 87, 547 – 550.

DeSutter, T., 2015. Saline and Sodic Soils: Understanding Differences and Management Solutions. Lecture for Tom DeSutter, on February 19, 2015, in NDSU: North Dakota State University.

Faunt, C.C., 2009. Groundwater Availability of the Central Valley Aquifer, California: US Geological Survey Professional Paper 1766, 225.

Gaines, R., 1998. Central Valley Project water development historical background, Economic impacts, Outlook. Water Resources Center Archives. University of California, Berkeley. Berkeley, CA, 94720.

Gartley, K.L., 2011. Recommended Soil Testing Procedures for the Northeastern United States Last Revised 5/2011.

Graham, R., and O'Geen, A., 2016. Part 4. Geomorphology and Soils. Ecosystems of California. University of California Press. Oakland, California. pp 47-70.

Haghverdi, A., Leib, B.G., Washington-Allen, R.A., Ayers, P.D., and Buschermohle, M.J., 2015. High resolution prediction of soil available water content within the crop root zone. *J. of Hydrology,* 530, 167-179.

Hart, Q.J., Brugnach, M., Temesgen, B., Rueda, C., Ustin, S.L., *et al.,* 2009. Daily reference evapotranspiration for California using satellite imagery and weather station measurement interpolation. *Civil Engineering and Environmental Systems* 26 (1), 19–33.

He, R., Jin, Y., Kandelous, M., Zaccaria, D., Sanden, B., Snyder, R., Jiang, J., and Hopmans, J., 2017. Evapotranspiration estimate over an almond orchard using Landsat satellite observations. *Remote Sens*., 9, 436.

Hilhorst, M.A., 2000. A pore water conductivity sensor. Soil Science Society of America Journal 64:6 1922-1925.

Jones, A., 1990. Soil Analysis. Modern instrumental techniques, second edition. Edited by Kieth A. Smith. Department of Biology. New York University, New York, New York.

Klute, A. and Dirksen, C., 1986. "hydraulic Conductivity and Diffusivity: Laboratory Methods. " Methods of Soil Analysis, Part 1. Agronomy Monograph No. 9, 2nd Ed., pp 687-734.

Kratzer, C.R., and Grober, L.F., 1991. San Joaquin River salinity: 1991 projections compared to 1977. *California Agriculture,* 45 (6), 24-27.

Li, X., Kang, Y., Wan, S., Chen, X., Liu S., Xu, J., 2016. The response of a salt-sensitive plant to processes of soil reclamation in two saline-sodic, coastal soils using drip irrigation with saline water, *Agric. Water Manage. J.*, 164, 223 – 234.

Maas, E.V., 1993. Testing crops for salinity tolerance. In *Proc. Workshop on Adaptation of Plants to Soil Stresses.,* 234, 247.

Maas, E.V., and Hoffman, G.J., 1977. Crop salt tolerance - current assessment. *J. Irrig. And Drainage Div., ASCE 103 (IR2)*, 115-134.

Machado, R., and Serralheiro, R., 2017. Soil Salinity: Effect on Vegetable Crop Growth. Management Practices to Prevent and Mitigate Soil Salinization. *Horticulturae J.,* (3), 30.

Mckenzie, R.C., Chomistek, W., and Clark, N.F., 1988. Conversion of electromagnetic inductance readings to saturated paste extract values in soils for different temperature, texture, and moisture conditions. J. Soil. Sci.
Downloaded from www.nrcresearchpress.com by 96.40.173.81 on 04/17/20.

METER Group., 2019. GS3 soil water permittivity, electrical conductivity, and temperature sensors user manual. METER Group, Inc. USA 2365 NE Hopkins Court Pullman, WA 99163. http://library.metergroup.com/Manuals/20429_GS3_Web.pdf.

METER Group, 2020a. Method A: Soil Specific calibrations for METER soil moisture sensors. https://www.metergroup.com/environment/articles/method-a-soil-specific-calibrations-for-meter-soil-moisture-sensors/, last log ins 2018- 2020.

METER Group, 2020b. library.metergroup.com/Manuals/20780_PARIO_Manual_Web.pdf.

Minhas P.S., T.B. Ramos, A. Ben-Gal, and L.S Pereira. 2020. Coping with Salinity in Irrigated Agriculture: Crop Evapotranspiration and Water Management Issues. *Agric. Water Manag. J.*, 227, 105832.

Owen, D., Cantor, A., Nylen N., Harter T., Kiparsky M., 2019. California groundwater management, Science-policy interfaces, and the legacies of Artificial Legal Distinctions. *Environ. Res. Letters*, 14 (1).

Peach, J.D., 1991. Ch2: Problems associated with irrigation practices carried out underwater services contracts. Reclamation law: Changes before water services contracts renew. Water Resources Center Achieves (WRCA), UC Berkeley.

Phogat, V., Skewes, M.A., Mahadevan, M., and Cox, J.W., 2013. Evaluation of soil-plant system response to pulsed drip irrigation of Almond tree under sustained stress conditions, *Agric. Water Manage.*, 118, 1-11.

Pratt, K.W., Koch, W.F., Wu, Y.C., and Berezansky, P.A., 2001. *Pure Appl. Chem*, 73, 1783.

Quinn, N.W.T., 2014. Chapter 3: The San Joaquin Valley: Salinity and Drainage Problems and the Framework for a Response. Springers.

Quinn, N.W.T., and Michael, L.D., 1994. Issues of sustainable irrigated Agriculture in the San Joaquin Valley of California in a Changing Regulatory Environment Concerning Water Quality and Protection of Wildlife. International Symposium on Water Resources in a Changing World Karlsruhe, Germany.

Rewald, B., Leuschner, C., Wiesman, Z., Ephrah, J.E. 2011. Influence of Salinity on root hydraulic properties of three olive varieties. *Plant Biosyst*., 145, 12-22.

Richards, L.A., 1954. Diagnosis and improvement of saline and alkali soils. US Salinity Laboratory Staff. Agric. Handbook. No. 60. USDA, Washington, DC, pp 160.

Schoups, G., Hopmans, J.W., Young, C.A., Vrugt, J.A., Wallender, W.W., Tanji, K.K., and Panday., S., 2005. Sustainability of irrigated agriculture in the San Joaquin Valley, California. *Proceedings of the National Academy of Sciences*, *102* (43), *15352-15356*.

Scudiero, E., Corwin, D., Anderson, R., Yemoto, K., W. Clary, W., Z. Wang, Z., and T. Skaggs, T., 2017. Remote sensing is a viable tool for mapping soil salinity in agricultural lands. *California Agriculture*, 71 (2) *1-8*.

Sanden, B., Ferguson, L., and Kallsen, C., 2014. Development of Pistachios with Saline Irrigation Water and Regional Salt Tolerance in Pistachio Production Fields. *Agricultural and Natural Resources*, University of California.

Sanden, B.L., Ferguson, L., Reyes, H.C., and Grattan, S.C., 2004. Effect of Salinity on Evaporation and yield of San Joaquin Valley Pistachios. Proceedings of IVth International Symposium on Irrigation of Horticultural Crops, *Acta Horticulturae* 664, 583 – 589.

Sepaskhah, A.R., and Maftoun, M., 1988. Relative salt tolerance of pistachio cultivars. *J. of Horticultural Science*, *63* (1), 157-162.

SIMIS, 2016-2018. Satellite Irrigation Management Support for monitoring, modeling, and forecast, USA. url link, last logged in 2019.

SJVDIP, 1998. Drainage Management in the San Joaquin Valley: A Status Report. Sacramento, CA, DWR, San Joaquin Valley Drainage Implementation Program.

SJVDP, 1990. The San Joaquin Valley Drainage federal-state interagency program. It was established to study agricultural drainage and drainage related problems in the western San Joaquin Valley.

Tindula, G.N., Orang, M.N., and Snyder, R.L., 2013. "Survey of Irrigation Methods in California in 2010," ASCE Journal of Irrigation and Drainage Engineering 139, 233-238.

Turk, J., Chadwick, O., Graham, R., 2012. Chapter 30: Pedogenic processes. Handbook of Soil Silences. Boca Raton: CRC Press, https://doi.org/10.1201/b11267.

UCCHM, 2014. UC Center for Hydrologic Modeling (UCCHM). Water Storage Changes in California's Sacramento and San Joaquin river basins from GrACe: Preliminary updated results for 2003-

2013. university of California, Irvine UCCHM Water Advisory #1, February 3, 2014. https://www.nrdc.org/sites/default/files/ca-water-supply-solutions-capstone-IB.pdf. NRDC: The Untapped Potential of California's Water Supply: Efficiency, Reuse, and Stormwater.

US Salinity Laboratory Staff, 1954. Methods for Measuring Soluble Salts, Soluble Salts by the Saturated Paste Method. Chapter 10. Recommended Methods for Measuring Soluble Salts in Soils. Recommended Soil Testing Procedures for the Northeastern United States Last Revised 5/2011.

USGS, 1999. PART I. San Joaquin Valley, California. Land subsidence in the united states. Menlo Park, California, US Geological Survey and US Department of Interior. http://pubs.usgs.gov/circ/circ1182/pdf/06SanJoaquinValley.pdf.

Van Der Lelii, A., 1983. use of an electromagnetic induction instrument (type EM-38) for mapping of soil salinity. Water Resourc∈s Commission. Murrumbidgee Division, Australia.

Van Reeuwijk, L.P., 2002. Procedures for Soil Analysis. 6th ed, Technical Paper/ International Soil Reference and Information Center, Wageningen, The Netherlands. Protokol_Soil_Exchangeable_Bases_CEC_20081127.doc.

West, G., Inze, D., Beemster, G.T., 2004. Cell Cycle modulation in the response of the primary root of *Arabidopsis* to salt stress. *Plant Physiol*. 135, 1050 -1058.

WSS, 2018. Web Soil Survey. United States Department of Agriculture. Natural Resources Conservation Service. logged in April 2018. https://websoilsurvey.sc.egov.usda.gov/App/HomePage.htm

Appendix 2. Soil Characterization Data

Table A2.1. Measured soil properties of the HWA site.

Location	Position	Depth	CEC	Exchangeable Sodium Percentage	Sodium Adsorption Ratio	EC_e	pH	Sand	Silt	Clay	Saturated hydraulic conductivity
		cm	$mmol_c/kg$	%	$mmolcL^{0.5}$	dS/m		%	%	%	$cm.d^{-1}$
Tower	Drip	0–20						49.5	20.1	30.4	
		20–40	62.57	22.15	3.6	2.4	6.7	40.9	28.9	30.2	16.15
		40–60	130.64	34.79	6.0	5.9	8.0				5.62
		60–80	151.47	32.02	5.0	7.0	8.0	5.2	59.2	35.6	0.5
		100–120	138.13	33.24	3.8	6.7	8.0	4.9	57.3	37.8	2.05
	Mid	0–20									
		20–40	7.79	22.40							
		40–60	8.51	16.32							
		60–80	56.41	1.21							
		100–120	47.71	1.47							
Outer 1	Drip	0–20									
		20–40			1.33	1.4	6.6				
		40–60			3.86	4.4	8.1				
		60–80			13.31	3.7	8.2	1.0	65.0	34.0	
		100–120			1.34	2.0	7.8				
	Mid	0–20									
		20–40			12.3	5.0	7.9				
		40–60			7.3	4.4	8.1				
		60–80			3.1	3.6	8.1				
		100–120			3.4	2.7	7.7				
Outer 2	Drip	0–20						45.2	23.4	31.4	
		20–40	63.24	23.88	2.8	3.0	8.4	40.8	27.0	32.2	10.83
		40–60	112.14	21.97	3.6	4.6	8.5				6.33
		60–80	134.43	22.72	5.3	5.9	8.4	10.2	49.6	40.2	2.87
		100–120	78.30	22.60	2.3	2.6	8.2	38.0	44.2	17.8	26.59
	Mid	0–20									
		20–40	73.43	22.36	1.5	0.3	8.1				
		40–60	109.50	20.44	2.0	-	-				
		60–80	113.17	22.50	3.2	0.5	8.3				
		100–120	99.94	27.34	3.3	0.5					

Table A2.2. Measured soil properties of the MWA site.

Location	Position	Depth	CEC	Exchangeable Sodium Percentage	Sodium Adsorption Ratio	EC_e	pH	Sand	Silt	Clay	Saturated hydraulic conductivity
		cm	mmol$_c$/kg	%	$mmolcL^{0.5}$	$dS.m^{-1}$		%	%	%	cm/d^{-1}
Tower	Drip	0–20						18.8	43.6	37.6	9.37
		20–40	124.49	5.17	1.5	1.3	8.5	17.7	43.5	38.8	3.38
		40–60	75.78	6.46	1.1	2.2	8.6				
		60–80	133.11	3.87	3.2	4.5	8.2	4.6	56.8	38.6	1.01
		100–120	115.22	4.95	2.0	3.9	8.2	7.0	66.4	26.6	8.72
	Mid	0–20									
		20–40			2.1	3.0	8.3				
		40–60			1.5	3.0	8.1				
		60–80			2.9	4.4	8.3				
		100–120			3.7	6.1	8.1				
Outer 1	Drip	0–20									
		20–40	100.28	15.05	16.0			15.7	40.5	43.8	
		40–60	125.34	16.96	9.9	3.5	8.1	22.7	37.5	39.8	
		60–80	128.82	20.19	15.1	6.1	8.4				
		80–100						15.3	49.7	35.0	
		100–120			16.6			13.0	47.0	40.0	
Outer 2	Drip	0–20						25.2	35.4	39.4	5.77
		20–40			0.9	1.3	7.9	23.2	37.0	39.8	2.27
		60–80			2.6	2.8	8.6				
		80–100			4.8	5.9	8.2	19.1	46.5	34.4	7.48
		100 -120			2.4	3.6	8.2	10.5	51.7	37.8	16.71

Table A2.3. Measured soil properties of the LEA site

Location	Position	Depth	CEC	Exchangeable Sodium Percentage	Sodium Adsorption Ratio	EC_e	pH	Sand	Silt	Clay	Saturated hydraulic conductivity
		cm	mmol$_c$/kg	%	$mmolcL^{0.5}$	dS/m		%	%	%	$cm.d^{-1}$
Tower	Drip	20–40	44.59	15.39		1.7	8.1	52.7	36.7	10.6	29.18
		40–60	48.19	16.80		0.9	8.2	48.5	37.9	13.6	17.74
		60–80	68.61	15.62		1.1	7.3	53.7	38.7	7.6	21.82
		100–120	78.01	15.68		1.7	8.1	58.6	35.2	6.2	27.78
	Mid	20–40	35.75	10.87	2.0	1.1	8.2				
		40–60	38.85	13.45	3.1	1.1					
		60–80	46.26	15.54	5.6	0.2	8.7				
		100–120	86.53	13.39	7.0	1.3	8.6				
Outer 1	Drip	20–40	35.14	22.90	6.0	1.6	8.6	45.0	33.0	22.0	
		40–60	34.38	17.73	5.7	2.5	8.3	48.3	27.7	24.0	
		60–80	31.37	17.09	6.8	0.8		51.3	26.7	22.0	
		100–120	29.72	23.90	6.8	1.0	8.3	51.0	29.0	20.0	
	Mid	20–40	33.90	10.61	1.9	0.7	7.5				
		40–60	30.36	13.21	2.7	1.4	7.9				
		60–80	32.60	10.82	2.6	1.2	8.2				
		100–120	33.01	16.60	4.0	1.1	7.6				
		20–40			16.8	3.0	8.9				
		40–60			13.3	3.0	8.8				
		60–80			14.3	4.0	8.2				
		100–120			17.7	4.5	8.5				

Table A 2.4. Measured soil properties of the HWP site.

Location	Position	Depth	CEC	Exchangeable Sodium Percentage	Sodium Adsorption Ratio	EC_e	pH	Sand	Silt	Clay	Saturated hydraulic conductivity
		cm	mmol$_c$/kg	%	$mmolcL^{0.5}$	dS/m		%	%	%	$cm.d^{-1}$
Tower	Drip	0–20						10.5	37.9	51.6	
		20–40	97.07	21.05	0.3	4	7.5	8.5	39.3	52.2	21.85
		40–60	120.64	20.58	0.9	1.5	8.5	14.3	38.1	47.6	7.03
		60–80	96.43	19.23	2.9	3.7	7.5				7.02
		100–120			2.6	4.8		24.2	35.2	40.6	13.57
	Mid	0–20									
		20–40									
		40–60									
		100–120									
Outer 1	Drip	0–20									
		20–40	126.53	10.30	2.16	5.0	7.8	9.2	39.2	51.6	
		40–60	119.59	10.21	2.89	5.8	7.8	7.3	38.9	53.8	
		60–80	129.58	8.04				8.7	35.4	55.9	
		100–120	53.07	12.13	13.32	5.5	7.4	19.1	37.2	43.7	
	Mid	0–20									
		20–40	103.42	11.23		2.6	7.3				
		40–60	106.44	10.12	14.1	2.3	7.4				
		60–80	118.36	8.01		3.7	7.2				
		100–120	106.34	5.73		4.9	7.0				
Outer 2	Drip	0–20									
		20–40	117.76	21.43	14.03	3.6	8.3				8.90
		60–80	124.53	23.20	14.05	3.8	8.4				3.79
		100 -120	166.82	25.59	34.48						9.79

Table A2.5. Measured soil properties of the LEP site.

Location	Position	Depth	CEC	Exchangeable Sodium Percentage	Sodium Adsorption Ratio	EC_e	pH	Sand	Silt	Clay	Saturated hydraulic conductivity
		cm	mmol/kg	%	$mmolcL^{0.5}$	dS/m		%	%	%	$cm.d^{-1}$
Tower	Drip	0–20						72.4	21.9	5.7	
		20–40	6.08	16.25	1.42	0.3	7.6	72.6	21.4	5.9	50.95
		40–60	8.10	7.96	1.47	0.2	6.9	70.0	22.5	7.5	30.33
		60–80	9.90	14.44	1.39	0.5	6.6	71.1	24.2	4.7	13.81
		100–120	30.46	11.50	1.33	1.1	7.9	56.7	35.6	7.7	11.20
Outer 1	Drip	0–20									
		20–40			1.2	1.1	7.9	63.0	13.8	23.2	
		40–60			2.0	2.6	8.0	59.0	10.0	31.0	
		60–80			2.0	1.1	7.9	60.3	8.0	31.7	
		100–120			1.3	0.6		50.2	8.0	41.8	
	Mid	0–20									
		20–40			0.5	0.9	8.4				
		40–60			0.6	0.7	8.2				
		60–80			0.3	0.9	8.2				
		100–120			0.6	0.6	7.8				
Outer 2	Drip	0–20									
		20–40	6.12	26.27	1.9	0.3	6.3	42.0	26.0	32.0	
		40 -60	8.03	16.07	2.3	1.1	6.9	38.0	36.0	26.0	
		60–80	54.88	1.31	7.1	5.0	7.2	48.0	22.0	30.0	
		100 -120	47.84	1.51	8.0	3.3	8.4	31.3	33.0	35.7	
	Mid	0–20									
		20–40	8.57	11.02	1.2	2.6	7.1	48.0	27.0	25.0	
		40–60	21.40	15.59	3.4	1.9	8.2	16.0	34.0	50.0	
		60–80	82.25	16.71	6.3	4.3	7.6	27.0	28.0	45.0	
		100–120	47.83	16.63	4.9	4.3	8.4	40.7	24.0	35.3	

Table A2.6. Irrigation water salinity, sodicity, and ionic composition.

	Sites	Day of irrigation	ECiw (Ds/m)	SAR (mmolc/L)$^{0.5}$	pH	Ca2+ (mmolc/L)	Mg2+ (mmolc/L)	Na+ (mmolc/L)	K+ (mmolc.l/L)
1	HWA	5/30/2017	0.3		7.78	0.32	0.32	1.29	0.17
		8/11/2017	0.24	1.4	7.14	0.35	0.35	1.54	0.09
		7/6/2018	0.43		7.6	1.04	0.51	2.24	0.1
		9/19/2018	0.54		6.95	0.31	0.29	1.09	0.07
		1/20/2019	0.79		7.8	1.1	1.16	4.76	0.19
2	MWA	5/30/2017	0.28	1.7	7.7	0.33	0.33	1.47	0.08
		5/17/2018	0.43		7.69	0.87	0.58	2.47	0.13
		7/6/2018	0.54	1.8	7.72	0.43	0.61	3.26	0.12
		7/6/2018	0.53	1.8	8	1.11	1.2	4.92	0.24
		9/19/2018	0.51		7.89	0.46	0.52	2.31	0.11
		1/5/2018	0.48		7.8	0.91	0.69	5.98	0.14
3	LEP	3/30/2017	0.05	0.48	7.64	0.1	0.02	0.19	0.05
		3/30/2017	0.04	0.6	7.6	0.08	0.01	0.13	0.04
		7/5/2017	0.24		7.8	0.49	0.24	1.15	0.07
		5/17/2018	0.04		7.2	0.08	0.02	0.19	0.04
		8/2/2018	0.05		8.06	0.07	0.01	0.15	0.04
4	HWP	2/20/2018	0.44		7.57	0.52	0.59	2.86	0.16
		8/31/2018	0.89	4.1	7.72	0.51	0.56	2.54	0.12
		9/19/2018	0.48	3	7.93	0.44	0.57	3.03	0.11
		1/30/2019	0.9		7.77	1.22	0.74	5.89	0.09

Table A2.7. Seasonal water balance in site HWA.

Year	Season	Season Start_ HWA	Applied Irrigation (cm)	Rain (cm)	Etc (cm)	ETa (cm)	Total precipitation	Apparent LF (cm)
2017	F 16	10/15/2016	7.49	3.76	13.56	11.47	11.25	-0.02
	W 17	12/15/2016	13.10	14.58	14.21	10.68	27.68	0.61
	SP 17	3/15/2017	50.32	4.01	46.55	45.32	54.33	0.17
	SU 17	6/15/2017	55.65	0.00	76.21	51.38	55.65	0.08
	Annual	**2017**	**126.56**	**22.35**	**150.52**	**118.85**	**148.91**	**0.20**
2018	F 17	9/15/2017	27.55	0.30	29.57	23.30	27.85	0.16
	W 18	12/15/2017	30.59	4.55	18.02	8.26	35.14	0.77
	SP 18	3/15/2018	50.85	6.10	42.40	51.05	56.95	0.10
	SU 18	6/15/2018	65.20	0.00	72.20	63.51	65.20	0.03
	Annual	**2018**	**174.20**	**10.95**	**162.19**	**146.12**	**185.15**	**0.21**
2019	F 18	9/15/2018	24.14	3.76	25.81	27.76	27.90	0.00
	W 19	12/15/2018	12.21	14.58	14.14	10.77	26.79	0.60
	SP 19	3/15/2019	50.32	4.01	43.16	51.58	54.33	0.05
	SU 19	6/15/2019	55.65	0.00	71.95	54.19	55.65	0.03
	Annual	**2019**	**142.32**	**22.35**	**155.06**	**144.30**	**164.67**	**0.12**

Average LF =18%, Average Eta/ETc = 87%

Table A2.8. Seasonal water balance in site MWA.

Year	Season	Season Start_ HWA	Applied Irrigation (cm)	Rain (cm)	Etc (cm)	ETa (cm)	Total precipitation	Apparent LF (cm)
2017	F 16	10/15/2016	22.26	4.01	13.56	10.54	26.27	0.60
	W 17	12/15/2016	6.68	**12.78**	14.21	10.10	19.46	0.48
	SP 17	3/15/2017	47.22	4.04	46.55	47.86	51.26	0.07
	SU 17	6/15/2017	50.98	0.00	76.21	50.37	50.98	0.01
	Annual	**2017**	**127.13**	**20.83**	**150.52**	**118.87**	**147.96**	**0.20**
2018	F 17	9/15/2017	22.35	0.28	29.57	23.52	22.63	-0.04
	W 18	12/15/2017	12.35	**4.70**	18.02	7.28	17.05	0.57
	SP 18	3/15/2018	50.22	6.02	45.84	54.29	56.24	0.03
	SU 18	6/15/2018	75.00	0.00	78.72	73.22	75.00	0.02
	Annual	**2018**	**159.92**	**11.00**	**172.15**	**158.30**	**170.91**	**0.07**
2019	F 18	9/15/2018	22.35	2.87	24.80	26.14	25.22	-0.04
	W 19	12/15/2018	6.68	**10.52**	12.25	9.30	17.20	0.46
	SP 19	3/15/2019	50.22	2.62	43.77	49.59	52.83	0.06
	SU 19	6/15/2019	65.00	0.00	72.20	64.49	65.00	0.01
	Annual	**2019**	**144.25**	**16.00**	**153.02**	**149.52**	**160.25**	**0.07**

Average LF = 11%, Average Eta/ETc = 90%

Table A2.9. Seasonal water balance in site LEA.

Year	Season	Season Start LEA	Applied Irrigation (cm)	Rain (cm)	Etc (cm)	ETa (cm)	Total precipitation	Apparent LF (cm)
2017	F 16	10/15/2016	20.16	6.55	10.95	9.27	26.71	0.65
	W 17	12/15/2016	35.19	14.00	13.19	12.37	62.24	0.80
	SP 17	3/15/2017	47.77	6.20	43.32	55.86	53.97	-0.04
	SU 17	6/15/2017	61.77	0.28	70.05	67.89	62.10	-0.09
	Annual	**2017**	**164.88**	**27.03**	**137.52**	**145.40**	**205.01**	**0.29**
2018	F 17	9/15/2017	29.32	2.36	25.06	20.12	31.68	0.37
	W 18	12/15/2017	14.42	8.69	15.48	11.29	23.20	0.51
	SP 18	3/15/2018	45.45	8.18	45.65	55.23	53.52	-0.03
	SU 18	6/15/2018	42.92	0.00	70.20	64.96	42.92	-0.51
	Annual	**2018**	**132.10**	**19.23**	**156.40**	**151.60**	**151.33**	**0.00**
2019	F 18	9/15/2018	21.38	7.65	22.65	19.14	29.03	0.34
	W 19	12/15/2018	36.16	16.00	13.29	16.62	57.55	0.71
	SP 19	3/15/2019	47.77	8.18	41.40	50.52	55.95	0.10
	SU 19	6/15/2019	61.77	0.00	69.72	59.19	61.77	0.04
	Annual	2019	167.08	31.82	147.06	145.46	204.29	0.29

Average LF =19%, Average Eta/ETc =101

Table A2.10. Seasonal water balance in site HWP.

Year	Season	Season Start_ LEP	Applied Irrigation (cm)	Rain (cm)	Etc (cm)	ETa (cm)	Total precipitation	Apparent LF (cm)
2017	F 16	10/15/2016	15.11	3.86	12.19	6.19	18.97	0.67
	W 17	12/15/2016	17.23	14.33	14.30	13.87	31.55	0.56
	SP 17	3/15/2017	38.23	3.35	40.09	38.56	41.58	-0.22
	SU 17	6/15/2017	69.08	0.03	66.70	63.47	69.11	0.08
	Annual	**2017**	**139.65**	**21.56**	**133.27**	**122.08**	**161.21**	**0.24**
2018	F 17	9/15/2017	15.73	0.61	25.84	13.77	16.34	0.16
	W 18	12/15/2017	17.48	4.34	16.48	10.36	21.82	0.53
	SP 18	3/15/2018	45.24	3.58	24.86	37.06	48.83	0.24
	SU 18	6/15/2018	40.00	0.00	63.66	29.01	40.00	0.88
	Annual	**2018**	**118.45**	**8.53**	**130.84**	**90.21**	**126.99**	**0.48**
2019	F 18	9/15/2018	16.45	3.38	24.58	15.21	19.83	0.23
	W 19	12/15/2018	17.23	10.01	13.16	13.71	27.23	0.50
	SP 19	3/15/2019	29.57	9.04	35.42	37.76	38.61	0.02
	SU 19	6/15/2019	67.74	0.00	60.48	67.26	67.74	0.01
	Annual	**2019**	**130.99**	**22.43**	**133.64**	**133.94**	**153.42**	**0.13**

Average LF =28%, Average Eta/ETc =87%

Table A2.11. Seasonal water balance in site LEP.

Year	Season	Season Start_ LEP	Applied Irrigation (cm)	Rain (cm)	Etc (cm)	ETa (cm)	Total precipitation	Apparent LF (cm)
2017	F 16	10/15/2016	17.67	6.55	10.43	9.50	24.22	0.61
	W 17	12/15/2016	14.19	20.00	13.68	11.64	34.19	0.66
	SP 17	3/15/2017	35.76	6.20	35.80	37.01	41.96	0.12
	SU 17	6/15/2017	65.56	0.28	63.42	66.16	65.84	0.00
	Annual	**2017**	**133.17**	**33.03**	**123.33**	**124.31**	**166.20**	**0.25**
2018	F 17	9/15/2017	15.19	2.36	23.22	21.51	17.55	-0.23
	W 18	12/15/2017	18.21	8.69	15.57	8.19	26.89	0.70
	SP 18	3/15/2018	38.19	8.18	23.55	36.30	46.37	0.22
	SU 18	6/15/2018	65.56	0.00	62.56	57.83	65.56	0.12
	Annual	**2018**	**137.14**	**19.23**	**124.91**	**123.83**	**156.37**	**0.21**
2019	F 18	9/15/2018	17.67	7.65	22.29	24.74	25.31	0.02
	W 19	12/15/2018	14.19	21.39	14.83	11.22	35.58	0.68
	SP 19	3/15/2019	35.76	8.18	35.34	34.85	43.94	0.21
	SU 19	6/15/2019	65.56	0.00	63.85	70.91	65.56	-0.08
	Annual	**2019**	**133.17**	**37.21**	**136.30**	**141.71**	**170.38**	**0.17**

Average LF = 21%, Average Eta/ETc =101%

Chapter 3 HYDRUS-1D Simulations of Almond and Pistachio Root Zone Salinity in the San Joaquin Valley, CA.

Abstract

This chapter aims to present numerical simulations of rootzone salinity in and below the root zone of almond and pistachio orchards and compare numerical results with experimental data. The numerical model is additionally used to quantitatively assess a seasonal increase in the soil salinity as a function of applied irrigation water and its salinity. Transient numerical simulations were carried out using the one-dimensional (1D) numerical model HYDRUS-1D to simulate dynamic water and solute changes in soils. The numerical model was used to evaluate the effects of saline irrigation water use through a drip irrigation system in the east and west regions of the San Joaquin Valley (SJV), CA. The numerical model was calibrated and validated using field measurements of soil water contents and soil solute bulk electrical conductivities at four rootzone depths of 25, 50, 75, and 100 cm, and measured values of soil hydraulic conductivities. The remaining soil hydraulic parameters were estimated inversely using the Marquardt-Levenberg method, which is directly implemented in the HYDRUS-1D code.

Observations and numerical simulations showed that regardless of whether the year was dry or wet, the effects of seasonal rainfall on soil salt concentrations in the rootzones with initially low salinity were higher than those with initially high salinities. The maximum reduction in simulated water uptake (7%) occurred in the west SJV (site HWA) in response to initially saline conditions and highly saline irrigation water applied. The minimum reduction (2.5%) in simulated water uptake occurred in the east SJV (site LEA) in response to both low initial soil salinity conditions and a wet year's rain (2017). The relationship at the early and late times of the growing season between the simulated water uptake reduction and the leaching fraction showed a variable

response dependent on the irrigation water salinity level. The primary factors, which influenced the water uptake reduction, were the salinity of irrigation water, soil leaching, and the annual total precipitation amount. The root water uptake reduction was much more correlated to the cumulative effects of using saline waters in prior years than to the leached amounts of salts during the same season, even when rain was sufficient to leach salts in a wet year. The results showed that irrigation water's salinity was the more important factor than the other two factors, i.e., leaching and the rain year type. In the western SJV, the increase in the water uptake reduction was significantly correlated with saline irrigation water use in previous years.

3.1. Introduction

Agricultural management practices need to be adjusted to account for the ongoing water scarcity and predicted climate change scenarios in California. It is essential to quantify and predict management effects on soil properties and model their consequent impact on production and the environment (Green *et al.*, 2003). Developing sustainable agricultural practices requires using methods that accurately describe salinity patterns and changes over time and space (Schoups *et al.*, 2005). A comprehensive understanding of the spatial distribution of deep percolation fluxes due to the spatial distribution of soil properties and spatial vegetation heterogeneities is still needed to develop such strategies (Lia *et al.*, 2016).

Soil salinity, similarly to soil water content, is often variable in time and space. The full analysis of salts' transient transport in the root zone requires extensive measurements, a long time, and significant efforts and costs. Numerical models, on the other hand, proved to be useful and efficient tools to carry out spatial-temporal analyses of agricultural systems to enhance their productivity under various irrigation schemes and to assess ongoing climate change effects on soil salinity (e.g., Li *et al.*, 2015; Phogat *et al.*, 2018; 2020; Ramos *et al.*, 2019). Hence transient salinity models are desirable for the analysis of management decisions (Suarez, 2012). Inherent soil salinity

problems integrate the effects of soil, climate, crops, methods of irrigation, and management practices. Transient state models provide solutions for quantifying the salinity build-up in the root zone due to these various processes and factors. These may additionally include irrigation-induced salinity, upward movement of salts from the saline groundwater table, and sodification processes (Minhas *et al.*, 2020).

There is a need to develop simple and practical (e.g., quicker and cheaper) methods to determine and evaluate soil salinity to improve decision-making processes and soil salinity stress management (Shrivastava and Kumar, 2015; Lobell *et al.*, 2010; and Rasouli *et al.,* 2013). The accuracy of the predictions of salinity build-up and water uptake by plants depends on selecting proper mathematical models (Kumar *et al.*, 2015). Modeling can explain how temporal and spatial aspects of soil water and solute fluxes are affected by irrigation practices (Šimůnek *et al.*, 2008). Feddes *et al.* (2004) summarized the progress, challenges, and applications of unsaturated-zone modeling.

Simulations using transient-state models for actual field conditions require information about the quality of waters entering the soil (e.g., rainwater, irrigation water, etc.). The continuous changes that occur throughout the root zone are a function of irrigation water salinity, amounts of applied water, rainfall, crop evapotranspiration (*ET*), and climate change (Oster *et al.*, 2010). Gigante *et al.* (2009) stated that vegetation's space-time distribution is crucial for a correct evaluation of soil evapotranspiration. However, some of the past analyses that compared steady-state and transient-based leaching requirements ignored rainfall and did not correctly represent field conditions (Letey *et al.*, 2011).

The HYDRUS-1D model (Šimůnek *et al.*, 2008) was used in many studies to assess problems associated with soil salinity, including those involving drip irrigation, through a one-dimension or two-dimensional analysis (Kaledhonkar and Keshari, 2006; Goncalves *et al.*, 2006;

Suarez 2006; Corwin *et al.*, 2007; Kaledhonkar *et al.*, 2012; Gonçalves *et al.*, 2011; Zeng *et al.*, 2014; Ramos *et al.*, 2019). For example, Gonçalves *et al.* (2011) concluded that HYDRUS-1D is a powerful tool for analyzing solute concentrations related to overall soil salinity and nitrogen species. Haj-Amor *et al.* (2016) used HYDRUS-1D to clarify the impact of different water salinities and irrigation practices on soil salinity (expressed as electric conductivity, *EC*), which exceeded the palm salt tolerance in their study. Li *et al.* (2015) used HYDRUS-1D to investigate the effects of soil water dynamics, soil salinization, and groundwater salinity. In their research, simulated soil water contents (*SWC*) and electrical conductivities (*ECs*) of the soil solution were in good agreement with the observations.

Models, such as HYDRUS, generally require extensive calibration to confirm that water flow and solute transport and all boundary conditions of the simulated scenarios are suitably addressed by the model structure (Ramos *et al.*, 2019; Rasouli *et al.*, 2013). Accurate predictions of such models rely on the precise determination of soil hydraulic characteristics (Wang *et al.*, 2014) or their estimation using pedotransfer function models, such as ROSETTA (Schaap *et al.*, 2001). The unsaturated soil hydraulic properties are described in the HYDRUS-1D model using the van Genuchten-Mualem hydraulic relations (van Genuchten, 1980). Studies have indicated that the laboratory-measured soil hydraulic parameters, e.g., α, n, and l in the van Genuchten-Mualem functions, in combination with pedotransfer functions and inverse optimization algorithms, are effective in simulating soil water contents and salinities (Feddes *et al.*, 1988; Jacques *et al.*, 2002; Šimůnek *et al.*, 2013). The pedotransfer functions implemented in the ROSETTA module (Schaap *et al.*, 2001) of HYDRUS-1D use neural networks to predict soil hydraulic parameters from soil texture and related data. The ROSETTA module predicts the following soil hydraulic parameters: the residual water content (θ_r), the saturated water content (θ_r), the saturated hydraulic conductivity

(K_s), and the fitting parameters n and α of the van Genuchten-Mualem soil hydraulic model (van Genuchten, 1980).

In the previous chapter (Chapter 2), we presented experimental data for several locations in the SJV, including soil hydraulic properties, measured rootzone soil water contents and electrical conductivities, and summarized seasonal averages and maximum values of the root zone salinity. The maximum values guided us towards the most critical worst-case scenarios that could happen. Depending on this data, we could determine the best times for soil leaching or other management practices.

In this chapter, we aim to use the experimental data presented in the previous chapter i) to calibrate the HYDRUS-1D numerical model simulating transient rootzone deep percolation and plant water uptake, ii) to relate salt leaching fluxes and accumulated salt concentrations to soil properties and irrigation water criteria, and iii) to establish base simulations of rootzone salinity using HYDRUS-1D for two regions of SJV, CA. These base simulations will then be used in the next chapter (Chapter 4) to compare simulations of future scenarios for different availabilities of expected water resources and climate change circumstances in these two regions.

3.2. Methods

3.2.1. Simulated Sites

Five agricultural sites with five levels of salinity were analyzed in this study. The sites were selected by scientists of the US Salinity Laboratory in Riverside, CA. A detailed description of these sites is given in Chapter 2. The western sites were chosen because they were irrigated with highly saline groundwaters before this study was initiated due to a prolonged historic drought. The initial soil salinity at the selected sites was classified as relatively high (H), medium (M), and low (L), which is referred to by the first letter of each site identifier.

Table 3.1. Description of experimental sites.

Region of SJV, CA	Simulated Site Identifier	Crop	Mean Rain (cm/y)	Soil Type	Initial Salinity (dS/m)	Initial SAR $(mmol/L)^{0.5}$
East	LEA	Almonds	125 -200	Sandy Loam	Low (1.3-1.9)	10-25
West	HWA	Almonds	<50- 75	Clay loam	High (2.2-4.1)	7-25
West	MWA	Almonds	<50-75	Silty Clay Loam	Medium (1.8-3.5)	7-20
East	LEP	Pistachio	125 -200	Sandy Loam	Low (1.1-2.1)	3-10
West	HWP	Pistachio	<50-75	Silty Clay	High (2.3-4.7)	5-15

As shown in Table 3.1, three sites are on the west side of SJV (W), two of which have almonds (A) and one pistachio (P). Two sites are on the east side of SJV (E), one of which is cultivated with almonds (A) and the other with pistachios (P). Rainfall on the east side of SJV is higher than on the western side (Hoover *et al.*, 2015). Increased rainfall on the eastern sites of SJV, i.e., LEA and LEP (Table 3.1), is due to the sites' locations near the La Sierra Nevada rain and snowfalls. The Sierra Nevada mountains' rain and snow provide low saline surface waters for irrigation in the east SJV. The irrigation water salinity at the studied eastern sites LEA and LEP is about 0.04-0.24 $dS.m^{-1}$. Initial soil salinities, defined by the electrical conductivity of the soil saturated extracted solutions, are shown in Table 3.2.

3.2.2. Model Setup

Simulations of transient soil water flow and solute transport were performed using the HYDRUS-1D model (Šimůnek *et al.*, 2008, 2016)). The model solves the Richards equation numerically for water flow and the convection-dispersion equations (CDEs) for solute transport in variably-saturated porous media. The Richards equation (Richards, 1952) that controls variably saturated water flow is described as follows:

$$\frac{\partial \theta}{\partial t} = \frac{\partial}{\partial z}[K\,(\frac{\partial h}{\partial z} + cos\,\alpha)] - S \qquad (3.1)$$

where θ is the soil water content [$L^3.L^{-3}$] t is time [T], z is the vertical space coordinate [L] (positive upward), K is the hydraulic conductivity [$L.T^{-1}$], h is the pressure head [L], S is the sink term accounting for root water uptake [$L^3.L^{-3}T^{-1}$], and α is the angle between the flow direction and the vertical axis (i.e., α=0º for vertical flow, α=90º for horizontal flow, and 0º<α<90º for inclined flow). The volumetric flux q_w is calculated using Darcy's law:

$$q_w = -K\left(\frac{\partial h}{\partial z} + cos\ \alpha\right) \tag{3.2}$$

The unsaturated soil hydraulic properties are described using the following van Genuchten-Mualem hydraulic relations (van Genuchten, 1980):

$$\theta_w(h)\begin{cases} \theta_r + \frac{\theta_s-\theta_r}{[1+|\alpha h|^n]^m} & h < 0 \\ \theta_s & h \geq 0 \end{cases} \tag{3.3}$$

$$K(h) = \begin{vmatrix} K_s K_r(h) & h<0 \\ K_s & h\geq 0 \end{vmatrix} \tag{3.4}$$

$$K_r = S_e^{1/2}\left[1-\left(1-S_e^{1l/m}\right)\right]^2 S_e^{1/2}\left[1-\left(1-S_e^{l/m}\right)\right]^2 \tag{3.5}$$

$$m = 1 - {}^{1}/_{n}\ , \quad n > 1 \tag{3.6}$$

$$S_e = \frac{\theta_w-\theta_r}{\theta_s-\theta_r} \tag{3.7}$$

where θ_r and θ_s denote the residual and saturated water contents [$L^3.L^{-3}$], respectively, K_s is the saturated hydraulic conductivity [$L.T^{-1}$], K_r is the relative hydraulic conductivity [-], S_e is the effective water content [-], and a [L^{-1}], m [-], and n [-] are empirical parameters in the water retention function.

Initial and Boundary Conditions

We measured the initial rootzone soil solute concentrations and water contents at four depths (25, 50, 75, and 100 cm) in the root zone layers. Atmospheric and free drainage time-variable boundary conditions were used at the top and bottom of the soil profile, respectively. The atmospheric variable boundary condition was defined using precipitation, irrigation, and evapotranspiration fluxes as a function of time. Potential evapotranspiration fluxes were obtained from the CIMIS meteorological data. Irrigation depths were calculated for each studied orchard using emitter discharges [$M^3.T^{-1}$] and distances between emitters per drip line. Irrigation fluxes were estimated based on seasonal allocations of irrigation provided by the farm managers. Farmers' estimates of irrigation are adjusted to fulfill the potential evapotranspiration demands (ET_0) for almond and pistachio.

Irrigation water samples were collected at different times of the growing season. Five replications are presented for each site in Table 3.2, f. All measured irrigation water salinity values were used to identify the time-variable concentration boundary conditions. The measured rain concentrations were averaged as 0.001-0.01 $dS.m^{-1}$.

Rainfall was measured by the Eddy covariance instruments in each orchard that was used in the simulations of the rootzone salinity during the 2016-2019 years. Measured rain depths were compared with rainfall values provided by the California irrigation management and information system (CIMIS) weather stations adjacent to the simulated sites at the western and eastern SJV. The CIMIS-provided data showed few differences from the on-orchard measured data used in this study's simulations. In the SJV, seasonal rain events occur mainly from December to March (the winter season). An alternative annual pattern of wet and dry winter seasons was reported by the historical SJV seasonal rain patterns (CVP-OPAC, 1992). In this study, 2017 was a wet rain year, and 2018 was a dry rain year.

Table 3.2. Irrigation water salinity, sodicity, and ionic composition at five simulated sites.

Sites	Day of irrigation	ECiw ($dS.m^{-1}$)	SAR ($(mmol_c/L)^{0.5}$)	pH	Ca2+	Mg2+	Na+	K+ ($mmol_c.L^{-1}$)
LEP	3/30/2017	0.05	0.48	7.64	0.1	0.02	0.19	0.05
	3/30/2017	0.04	0.6	7.6	0.08	0.01	0.13	0.04
	7/5/2017	0.24		7.8	0.49	0.24	1.15	0.07
	5/17/2018	0.04		7.2	0.08	0.02	0.19	0.04
	8/2/2018	0.05		8.06	0.07	0.01	0.15	0.04
HWA	5/30/2017	0.3		7.78	0.32	0.32	1.29	0.17
	8/11/2017	0.24	1.4	7.14	0.35	0.35	1.54	0.09
	7/6/2018	0.43		7.6	1.04	0.51	2.24	0.1
	9/19/2018	0.54		6.95	0.31	0.29	1.09	0.07
	1/20/2019	0.79		7.8	1.1	1.16	4.76	0.19
MWA	5/30/2017	0.28	1.7	7.7	0.33	0.33	1.47	0.08
	5/17/2018	0.43		7.69	0.87	0.58	2.47	0.13
	7/6/2018	0.54	1.8	7.72	0.43	0.61	3.26	0.12
	7/6/2018	0.53	1.8	8	1.11	1.2	4.92	0.24
	9/19/2018	0.51		7.89	0.46	0.52	2.31	0.11
	1/5/2018	0.48		7.8	0.91	0.69	5.98	0.14
HWP	2/20/2018	0.44		7.57	0.52	0.59	2.86	0.16
	8/31/2018	0.89	4.1	7.72	0.51	0.56	2.54	0.12
	9/19/2018	0.48	3	7.93	0.44	0.57	3.03	0.11
	1/30/2019	0.9		7.77	1.22	0.74	5.89	0.09

Table 3.3. Growing seasons in SJV, CA, for almond and pistachio.

Crop	Growing Season in SJV, CA	Early Season	Late Season
Almond	February - August	February - March	July - August
Pistachio	April - September	April - May	August - September

The growing season in Table 3.3 is defined as the time of maximum tree evapotranspiration. Almond's growing season in SJV, CA, starts in mid-February, after a winter dormancy period in December and January (California Almond Board, 2018). We refer in our analysis to the months of February and March as an early growing season (Early). The time after

harvest in August is considered as a late season (Late). The blooming of pistachio trees starts after almonds. Early season time for pistachios is considered from mid-April and late-season time is September. We used the term "early" to discuss temporal changes of root zone salinity as affected by winter rains in the early part of the tree growing season. Salinity trends in the late part of the growing season are related to using irrigation waters of different qualities (Table 3.2) at various simulated Sites.

In the HYDRUS- 1D model, Leaf Area Index (*LAI*) or Surface Cover Fraction (*SCF*) of soil by plants are used to estimate potential evaporation (E_p) and potential transpiration (T_p) from potential evapotranspiration (ET_p) (Allen *et al.*, 1998; Šimůnek *et al.*, 2008; Raz-Yaseef *et al.*, 2012; Zheng *et al.*, 2017). The leaf area index values (*LAI*) and the crop coefficients (K_c) for the studied sites were obtained from the satellite data (SIMS – Satellite Irrigation Management Support) for the 2016 – 2018 years. The *LAI* values were used to estimate the soil cover fractions (*SCF*) by the canopy at the studied sites (Equation 3.9). The *SCF* was then used to divide potential evapotranspiration ET_p into potential evaporation (E_p) and potential transpiration (T_p) using equations (3.10) and (3.11), respectively:

$$ET_P = ET_0 * k_c \tag{3.8}$$

$$SCF = 1 - \exp(-r\ Extinct * LAI) \tag{3.9}$$

$$T_P = ET_P * SCF \tag{3.10}$$

$$E_P = ET_P * (1 - SCF) \tag{3.11}$$

where r_{Extent} is the radiation extinction coefficient (=0.463).

The HYDRUS-1D model relates root water uptake with the root density distribution. The spatial root distribution was determined from measured weights of almond (Figure 3.1) and pistachio (Figure 3.2) roots in six root zone soil layers.

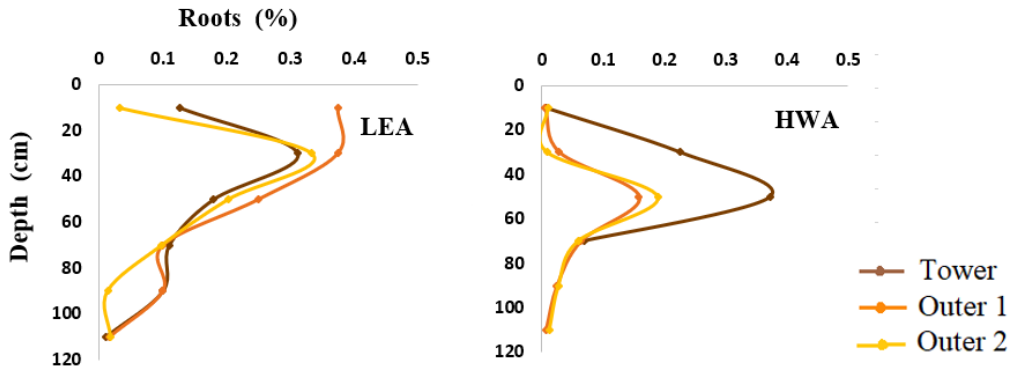

Figure 3.1. Measured spatial distribution of root densities of almond trees at the LEA (left) and HWA (right) sites.

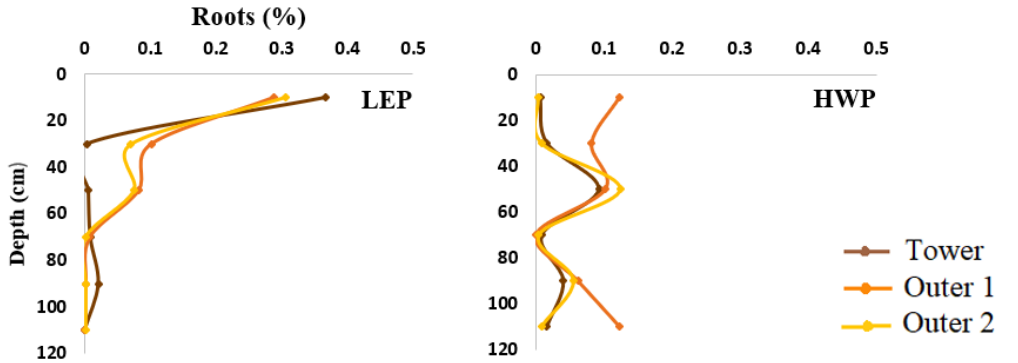

Figure 3.2. Measured spatial distribution of root density of pistachio trees at the LEP (left) and HWP (right) sites.

3.2.3. Model Calibration and Validation

The numerical model HYDRUS-1D was calibrated for the five experimental sites. Soil water contents and soil salinities at depths of 25, 50, 75, and 100 cm measured during the years of 2016-2018 (measurement methods are described in Chapter 2) were used in calibration. The model was validated using the third-year data sets from 2018-2019.

Table 3.4. The soil hydraulic parameters for four depths of five experimental sites.

Sites	*Depth* (cm)	θ_r ($cm^3.cm^{-3}$)	θ_s ($cm^3.cm^{-3}$)	α (cm^{-1})	n (-)	K_s ($cm.d^{-1}$)
LEA	25	0.039	0.395	0.020	1.477	29.18
	50	0.041	0.464	0.020	1.512	17.74
	75	0.047	0.404	0.014	1.478	21.82
	100	0.036	0.349	0.017	1.530	27.78
HWA	25	0.072	0.343	0.009	1.304	16.15
	50	0.098	0.433	0.002	1.705	5.60
	75	0.117	0.847	0.003	1.751	0.50
	100	0.116	0.935	0.003	1.655	2.05
MWA	25	0.098	0.503	0.014	1.386	19.79
	50	0.094	0.486	0.013	1.312	18.33
	75	0.092	0.490	0.010	1.484	20.57
	100	0.092	0.490	0.010	1.484	20.57
LEP	25	0.038	0.523	0.040	1.546	50.96
	50	0.111	0.210	0.024	1.260	30.44
	75	0.040	0.550	0.036	1.498	30.33
	100	0.035	0.376	0.041	1.520	13.81
HWP	25	0.101	0.480	0.016	1.328	21.85
	50	0.101	0.503	0.016	1.326	7.03
	75	0.099	0.494	0.015	1.353	7.03
	100	0.093	0.478	0.013	1.397	13.57

Soil Hydraulic Parameters

The HYDRUS-1D codes are physically based models and, as such, require little calibration when all necessary input parameters are experimentally determined. In this study, we measured the saturated soil water content (θ_s), the average field capacity (θ_{FC}) moisture content at 0.33 bar, percentages of sand, silt, and clay fractions, the soil bulk density, and the saturated hydraulic conductivity (K_s). The above-listed soil properties were measured for four layers of each simulated location. The ROSETTA (Schaap *et al.*, 2001) pedotransfer function software was used to predict soil hydraulic parameters θ_r, α, and n of the soil-water characteristics retention curve. We first used the measured and ROSETTA-estimated soil hydraulic parameters. We then applied the inverse

optimization of the soil hydraulic parameters implemented in the HYDRUS-1D model to adjust these parameters further. The soil hydraulic parameters for four depths of five experimental sites were calibrated (Table 3.4).

Root water uptake - Salinity stress reduction module

Root water uptake and yield reductions occur when salts accumulate in the root zone to the extent that the crop cannot extract enough water from the salty soil solution due to the osmotic (salt) and saturation stresses. The root water uptake (transpiration) reduction due to the salinity stress is computed in the HYDRUS-1D model using either the threshold and slope function (Mass, 1990) or the S-Shape function of van Genuchten (1987). In this research, the S-Shape root water uptake model (van Genuchten, 1987) is used to simulate the plant water uptake reduction due to salinity. The parameters of the root water uptake stress response function of the van Genuchten (1987) S-Shape function were obtained from the most recent reference values of the salinity reduction slope and threshold values for the studied varieties of almond (*Prunus duclis*) and pistachio (*Pistacia vera L.*).

Crop growth and yield do not respond to salinity until a salinity threshold is reached. Early studies found that almonds have a salinity threshold of 1.8 $dS.m^{-1}$ (e.g., Mass and Hoffman 1977; Mass 1993; Sanden and Ferguson 2004). In a more recent study in California, yield starts to decrease at 1.8 $dS.m^{-1}$, with a 50% yield reduction at much higher salinity of ECe = 4 $dS.m^{-1}$ (Sanden and Ferguson 2004, Figure. 3.3). For pistachios, early studies found that shoot growth of Pistachio (*P. vera*) is reduced at root zone salinity of 7.9 to 10 $dS.m^{-1}$ (Sepaskhah and Maftoun, 1988). The threshold value for the start of pistachio yield reduction was taken at 10 $dS.m^{-1}$ and the 50% reduction at 14-15 $dS.m^{-1}$ (Sanden and Ferguson 2004, Figure 3.3).

In the S-Shape model, the c_{50} coefficient (salinity at which the root water uptake reduction is 50%) is evaluated as follows:

$$c_{50} = 50/s + c_T \quad (3.12)$$

where c_T is the salinity threshold, and s is the slope of the yield reduction curve. The coefficients of the root water uptake reduction (c_{50}) for almonds and pistachios in this research are calculated as follows:

$$c_{50\ \text{Almond}} = 50/(19/2) + (1.5*2) = 8.263 \quad (3.13)$$

$$c_{50\ \text{Pistachio}} = 50/(10/2) + (5\text{-}6*2) = 20\text{-}22 \quad (3.14)$$

Conversion from the *EC* of the saturated extract (EC_e) to the *EC* of water (EC_w) is as follows: $EC_w \approx k_e * EC_e$, where k_e is approximately 2 (Skaggs *et al*., 2006). Consequently, almond and pistachio salinity threshold values were multiplied by the coefficient k_e (=2), and the slope values were divided by k_e (Equations 3.13 and 3.14).

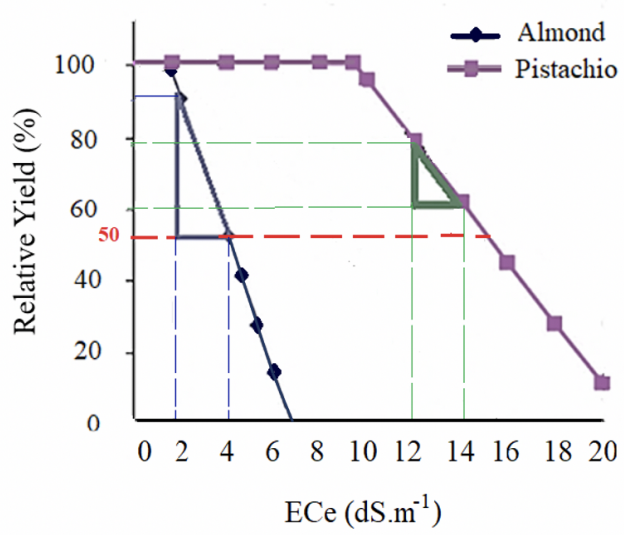

Figure 3.3. The salinity stress response functions for almonds and pistachios. A reduction of 50% due to salinity is indicated by a red line (Sanden and Ferguson, 2004).

3.3. Results and Discussion

3.3.1. Root Zone Soil Water Contents

Defining the salinity control parameters, e.g., soil salinity and salt leaching, requires information about water movement in the soils (Grismer, 2014). Root zone water contents and salinities were analyzed and compared at four sites of the east and west hydro-geological regions of SJV, CA. The sites LEA and LEP represent the east SJV, and the sites HWA and WHP represent the west SJV. The HYDRUS-1D simulated and measured soil water contents (SWCs) showed a good agreement and corresponded to the rain and irrigation fluxes and (Figure 3.4).

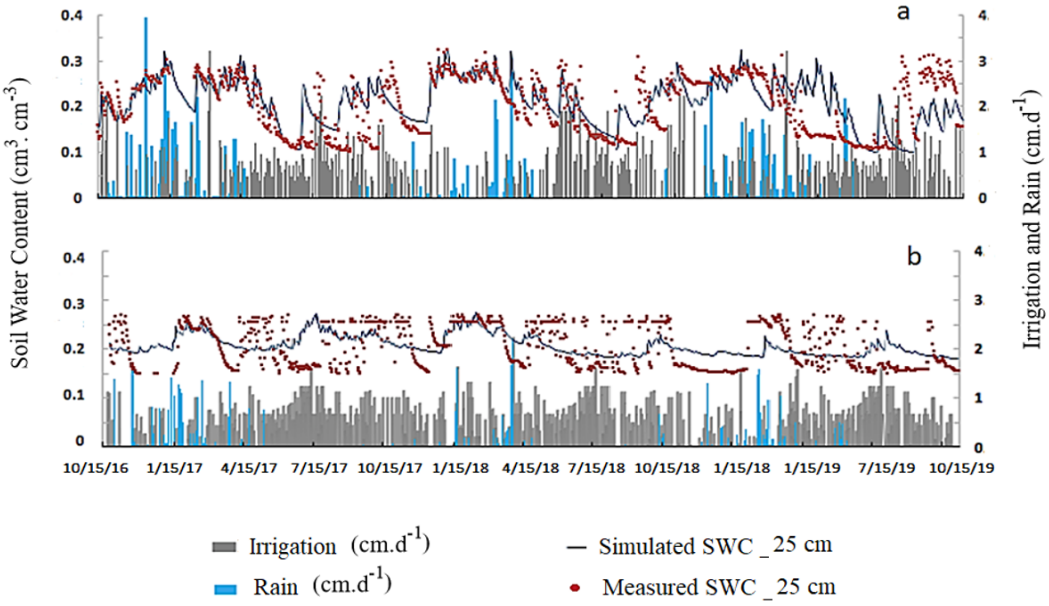

Figure 3.4. Effects of irrigation and rain on the measured and HYDRUS-1D simulated daily soil water contents at a depth of 25 cm at the LEA site, east SJV, CA (a), and the HWA site, west SJV, CA (b).

The effects of daily irrigation in spring and rains in winter on soil water contents in the top root zone of HWA and LEA are shown in Figure 3.4. The eastern scenario LEA (Figure 3.4a) showed an apparent increase in the simulated and measured SWCs during the irrigation season (April). The seasonal SWC trend shows high water contents during the growing season (Jan.-July) due to irrigation and low SWCs during summer with dry conditions. Daily fluctuations in summer were lower at the LEA site (the eastern SJV side) than at the HWA site (the western SJV side).

The western site HWA (see Figure 3.4b) had less abrupt seasonal SWC changes between winters and summers than the eastern LEA site (Figure 3.4a). In summer, the dry and wet events fluctuated more at the HWA site (Figure 3.4b). Contrary to that, at the LEA site (Figure 3.4a), a long-term stable trend of low SWCs was observed in summer. The HWA site had a higher soil clay percentage, initial salinity, and SAR than the LEA site (Table 3.1). The rain total was lower at the HWA site than at the LEA site. Due to these factors, the two regions had a different frequency of the topsoil's wetting and drying patterns.

At the eastern SJV hydro-geological site LEA, values of simulated and measured SWCs were highly correlated in all root zone depths from 25 to 100 cm, with a correlation coefficient of 0.91, 0.94, and 0.96 at depths of 25, 75, and 100 cm, respectively (Figure 3.4a, Figure 3.5). At the western hydro-geological site HWA (Figure 3.4b), the simulated and measured SWCs in the top 25 cm of the root zone were correlated in all seasons, in both wet and dry years of 2017 and 2018, respectively. Correlations between simulated and measured SWCs at other depths varied in different seasons (Appendix 3, Figure A3.12). Correlation coefficients of 0.99, 0.82, and 0.72 at depths of 50, 75, and 100 cm, respectively, were observed during the winter season. In spring, the highest correlations of 0.98 and 0.94 were obtained for deep root zone depths of 75 and 100 cm, respectively. The correlation coefficients for the topsoil layer (25 cm) were 0.62 and 0.6 cm during the spring and winter seasons, respectively.

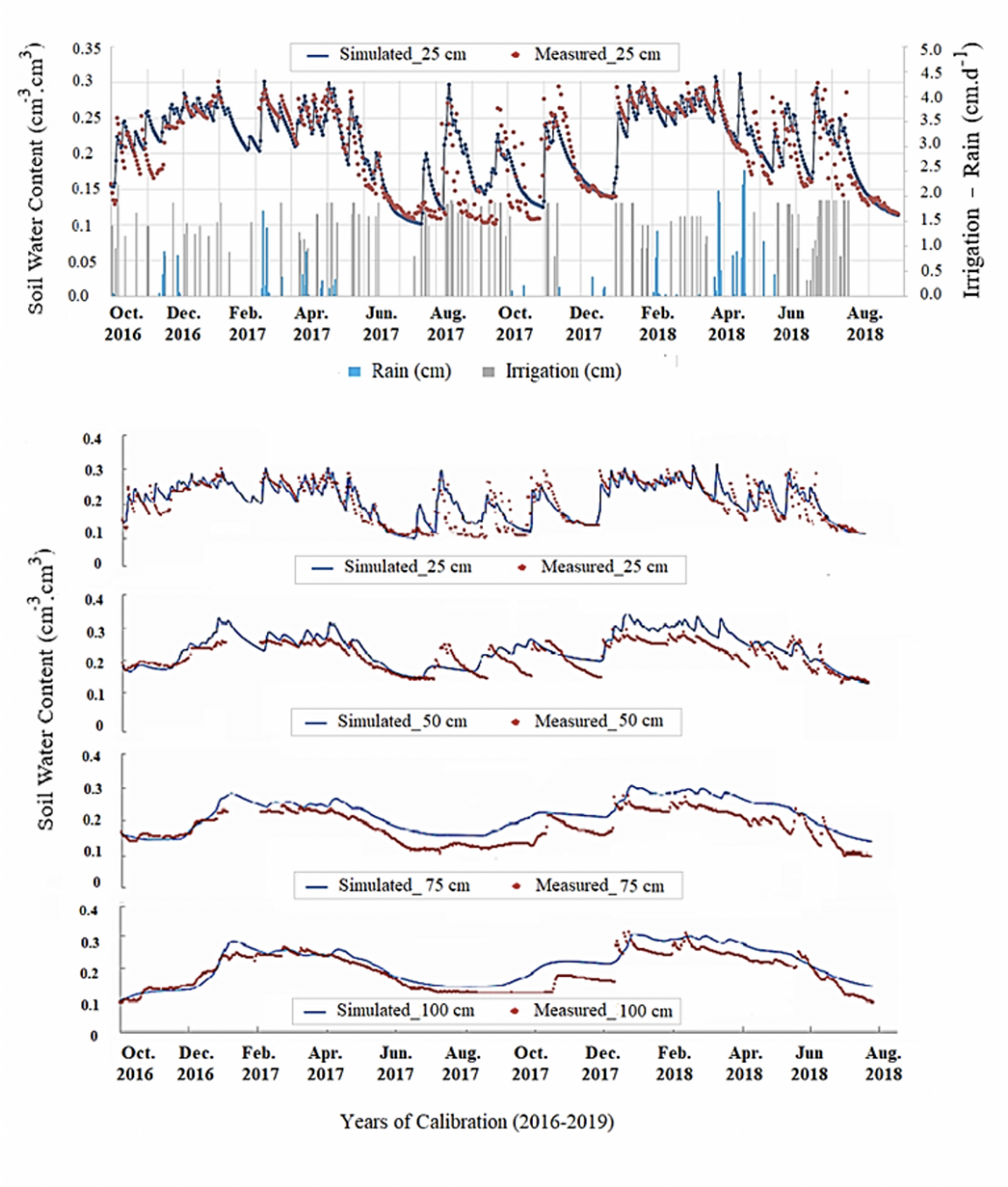

Figure 3.5. Measured (dots) and simulated (lines) soil water contents at four root zone depths of 25, 50, 75, and 100 cm at the LEA site in East SJV.

Calibration and validation of the simulated SWCs ($m^3.m^{-3}$) (presented as 20-d averages) at root zone depths of 25, 50, 75, and 100 cm for all five studied sites are presented in Appendix 3 (Figures A3.11-A3.15). The correlations between measured and simulated water contents were, for various reasons, less good at the other three sites than at the LEA and HWA sites. Saturation conditions hindered the fitting in deep layers at the MWA site (Figure A3.3). These observations in the deep layers reflect the properties of the third root zone layer (75 cm), which is a clogged semi-permeable dense clay with a measured saturated hydraulic conductivity of 0.5 cm/day.

The HWP site (Appendix 3, Figure A3.15) has a sodic clay soil, where physicochemical reactions cause slaking of soil aggregates and swelling and dispersion of clay minerals. This leads to a reduction in the soil hydraulic conductivity and a corresponding reduction in the infiltration of applied water and hence the yield. The highest Na concentration measurements were obtained for irrigation waters used at the MWA and HWP sites (Table 3.2). Additionally, the soils at the MWA and HWP sites have a fine texture and high initial soil solution SAR. The high SAR reduced the soil hydraulic conductivity at both sites (as described in Chapter 2). We relate the periods of different simulated and measured SWCs at the MWA and HWP sites (Appendix 3, Figures A3.13 and A3.15) to the previously discussed soil SAR effects on the soil hydraulic conductivity.

On the other hand, the calibration of the model at the LEP site (Appendix 3, Figure A3.14) showed an acceptable agreement between measured and simulated SWCs. Some overestimations occurred during the third year of data validation. The high saturated hydraulic conductivity of sandy layers above a depth of 50 cm, combined with deep, poorly drained duri-pan layers observed at depths of 70–80 cm, hindered the validation of HYDRUS-1D for the soil layers above 70 cm.

3.3.2. Root Zone Salinity

Measured and simulated rootzone salinities, i.e., soil water electrical conductivities, are discussed for the western and eastern SJV almond sites during two consecutive wet and dry years of 2017 and 2018, respectively.

Salinity increased during the irrigation season (from April to June) at the LEA site in the east SJV (Figure 3.6). During the dry year 2018, the soil water salinity reached 6-8 $dS.m^{-1}$ at depths of 50 and 100 cm, which is marginally higher than the tolerance threshold of almond (Figure 3.3). During the wet rainy year 2017, during the irrigation season (from April to June), the rootzone salinity decreased to an average of 2-3 $dS.m^{-1}$, which is less than half of what was observed in the dry year of 2018. The rain (from December to February) played a significant role in decreasing the root zone salinity to 2-4, 4-6, and 4-6 $dS.m^{-1}$ at depths of 25, 50, and 100 cm, respectively. The rain reduced the rootzone salinities during December and January in all root zone depths in both wet and dry years. The correspondence between simulated and measured rootzone salinities and SWCs indicates that HYDRUS-1D can be reliably used to predict future root zone salinity trends at the LEA site. Correlation coefficients between the measured and simulated salinities were significant at the LEA site in all wet and dry years.

Salinity increased considerably after the irrigation season (April-June) at the HWA site in the west SJV (Figure 3.7). Rainfall has a lower effect on reducing the root zone salinity at the HWA site, which has a relatively higher initial root zone salinity than at the LEA site.

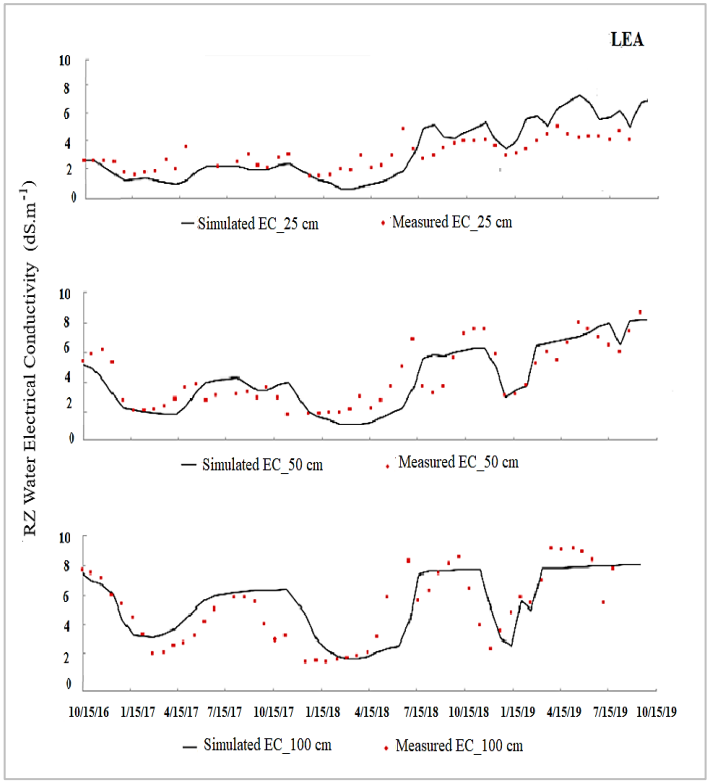

Figure 3.7. Measured (dots) and simulated (lines) salinities at three observation depths of 25, 50, and 100 cm at the LEA site, east SJV, CA

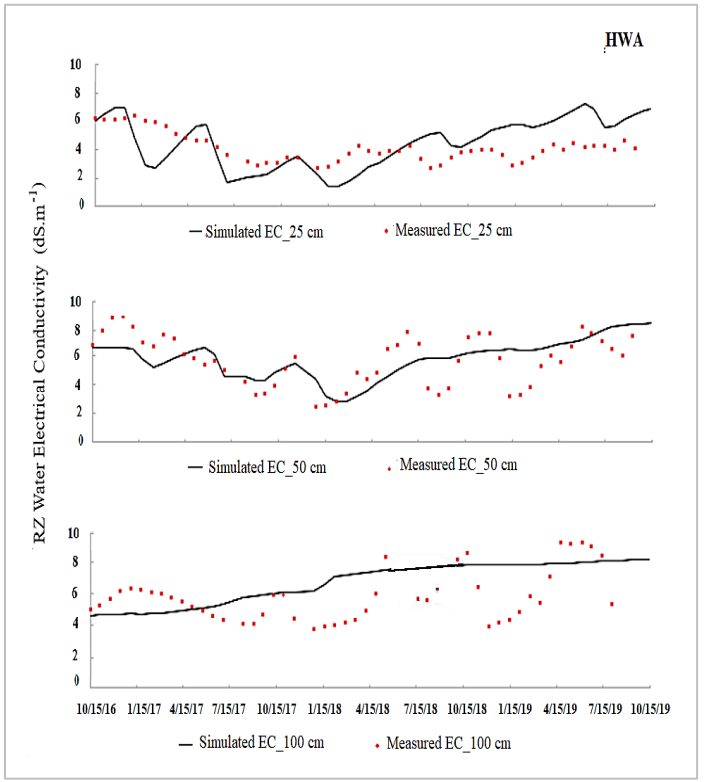

Figure 3.6. Measured (symbols) and simulated (lines) salinities at three observation depths of 25, 50, and 100 cm at the HWA site, west SJV, CA.

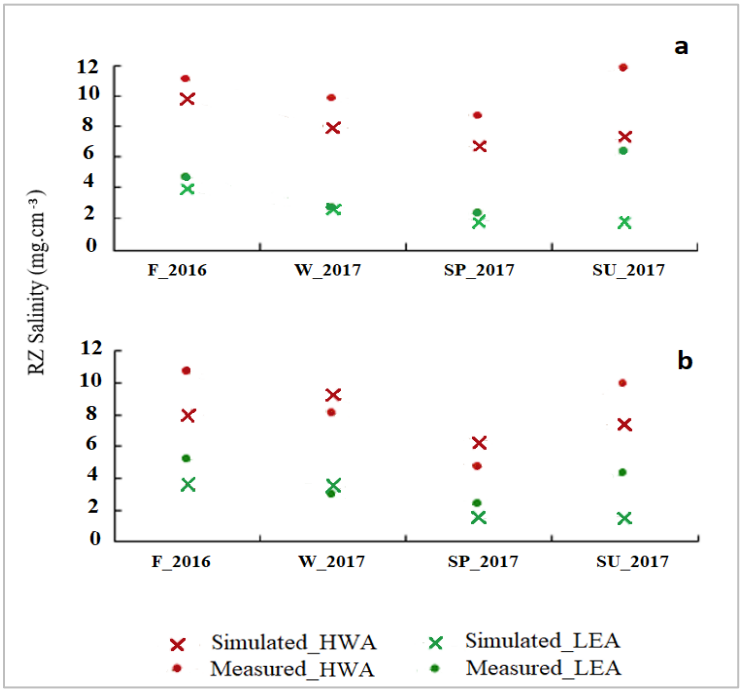

Figure 3.8. Seasonal (F- fall, W - winter, SP – spring, and SU – summer) simulated and measured root zone salinities at the low and high saline LEA and HWA sites, respectively, during the wet year 2017 (a), and the dry year 2018 (b).

Simulated and measured concentrations of root zone soil water were averaged over different seasons (spring, summer, fall, and winter), i.e., seasonal salinities in terms of electrical conductivities (*ECs*) were defined as:

$$EC_S = \frac{\sum Daily\ EC}{Number\ of\ days\ per\ season} \tag{3.15}$$

Simulated and measured data were then grouped for different regions (i.e., the eastern (LEA) and western (HWA) SJV regions) and various seasons (fall, winter, spring, and summer) during both the wet year 2017 (Figure 3.8a) and the dry year 2018 (Figure 3.8b). Initial salinity conditions controlled both irrigation and rain effects on increasing and reducing seasonal salinities.

The two data sets are very distinct. Salinities are mostly in the low range of 2-6 $dS.m^{-1}$ at the LEA site (green lines) and in the high range of 6-12 $dS.m^{-1}$ at the HWA site (orange lines). The

lower range of seasonal salinities in the eastern SJV reflects the effect of the relatively higher mean annual precipitation of 125-200 cm/y. On the other hand, in the western SJV, the higher range of seasonal salinities reflects high soil SAR (Table 3.1) and a mean annual rainfall of 50-75 cm/y, i.e., less than half of the mean yearly rains of the eastern region. Seasonal salinities were reduced in the middle of the winter seasons of both wet and dry years at both high and low salinity (HWA and LEA) sites. In the wet year, the rain effect was higher on reducing soil salinity than the impact of initial salinity.

Simulated and measured seasonal salinities were the highest in the fall and summer of both wet and dry years of 2017 and 2018, respectively. This increase in soil water salinity reflects the effect of applied irrigation water, in addition to the impacts of the initial soil salinity and SAR conditions. The salinity risk at the initially high saline HWA site due to irrigation practices is high. Soil reclamation and amendments to lower initial salinity levels at the beginning of the growing season would increase the efficiency of winter rains in reducing the root zone salinities and minimizing the risk of salinity during the irrigation season. At the LEA site, irrigation water caused only a small increase in seasonal salinities after winter rains and an acceptable salinity range. In summer, measured salinity was higher than simulated salinity, which could be related to the irrigation events and dry root zone conditions.

The *EC* measured by GS3 sensors depends on a specific range of soil water contents. When SWC is less than about 0.10 $m^3.m^{-3}$, the denominator in the pore water conductivity equation for water permittivity becomes very small, leading to significant potential errors (METER Group, 2019). Accordingly, that can lead to the overestimation of measured soil solution electrical conductivities. This would explain some too high measured values of salinities when SWC is lower than 0.10 $m^3.m^{-3}$.

The clogged layers at the HWP site and heterogeneous duri-pan layers at the LEP site, with low SWC measurements, prevented HYDRUS-1D to be successfully calibrated against salinities at deeper depths of these two sites. As a result, only the simulations of root zone salinities at the LEA and HWA sites will be used for further analysis.

3.3.3. Reduction of Root Water Uptake due to Salinity

The measured evapotranspiration fluxes (ET_a) were estimated from measured carbon dioxide and heat fluxes using Eddy covariance (installed as a part of the USSL project). The actual measured ET_a fluxes were compared with the actual evapotranspiration fluxes simulated using the HYDRUS-1D model (Figure 3.9). Simulated actual evapotranspiration (root water uptake + evaporation) showed a good agreement with the measured values of actual evapotranspiration (Figure 3.9).

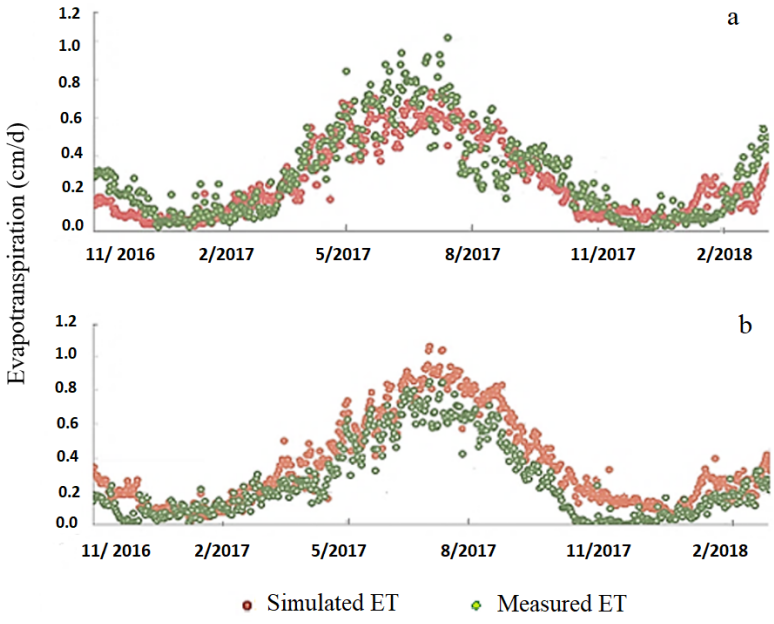

Figure 3.9. Simulated and measured actual evapotranspiration at two sites, HWA (top) and HWP (bottom), west SJV, CA.

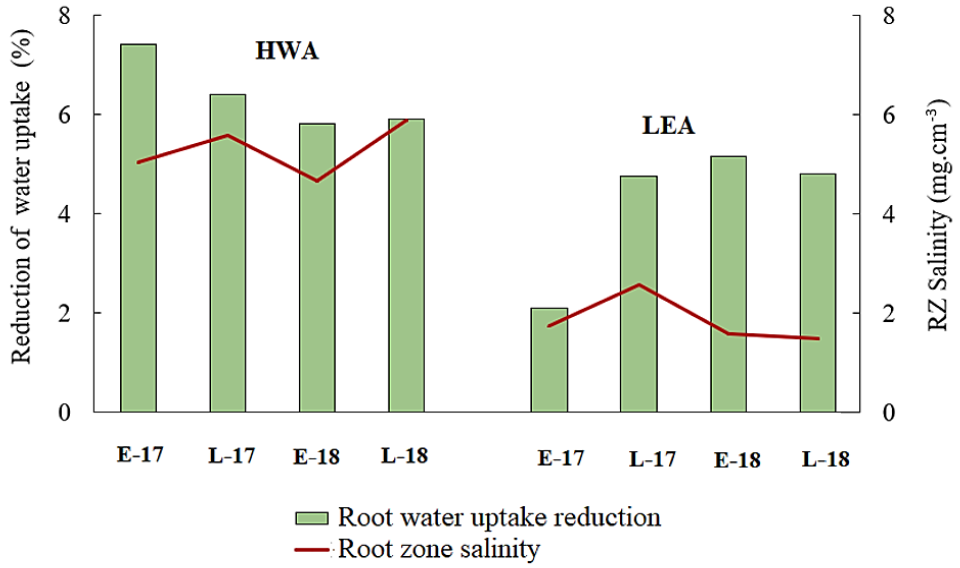

Figure 3.10. Simulated root zone salinities and corresponding reductions in tree water uptake at the HWA site (west SJV) and the LEA site (east SJV). "E" refers to the early time of the growing season (February-March period), and "L" refers to the late time of the growing season (July-August period).

The reduction of water uptake by trees (T_r reduction) due to the salinity stress was estimated as follows:

$$T_{r\ reduction} = 1 - \frac{Actual\ root\ water\ uptake/season}{Potential\ root\ water\ uptake/season} \tag{3.16}$$

The reduction in HYDRUS-1D-simulated actual transpiration fluxes (i.e., root water uptake) were related to root zone salinities in Figure 3.10 for different parts of the growing season. In SJV, CA, the almonds growing season starts after a winter dormancy in January and ends in August. The growing season of pistachios begins in late March and ends in September (Table 3.3). We analyzed the effects of simulated root zone salinities on the water uptake reduction in the west and east of SJV by comparing the HWA and LEA sites, respectively. The comparison was during two periods, the early time of the growing season ("E") and the late time of the growing season ("L").

The analysis includes the wet year 2017, followed by the dry year 2018. The seasonal deficit in crop growth is assumed to be related to the reduction of root water uptake (tree transpiration) due to the salinity stress.

The early time of the growing seasons ("E"), which refers to the February-March period, is when soil salinity reflects the impact of winter rains. The effect of precipitation in the early season in both east and west SJV is shown in Figure 3.10. The initially measured soil salinity at the HWA site in the west SJV is relatively high. The salts accumulated from previous seasons interacted reversely with the rain during the early season of the wet year 2017. As shown for the HWA site for E-17 (an early season of 2017), the initial high salinity causes a relatively high reduction in root water uptake (over 5%). On the other hand, the effect of rains during the early time of the wet year 2017 (E-17) was not noticeable until the second year (E-18), in which the impact of rain during a prior wet year and leaching practices reduced the soil water salinity.

The rain effect was more immediate at the LEA site in the east SJV. The measured initial root zone soil salinity at the LEA site is relatively lower than at the HWA site. Accordingly, at the LEA site, the reduction in root water uptake was the lowest in the wet year (E-17) and increased in the dry year (E-18). There was a significant impact of rain in both dry and wet years when the initial soil salinity was lower, and irrigation with less saline water was used.

The late time of the growing seasons ("L") is when soil salinity reflects the impact of irrigation after the end of the growing and irrigation season. The effect of irrigation was higher at the HWA site (with initial high salinity) than at the LEA site (with initial low salinity). At the HWA site, root zone soil's water salinity in the late-season increased during both wet and dry years (i.e., L-17 and L-18, respectively). At the LEA site, the root zone soil's water salinity increased only in the wet year (L-17) but decreased in the dry year (L-18). The degree of increase or decrease of root

zone salinity did not show any significant effect on the root water uptake reduction in both years at the LEA site (with initial low salinity). We relate the reduction in root zone salinity during L-18 at the LEA site to the leaching practice, in which leaching successfully maintained root water uptake during both dry (i.e., L-18) and wet (i.e., L-17) years.

The HWA and LEA sites are commercial orchards where current root zone salinities are mostly below the almond and pistachio salinity threshold values (discussed in Section 3.2.2). The maximum reduction of potential water uptake (7%) occurred at the (initially saline) HWA site. This simulated high reduction of root water uptake reflects the effects of continued irrigations with highly saline water in the west SJV. The reduction of water uptake at the LEA site was lowest (2.5%), in response to both low initial soil salinity conditions and the wet year (LEA, E-17). In conclusion, the minimum reduction of root water uptake occurred during the wet year 2017 at the site with low root zone salinity at the beginning of the growing season.

3.3.4. The Effect of Salinity Leaching on Root Water Uptake

The leaching fraction indicates the degree to which salts are leached from the root zone (US Salinity Laboratory Staff 1954). The leaching efficiency of micro-irrigation can be expressed as the ratio of salt reduction to the equivalent leaching depth (Burt and Isbell 2005).

The leaching fraction is defined as a fraction of applied irrigation and precipitation that drains beyond the root zone (Corwin and Grattan, 2018). Fractions of water leached below the root zone were estimated from the applied and drained water fluxes using the simulated top and bottom cumulative water fluxes. Leaching fractions showed a similar increase spike at all sites during winter (Dec. 2016 and Dec. 2017), when the uptake reductions decrease at all sites accordingly.

Table 3.5. Pearson correlation between a reduction of root water uptake and leaching fractions.

HWA, West SJV, CA.				LEA, East SJV, CA.			
Wet 2017		**Dry 2018**		**Wet 2017**		**Dry 2018**	
Early	Late	Early	Late	Early	Late	Early	Late
-.912**	0.236	0.236	.955**	.419**	-.949**	-.933**	-.436**

** Correlation is significant at the 0.01 level (2-tailed).

* Correlation is significant at the 0.05 level (2-tailed).

Most values in the table above showed a significant negative correlation between leaching fractions (which have a positive effect on reducing root zone salinity) and water uptake reduction. Negative correlations (Table 3.5) indicate that the lower the leaching fraction is, the higher the water uptake reduction is. For example, at the HWA site in the west SJV, a significant negative correlation (-91%) between the leaching fraction and root water uptake reduction was achieved, which means that decreased leaching at the early time of 2017 was correlated with an increase in root water uptake reduction. Also, at the LEA site in the eastern SJV, root water uptake reduction was always negatively associated with the leaching fraction (-95%, -93%, and -45%) except for the early time of the wet year 2017. This explains higher leaching at the eastern side with lower water uptake reduction in all (three) seasons, except in early 2017.

When leaching fractions showed a low positive correlation with root water uptake reduction (i.e., 23% at the HWA site and 0.41% at the LEA site, Table 3.3), then an increase in leaching was positively correlated with an increase in water uptake reductions. This increase in water uptake reduction is more closely correlated with the effect of the saline irrigation water use in prior years than with the rain year type (and thus leaching) during the measurement time.

3.4. Conclusions

The HYDRUS-1D simulations of the LEA and HWA sites were used to compare the effects of two different irrigation waters, initial soil water salinities, and regional mean rainfalls in the east and west regions of SJV, CA. The calibration and validation of the HYDRUS-1D model were conducted using measured soil water contents and electrical conductivities.

Root zone water leaching and root water uptake were estimated for the four sites HWA, LEA, HWP, and LEP. Soil salinity concentrations in different root zone depths were simulated for the LEA and HWA sites. The HWP and LEP sites were successfully analyzed only in terms of root zone water contents and root water uptake.

The reduction in root water uptake due to salinity and saturation stresses was simulated using the S-shape stress response functions in HYDRUS-1D. Simulated actual evapotranspiration (*ET*) showed a good agreement with on-site eddy covariance measurements of actual *ET*. The minimum root water uptake reduction was obtained during the wet year 2017 at the site with low root zone salinity at the beginning of the growing season (i.e., at the LEA site). The simulated water uptake reduction was highly negatively correlated with the leaching fraction. The more water drained (and salts leached), the less root water uptake was reduced.

The effect of precipitation on soil salinity was discussed for 'early times of the growing season' when rain is the dominant factor for soil salinity and 'late times of the growing season' when the irrigation water salinity is the dominant factor. Simulated higher leaching fractions showed higher root water uptake reductions in late seasons than in early seasons (Figure 3.10). The root water uptake reduction at the HWA site during the early season was mainly caused by salinity accumulated during prior seasons and not leached with adequate water amounts. Securing low salinity at the beginning of the growing season (either by winter rains or additional irrigation) is

crucial for minimizing the risk of substantial crop water uptake reductions due to the potential high salinity of irrigation water.

The good correspondence between simulated and measured rootzone salinities and SWCs obtained in this study indicates that we can use HYDRUS-1D to predict future root zone salinity trends at the LEA and HWA sites. The soil type is an important key factor for increasing root water uptake, decreasing soil salinity, optimizing leaching, and reducing the risk of groundwater salinization due to leaching.

3.5. References

Ahuja, L.R., DeCoursey, D.G., Barnes, B.B., and Rojas, K.W., 1993. Characterization of macropore transport studied with the ARS. Root Zone Water Quality Model. *Trans. ASAE,* 36 (2), 369-380.

Allen, R.G., Pereira, L., Raes, D., and Smith, M., 1998. Crop evapotranspiration-Guidelines for computing crop water requirements- FAO Irrigation and Drainage paper 56. FAO – Food and Agriculture Organization of the United Nations, Rome.

Burt, C.M., and Ishell, B., 2005. Leaching of accumulated soil salinity under drip irrigation. *Trans. ASAE,* 48, 2115 -2121.

California Almond Board, 2018, Annual report ALMOND ALMANAC. https://www.almonds.com/sites/default/files/Almanac%202018.pdf.

CIMIS, California Irrigation Management, and Irrigation System. Data of 2016-2018.

Corwin, D.L., Grattan, S.R., 2018. Are existing irrigation salinity requirements guidelines overly conservative or obsolete? J. Irrig. Drain. Engr. 144 (8), 02518001.

Corwin, D.L., Rhoades, J.D., Šimůnek, J., 2007. Leaching requirements for soil salinity control: steady state versus transient models. *Agric. Water Manage.* 90, 165–180.

Cullen, B., Johnson, I., Eckard, R., Lodge, G., Walker, R., Rawnsley, R., and McCaskill, M., 2009. Climate change effects on pasture systems in south-eastern Australia. *Crop Pasture Sci., 60* (10), 933–942.

CVP-OCAP, 1992. Long-Term Central Valley Project Operations Criteria and Plan, 1992. US Department of the Interior Bureau of Reclamation, Mid-Pacific Region, Sacramento, CA. Water Resources Center Archives, UC Berkeley.

Decagon team, 2016. Operator manual of GS3 sensors for measuring soil water content, electrical conductivity, and temperature. Decagon Devices, Inc., Version: March 11, 2016.

Dellavalle, NB, 1992. Determination of soil-paste pH and conductivity of saturation extract. In Handbook on Reference Methods for Soil Analysis. Pp. 40-43. *Soil and Plant Analysis Council, Inc., Athens*, GA.

Feddes, R. A., Bresler, E., and Neuman, S.P., 1974. Field test of a modified numerical model for water uptake by root systems, Water Resour. Res., 10(6), 1199-1206, 1974.

Feddes, R.A., Kabat, P., Van Bakel, P.J.T., Bronswijk, J.J.B., Halbertsma J., 1988. Modeling soil water dynamics in the unsaturated zone — State of the art. *J. of Hydrology*, vol. 100 (1–3): 69-111.

Feddes, R.A., Raats, P.A.C., 2004. Parameterizing the soil–water–plant–the root system. In: In Feddes, RA, de Rooij, GH, van Dam, J.C. (Eds.), Proceedings of the Unsaturated Zone Modelling: Progress, Challenges and Applications, vol. 6. Kluwer Academic Publishers, Dordrecht, The Netherlands, pp. 95–141 Wageningen UR Frontis Series.

Gardner, W.K., Fawcett, R.G., Steed, G.R., Pratley, J.E., Whitfield, D.M., Rees, H., and Van, R.H., 1992. Crop production on duplex soils in south-eastern Australia. *Australian J. of Experimental Agriculture 32(7):915-927*.

Gartley, K.L., 2011. Ch10: Recommended Methods for Measuring Soluble Salts in Soils. Recommended Soil Testing Procedures book for the Northeastern United States Last Revised 5/2011.

Gerke, H.H., 2006. Preferential flow descriptions for structured soils. *Journal of Plant Nutrition and Soil Science* **169**, 382-400.

Gigante, V., Iacobellis, V., Manfreda, S., Milella, P., and Portoghese, I., 2009. Influences of leaf area index estimations on water balance modeling in a Mediterranean semi-arid basin. *Natural Hazards and Earth System Science*, *9*(3), 979–991.

Gonçalves, M.C., Martins, J.C., Prazeres, A., Castanheira, N.L., Pereira, L.S., Ramos, T.B., and Šimůnek, J., 2011. Field evaluation of a multicomponent solute transport model in soils irrigated with saline waters, *J. of Hydrology* 407, 129–144.

Gonçalves, M.C., Šimůnek, J., Ramos, T.B., Martins, J.C., Neves, M.J., Pires, F.P., 2006. Multi-component solute transport in soil lysimeters irrigated with waters of different quality. *Water Resour. Res.*, 42, 1–17.

Greco, R., 2002. Preferential flow in macroporous swelling soil with internal catchment: model development and applications. *J. of Hydrology*, 269, 3–4.

Green, T.R., Ahuja, L.R., and Benjamin, J.G., 2003. Advances and challenges in predicting agricultural management effects on soil hydraulic properties. *Geoderma,* 116, 3-27.

Grismer, M. E., 2014. Leaching fraction, soil salinity, and drainage efficiency. *California Agriculture*, 44: (6).

Hadi, M., 2011. Effect of antecedent soil moisture on infiltration and preferential flow in texture contrast soils. Ph.D. thesis, School of Agricultural Science. The University of Tasmania, Australia.

Haj-Amor, Z., Ibrahimi, M.K., Feki, N., Lhomme, J.P., and Bouri, S., 2016. Soil salinization and irrigation management of date palms in a Saharan environment. *Environmental Monitoring and Assessment*, *188*(8), p. 497.

Hanneman, R.A., Kposowa, A.J., and Riddle, M.D., 2013. Basic Statistics for Social Research.1st edition, Jossy-Bass, a Wiley Imprint, San Francisco, USA.

Hardie, B. M., 2011. Effect of antecedent soil moisture on infiltration and preferential flow in texture contrast soils, Ph.D. thesis, School of Agricultural Science. The University of Tasmania.

Hilhorst, M.A., 2000.A pore water conductivity sensor. *Soil Science Society of America Journal*, 64(6), 1922-1925.

Hoffman, G.J., 2010. Salt Tolerance of Crops in the Southern Sacramento-San Joaquin Delta Final Report. California Environmental Protection Agency State Water Resources Control Board Division of Water Rights. *Hydrology and Hydromechanics*, 50, 3-19.

Hoover, D. J., K. O. Odigie, P. W. Swarzenski, and P. Barnard, 2015. Sea-level rise and coastal groundwater inundation and shoaling at select sites in California, USA. *Journal of Hydrology: Regional Studies*, *11* , 234–249.

Jacques, D., Šimůnek, J., Timmerman, A., and Feyen, J., 2002. Calibration of Richards' and convection–dispersion equations to field-scale water flow and solute transport under rainfall conditions. *J. of Hydrology*, *259* (1), 15-31.

Kaledhonkar, M.J., and Keshari, A.K., 2006. Modeling the effects of saline water use in agriculture. *J. of Irrig.and Drain.*, 55, 177 -190.

Kaledhonkar, M.J., Sharma, D.R., Tyagi, NK, Ashwani, K., Van Der Zee, SEATM, 2012. Modeling for conjunctive use irrigation planning in sodic groundwater areas. *Agricultural Water Management, 107, 14 -22.*

Katerji, N., van Hoorn, J.W., Hamdy, A., Mastrorilli, M., 2000. Salt tolerance classification of crops according to soil salinity and to water stress day index. Agric. Water Manage.

Kumar, R., Shankar, V., and Jat, MK, 2015. Evaluation of root water uptake models – a review, *ISH Journal of Hydraulic Engineering,* 21 (2), 115-124.

Larsbo, M., and Jarvis N., 2005. Simulating solute transport in a structured field soil: Uncertainty in parameter identification and predictions. *Journal of Environmental Quality*, 34, 621-634.

Letey, J., Hoffman, G.J., Hopmans, J.W., Grattan, S.R., Suarez, D., Corwin, D.L., Oster, J.D., Wu, L., Amrhein, C., 2011. Evaluation of soil salinity leaching requirement guidelines. Agric. Water Manage., 98 (4), 502–506.

Li, H., Yi, J., Zhang, J., Zhao, Y., Si, B., Hill, R. L., Cui, L., and Liu, X., 2015. Modeling of soil water and salt dynamics and its effects on root water uptake in Heihe arid wetland, Gansu, China. *Water (Switzerland)*, *7* (5), 2382–2401.

Li, X., Kang, Y., Wan, S., Chen, X., Liu, S., and Xu, J., 2016. Response of a salt-sensitive plant to processes of soil reclamation in two saline-sodic, coastal soils using drip irrigation with saline water. *Agricultural Water Management*, *164*, 223–234.

Lobell, D.B., and Marshall, B.B., 2010. On the use of statistical models to predict crop yield responses to climate change. J. of Agricultural and Forest Meteorology, 150, 1443 – 1452.

Mass, EV, 1990. Crop salt tolerance. In: Tanji, K.K. (Ed.), Agricultural Salinity Assessment, and Management. Manual Eng. Pract., vol. 71. Am. Soc. of Civ. Eng., Reston, VA, pp. 262–304.

Minhas, P.S., Ramos, T.B., Ben-Gal, A., and Pereira, L.S., 2020. Coping with salinity in irrigated agriculture: Crop evapotranspiration and water management issues. *Agricultural Water Management*, *227*.

METER Group, 2019. GS3 soil water permittivity, electrical conductivity, and temperature sensors user manual. METER Group, Inc. USA 2365 NE Hopkins Court Pullman, WA 99163. http://library.metergroup.com/Manuals/20429_GS3_Web.pdf.

Novak, V., Šimůnek, J., van Genuchten, M.Th., 2002. Infiltration of water into soil with cracks. *Journal of Irrigation and Drainage Engineering* 126, 41-47.

Oster, J., Wu, L., Ayars, J., Letey, J., Vaughan, P., French, C., and Qadir, M., 2010. Comparison of models that include salinity and matric stress effects on plant growth. 19th World Congress of Soil Science, Soil Solutions for a Changing World 1 – 6 August 2010, Brisbane, Australia.

Pearson, C.J., David, W., Norman, J., Dixon, 1995. Sustainable Dryland Cropping in relation to Soil Productivity. Food and Agriculture Organization of the United Nations.

Philip, J.R., 1968. The theory of absorption in aggregated media. *Australian Journal of Soil Research* 6 (1): 1 – 19.

Phogat, V., Cox, J.W., and Šimůnek, J., 2018. Identifying the future water and salinity risks to irrigated viticulture in the Murray-Darling Basin, South Australia. *Agricultural Water Management*, *201*, 107–117.

Phogat, V., Mallants, D., Cox, J.W., Šimůnek, J., Oliver, D.P., and Awad, J., 2020. Management of soil salinity associated with irrigation of protected crops. *Agricultural Water Management*, 227.

Ramos, T.B., Darouich, H., Šimůnek, J., Gonçalves, M.C., Martins, J.C., 2019. Soil salinization in very high-density olive orchards grown in southern Portugal: Current risks and possible trends. *Agric. Water Manage*. 217, 265–281.

Rasouli, F., Pouya, A.K., Šimůnek, J., 2013. Modeling the effects of saline water use in wheat-cultivated lands using the UNSATCHEM model. *Irrig. Sci*. 31, 1009–1024.

Rassam, D., Šimůnek, J., Mallants, D., and van Genuchten, M.Th., 2018. The HYDRUS-1D Software Package for Simulating the one- Dimensional Movement of Water, Heat, and Multiple Solutes in Variably Saturated Media: Tutorial. Version 1.00, *Land, and Water. CSIRO*.

Raz-Yaseef, N., Yakir, D., Schiller, G., and S., Cohen, S., 2012. Dynamics of evapotranspiration partitioning in a semi-arid forest as affected by temporal rainfall patterns, *Agricultural and Forest Meteorology*. 157, 77-85.

Reeuwijk, L, van, P., 2000. Procedures for Soil Analysis. 6TH edition. -Technical Paper/International Soil Reference and Information Centre, Wageningen, The Netherlands.

Sanden, B., Ferguson, L., and Kallsen, C., 2014. Development of Pistachios with Saline Irrigation Water and Regional Salt Tolerance in Pistachio Production Fields. Agricultural and Natural Resources, University of California.

Sanden, B.L., Ferguson, L., Reyes, H.C., and Grattan, S.C., 2004. Effect of Salinity on Evaporation and yield of San Joaquin Valley Pistachios. Proceedings of IVth International Symposium on Irrigation of Horticultural Crops, *Acta Horticulturae*, 664, 583 – 589.

Schaap, M.G., Leij, F.J., and van Genuchten, M.Th., 2001. Rosetta: A computer program for estimating soil hydraulic parameters with hierarchical pedotransfer functions. *J. Hydrol. (Amsterdam)*, 251, 163– 176.

Schoups, G., Hopmans, J.W., Young, C.A., Vrugt, J.A., Wallender, W.W., Tanji, K.K., and Panday, S., 2005. Sustainability of irrigated agriculture in the San Joaquin Valley, *California*, *102*(43).

Scudiero, E., Skaggs, T.H., Corwin, D.L., 2014. Regional-scale soil salinity assessment using Landsat ETM + canopy reflectance. Remote Sensing of Environment, 169, 335- 343.

Sepaskhah, A.R., and Maftoun, M., 1988. Relative salt tolerance of pistachio cultivars. J. Hort. Sci. 1988, 63 (1), 157–162.

Sepaskhah, A.R., Maftoun, M., and Karimian, N., 1985. Growth and chemical composition of pistachio as affected by salinity and applied iron. J. Hort. Sci. 1985, 60 (1), 115–121.

Shrivastava, P, Kumar, R, 2015. Soil salinity: a serious environmental issue and plant growth-promoting bacteria as one of the tools for its alleviation. Saudi J Biol Sci 22:123–131.

SIMIS, data of 2016-2018. Satellite Irrigation Management Support for monitoring, modeling, and forecast, USA.

Šimůnek, J., Šejna, M., Saito, H., Sakai, M., and van Genuchten, M.Th., 2008. The HYDRUS-1D software package for simulating the one-dimensional movement of water, heat, and multiple solutes in variably saturated media version 4.0. Department of Environmental Sciences, University of California Riverside, California.

Šimůnek, J., Šejna, M., Saito, H., Sakai, M., van Genuchten, M.Th., 2013. The HYDRUS-1D Software Package for Simulating the Movement of Water, Heat, and Multiple Solutes in Variably Saturated Media, Version 4.17, HYDRUS Software Series 3. Department of Environmental Sciences, University of California Riverside, Riverside, California, USA.

Šimůnek, J., van Genuchten, M.Th., Šejna, M., 2016. Recent Developments and Applications of the HYDRUS Computer Software Packages. *Vadose Zone Journal* 15, 7.

Skaggs, T. H., Shouse, P. J., and Poss, J. A., 2006. Irrigating Forage Crops with Saline Waters. 2. Modeling Root Uptake and Drainage, *Vadose Zone J.,* 5, 824-837.

Smith, K.A. (1991). Soil Analysis, modern Instrumental Techniques, New York, NT, 10016.

Snyder, R., Geng, S., Orange, M, and Sarreshteh, S., 2012. Calculation and Simulation of Evapotranspiration of Applied Water. *J. Integrative Agriculture*, 11(3), 489–501.

Suarez, D.L., 2012. Modeling transient root zone salinity (SWS Model). In: W.W. Wallender and KK.

Suarez, D.L., Wood, J.D., Lesch, S.M., 2006. Effect of SAR on water infiltration under a sequential rain–irrigation management system. Agric. Water Manage. 86, 150–164.

Taylor, S.A., and Ashcroft, G.M., 1972. Physical Edaphology. Freeman and Co., San Francisco, California, p. 434-435.

US Salinity Laboratory Staff, 1954. Diagnosis and Improvement of Saline and Alkaline Soils, USDA Handbook 60, Washington, U.S.A.

van Genuchten, M.Th., 1978. Mass transport in saturated-unsaturated media: one-dimensional solutions, *Research Rep. No. 78-WR-11*, Water Resources Program, Princeton Univ., Princeton, NJ.

van Genuchten, M.Th., 1980. A closed-form equation for predicting the hydraulic conductivity of unsaturated soils. *Soil Sci. Soc. Am. J.* 44, 892–898.

van Genuchten, M.Th., 1987. A numerical model for water and solute movement in and below the root zone, Unpublished Research Report, US Salinity Laboratory, USDA, ARS, Riverside, CA.

Wang, J., Bai, Z., Yang, P., 2014. Mechanism and numerical simulation of multi-component solute transport in sodic soils reclaimed by calcium sulfate. Environ. Earth Sci. 72, 157–169.

Wesseling, J.G., Elbers, J.A., Kabat, P., and Van den Broek, B.J., 1991. SWATRE: instructions for input, Internal Note, Winand Staring Centre, Wageningen, the Netherlands.

Willigen and Van Noordwijk. 1987. Roots. Plant production and nutrient use efficiency. Wageningen, Netherlands. ISN 312978.

Zeng, W., Xu, C., Wu, J., Huang, J., 2014. Soil salt leaching under different irrigation regimes: HYDRUS-1D modeling and analysis. Journal of Arid Land 6, 44–58.

Yang, T., Šimůnek, J., Mo, M., Mccullough-Sanden, B., Shahrokhnia, H., Cherchian, S., and Wu L., 2019. Assessing salinity leaching efficiency in three soils by the HYDRUS-1D and -2D simulations. *Soil and Tillage Research*, 194, 104342.

Zheng, C., Yudong, L., Xiaohua, G., Huanhuan, L., Jiamei, S., and Xiuhua, L., 2017. Application of HYDRUS 1D model for research on irrigation infiltration characteristics in the arid oasis of Northwest China. Environ Earth Sci., 76: 785.

Appendix 3. Water Content Calibration Graphs

Calibration and validation of the simulated SWCs ($m^3.m^{-3}$) (presented as 20-d averages) are presented below in Figures A3.11-A3.15. The first two years were used for calibration and the third year for validation.

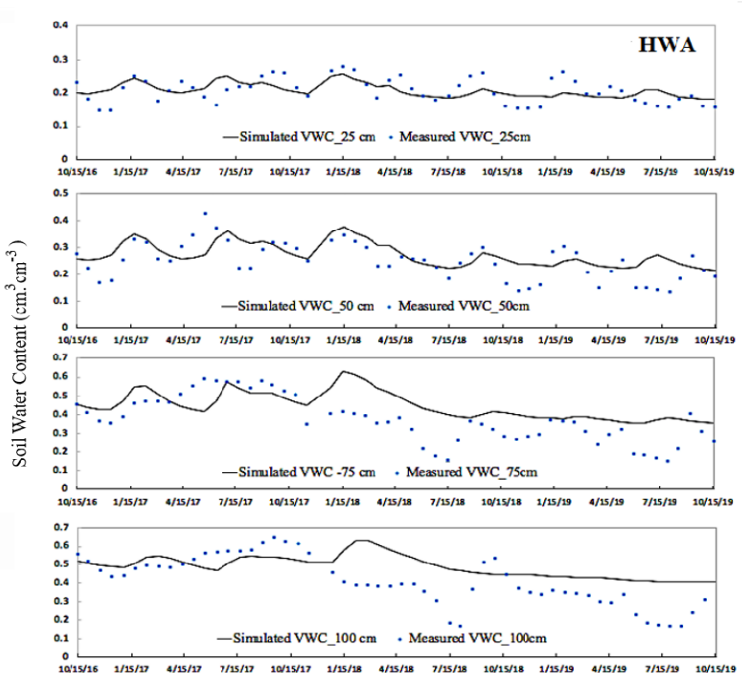

Figure A3.12. The measured and HYDRUS-1D simulated soil water contents (displayed as 20-d means) at depths of 25, 50, 75, and 100 cm of the almond rootzone at the HWA site, west SJV, CA.

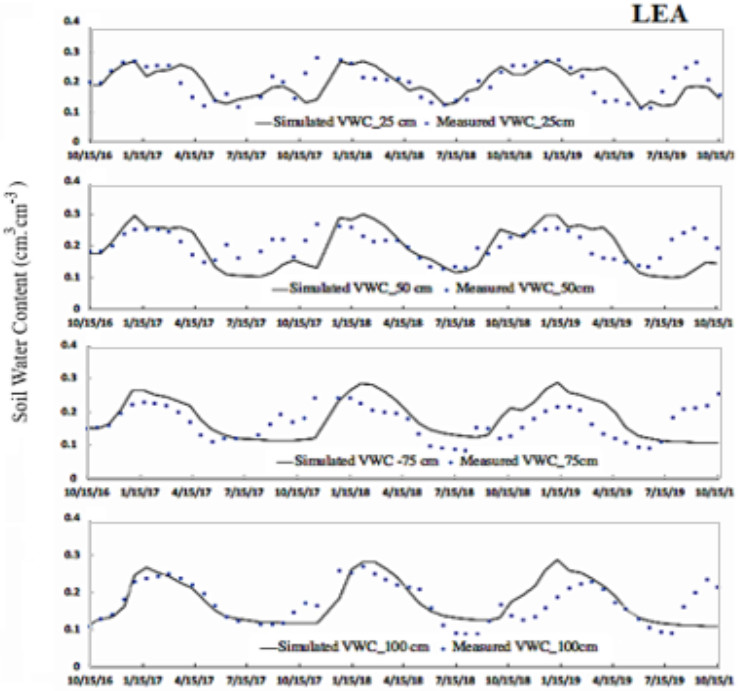

Figure A3.11. The measured and HYDRUS-1D simulated soil water contents (displayed as 20-d means) at depths of 25, 50, 75, and 100 cm of the almond rootzone at the LEA site, east SJV, CA.

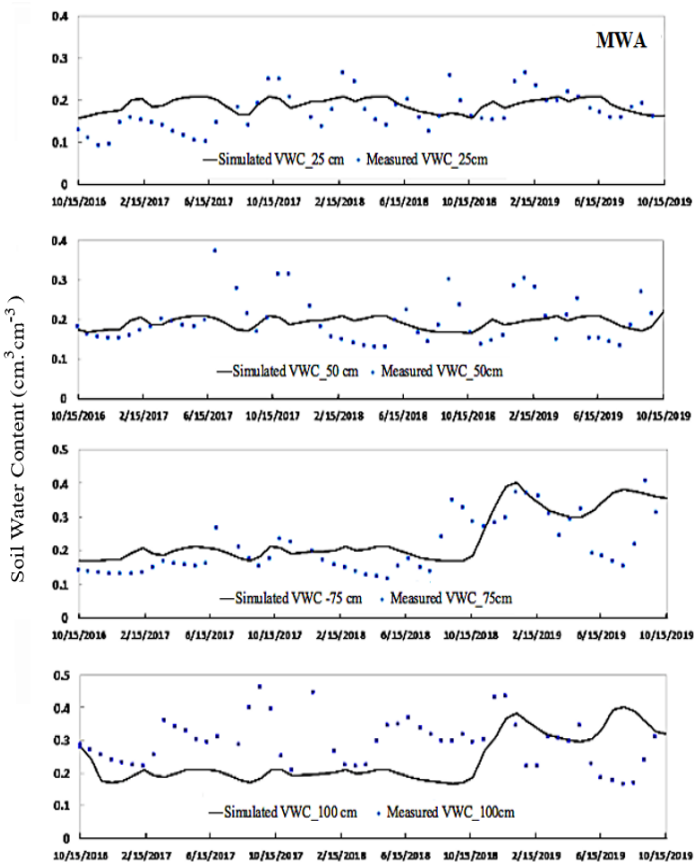

Figure A3.13. The measured and HYDRUS-1D simulated soil water contents (displayed as 20-d means) at depths of 25, 50, 75, and 100 cm of the almond rootzone at the MWA site, west SJV, CA.

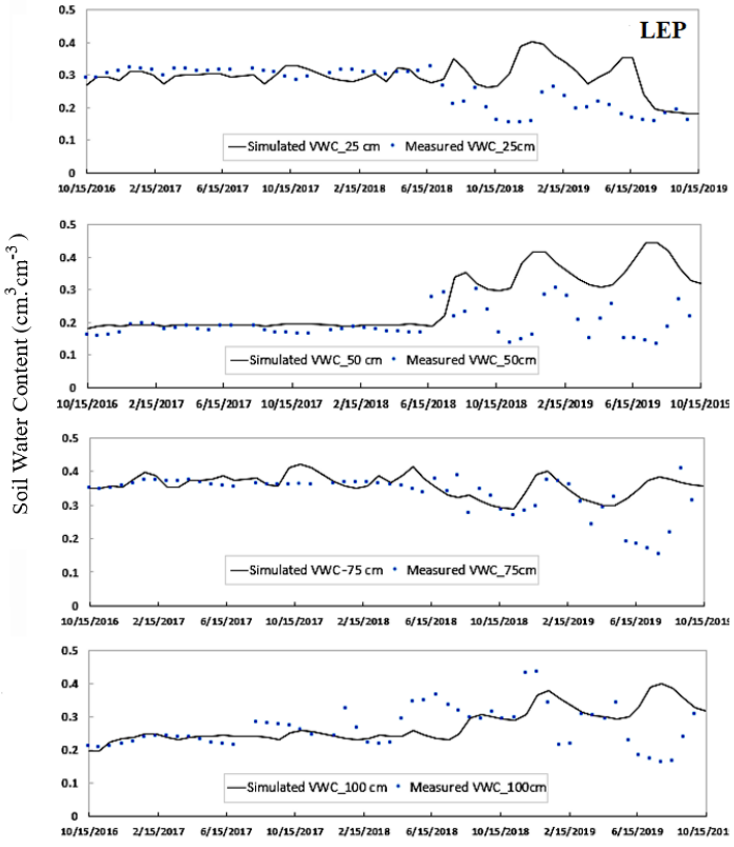

Figure A3.14. The measured and HYDRUS-1D simulated soil water contents (displayed as 20-d means) at depths of 25, 50, 75, and 100 cm of the pistachio rootzone at the LEP site, east SJV, CA.

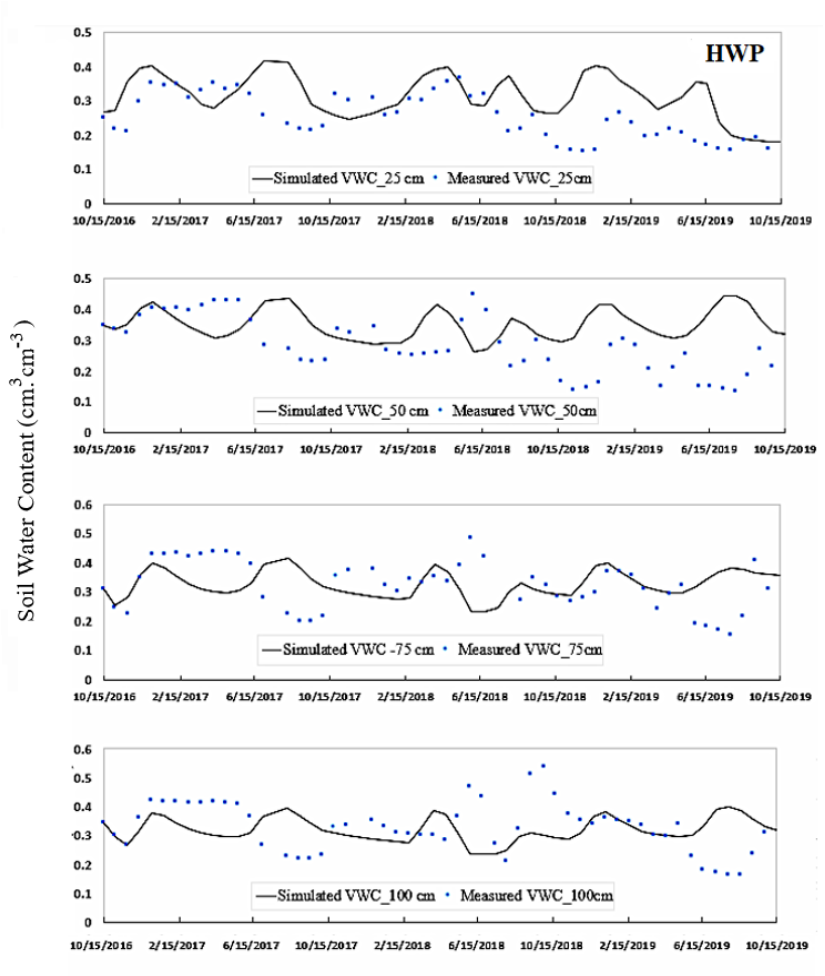

Figure A3.15. The measured and HYDRUS-1D simulated soil water contents (displayed as 20-d means) at depths of 25, 50, 75, and 100 cm of the almond rootzone at the HWP site, west SJV, CA

Chapter 4 Simulations of Future Seasonal Salinity in Almond trees' Rootzone Layers in Eastern and Western SJV, CA.

Abstract

Long-term changes in precipitation and climate trends are expected to increase soil surface evaporation and increase the reliance on higher salinity groundwater for irrigation and thus the root zones' salinity. Climate change is expected to significantly impact irrigated agriculture in California, with large uncertainty in precipitation. Hence, in this study, we relate root zone soil water and solute transport to diminishing water resources and climate change. To understand the potential impacts of climate change on the reliability of surface water resources, three irrigation resource patterns of 20, 50, and 80% groundwater proportions of irrigation water were studied in the San Joaquin Valley (SJV), California, USA. The effects of groundwater irrigation criteria on the root zone salinity during the near future decade (2020-2050) were simulated using the HYDRUS-1D soil water, solute, and temperature model. The annual impact of rains on the root zone salinity would vary according to different future climate scenarios, besides the expectations of altered future water use and changing soil characteristics. Thus, we used two future rain intensity predictions in twelve HYDRUS-1D simulations. Climate models were used to depict the used future rain intensity trends. First, the climate model CSM4_mid-range precipitations (CalAdapt, 2018), of which predictions are closest to a mean future rain scenario, were used. Second, the Climate Model CNRM_CM5_wetter precipitations (CalAdapt, 2018), of which predictions are closest to ensemble a wet future rain scenario, were used. The rain distribution within each year was upscaled from the average historical precipitation distribution of the western and eastern SJV.

The transient water uptake reduction sometimes approaches a steady state when viewed over the simulated 30 years period. In the coming decades, the rain amount correlated with the

fluxes through the rootzone deep layers, where the deep solute fluxes were noticeably higher in the eastern SJV than the western SJV. The salinity leaching fractions varied according to the different soil types. When the soils were initially saline, and more saline irrigation scenarios are assumed, the low root zone solute leaching fluxes were indicative of infiltration problems, which are expected due to an increase in the rootzones' sodicity. Precipitation provided an insufficient leaching effect when the fraction of irrigation water from groundwater exceeded 80% in the western SJV. These precipitation effects will play a significant role in increasing the salinity of shallow groundwater in the eastern region of SJV if the simulated fractions of leached salinities under the simulated irrigation criteria are used over the coming 30 years.

4.1. Introduction

Future expected reduced precipitation and warmer temperatures will lead to an increase in evapotranspiration and a decrease in mountain snow mass, implying stress on water resources (Cook et al., 2014; Allen and Anderson, 2018). One-fifth of the world's population will live in areas plagued by water scarcity (with annual water supplies dropping below 1,000 m^3 per person) by 2025. Two-thirds of the world's population will live in water-stressed regions (with annual water supplies dropping below 1,700 m^3 per person) (UN water, 2014). According to the existing climate change, half the world's population will be living in areas with high water stress by 2030 (UN water, 2018). California's climate pressures will make it harder to protect freshwater ecosystems. Making this system more climate-ready is a major challenge that will require better groundwater management. Water supply management must adapt to a warmer, more variable climate. Analyses suggest an era of new hydrological conditions for many, if not most southern California watersheds by the end of the century (Dettinger *et al*., 2011; Underwood *et al*., 2018). AghaKouchak *et al*. (2014) found that winter water shortages are of critical concern for decision-makers as this is the season in which water supplies accumulate for the rest of the year.

To understand the impacts of intensified agricultural activities, relations with the climate system is a major scientific and engineering endeavor for humankind (Wheeler and von Braun 2013; Liu *et al*., 2017). Balancing water supplies and demands by reducing demands will lead to groundwater quality challenges and reduced long-term agricultural prosperity. This challenge is amplified by the increased presence of perennial crops (such as almonds and pistachios) that require consistent irrigation over a multi-decade period. On this same timescale, farmers will also need to manage water quantity and quality together, to avoid unintended consequences (Hanak *et al*., 2019). In SJV, the state's Sustainable Groundwater Management Act (SGMA) requires local water users to bring groundwater use to sustainable levels by the early 2040s, which will have a broad impact on the valley agriculture and the regional economy in the coming years (Hanak *et al*., 2019).

Precipitation mitigates the impact of irrigation with saline waters. However, rainfalls are highly variable both seasonally and annually. The variation of seasonal rainfall quantities is the most uncontrolled factor causing non-steady-state RZ salinity (Minhas and Gupta, 1992). Temporal rain distributions may have an important influence on seasonal root zone salinity (Isidoro and Grattan, 2011). An earlier study by MacGillivray and Jones (1989) assessed relationships between total rain and the change in soil water content in the Central Valley of California. A later study by Schoups *et al*. (2005) showed that soil salinization is related to groundwater use during periodic droughts. Recent variable soil salinity distribution was surveyed and mapped for California agricultural lands, including the SJV, CA (Scudiero *et al*., 2017). The SJV historical pattern of annual rain years shows alternative rounds of droughts and wet seasons (CVP-OPAC, 1992), as shown in Appendix 4 (Table A4.1).

Addressing long-occurring water and soil quality problems in irrigated agriculture requires new analytical tools that improve our predictive capabilities (Jury *et al*., 2011). Future studies should focus on the use of decision-oriented models (Lobell *et al*., 2010; Rasouli *et al*., 2013; Bellvert, 2018). Soil moisture and salt balance equations have been used to analyze the long-term soil salinization trends (Allison *et al*., 1994; Hillel, 2000). Schoups *et al*. (2005) showed that soil salinization is related to groundwater use during periodic droughts. Groundwater salinity was shown to increase due to the leaching of salts from agriculture and the continued dissolution of gypsum present in the alluvial deposits. Hopmans *et al*. (2008) suggested that future work should consider additional irrigation water scenarios and evaluate the system's vulnerability to further increases in groundwater pumping. Also, more work is needed to quantify uncertainties in projected impacts caused by uncertain climate projections and uncertainties in the hydro-salinity model. To estimate site-specific water quality standards, rainfall should be considered, among other factors such as soil texture and crop tolerance (Minhas, 1996). Different hypotheses of future change can be used to develop differing management approaches that may be carried out and compared as climatic and other conditions change (Underwood *et al*., 2018). Seasonal rainfall effect on root zone soil salinity, soil water distribution, salt accumulation, and other existing trends are not only a function of soil properties and irrigation regimes but are also altered by plant water uptake, precipitation patterns, and micro-climate (Bah *et al*., 2009).

In this research, we used the numerical HYDRUS-1D model (Šimůnek *et al*., 2016) to simulate the root zone (RZ) salinity trends under different predicted climate forecasts for the early coming decade (2020-2050). We used HYDRUS-1D also to predict the effects of the continuing use of degraded high saline irrigation water on the RZ solute distribution in two almond sites, eastern and western SJV. As discussed in previous chapters, precipitation in the SJV, CA, decreases from the north to the south. Precipitation is much higher (200 cm/y) in the mountain ranges

surrounding the valley floor, as shown in Figure 4.1 (Gaines, 1998; Hoover et al., 2017). Most precipitation continues to occur in winter and is derived from North Pacific winter storms. Suweis et al. (2010) concluded that small rainfall reductions in warmer climates might cause dramatic shifts in the long-term soil salinization trends.

4.2. Methods

4.2.1. Simulations Setup

The future simulations are based on three-year calibrated simulations. The HYDRUS-1D simulations were calibrated during 2016-1019 using ongoing trends of moisture and soil solute salinity using soil moisture, electrical conductivity (*EC*), and temperature sensors (GS3, Decagon/METER Inc., Pullman, Washington, USA). Soils were sampled at six depth increments (0-20, 20-40, 40-60, 60-80, 80-100, and 100-120 cm) of a 120 cm RZ profile to determine the soil hydraulic and chemical properties.

4.2.2. Simulation initial and boundary conditions

Annual future rainfall intensity and distribution were downscaled using measured rainfalls of the studied locations between 2016-2019 (Figure 4.1), and the rainfall distribution pattern of the annual precipitation in the studied regions of SJV, CA (Figure 4.2). The future annual assumptions are based on both State of California, the State Water Project (SWP), and the Central Valley Project (CVP) historical data (Appendix 4, Table A.4.1). Future crop water demands timing were assumed the same, with no seasonal demands, daily allocation, or crop growth period shifting. The groundwater salinity is 1.35 - 1.5 dS/m, according to the USGS records of the wells in that region (USGS NWIS, 2018), and surface water average salinity is assumed 0.44 dS/m, as shown in (Appendix 4, Figure A4.12).

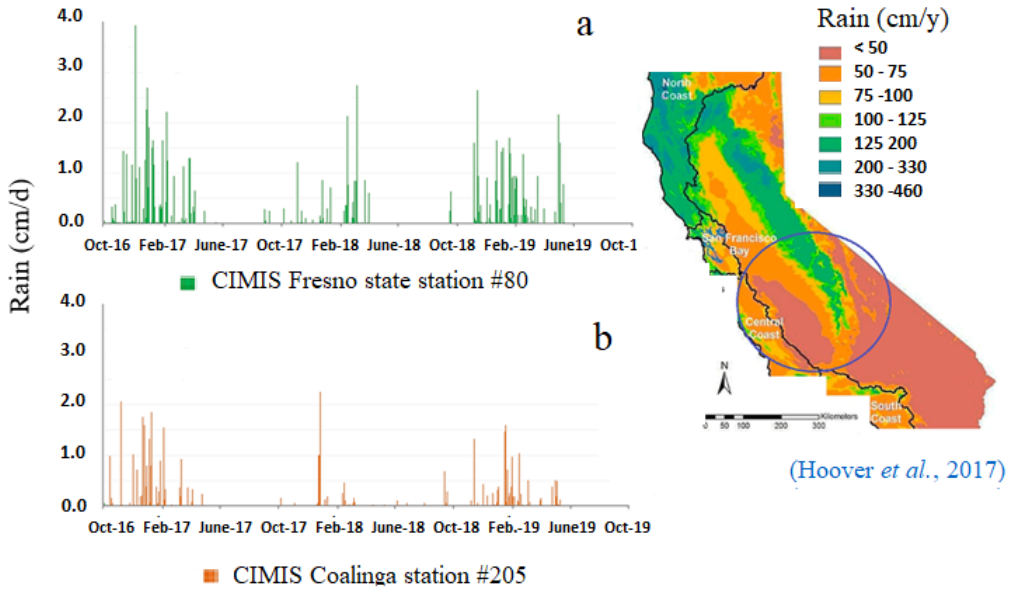

Figure 4.1. Measured daily rains in the east (a) and west (b) SJV during 2017 -2019. The map of SJV hydrological rain regions, depicted from (CIMIS, 2017; Hoover et al., 2017).

Three long-term irrigation water source scenarios were used to simulate the rootzone salinity dynamics for both the east and west of SJV, CA. The three irrigation source scenarios were simulated under two general climate scenarios commonly found in climate ensemble modeling. The first climate scenario assumes moderate temperature and rain projections. The second scenario assumes a warmer climate projection with an increase in rains. We used the future two rainfall projections of the early century (2020-2050). Two Global Climate Models were selected by the California Department of Water Resources team as having a good simulation of California's climate (Cal-Adapt., 2018). The first is CCSM 4. The second model is CNRM-CM5. The differences in the two models are regarding future precipitation. All the models predict temperature increases. They differ more in predictions of precipitation.

The two climate models are identified based on stakeholder feedback in the Climate Model Intercomparison Project, version 5 (CMIP5), of which the projection, which was closest to the ensemble mean of the other 17 climate models, is the CCSM4_Climate model, by the National Center for Atmospheric Research, USA. The warmer wetter projection is the CNRM-CM5 Climate model, by the Centre National des Recherches Météorologiques, France. Notably, the CCSM4 and CNRM-CM5 models were also selected as two of ten models best-suited for the research in California's Fourth Climate Change Assessment (Pierce *et al*., 2016).

Three irrigation quality scenarios under the previously chosen two rain scenarios gave the following assumed future scenarios for the study of root zone salinity. First, the six projected simulations were conducted using the western SJV studied site precipitation, crop evapotranspiration, and soil criteria. Then, the six scenarios were repeated using the eastern SJV site precipitation, soil, and crop evapotranspiration criteria.

The surface versus groundwater contributions to irrigation was selected based on expert input from the dissertation committee. These scenarios are arbitrary, but the availability of surface water for irrigation depends on a complex interaction between seasonal meteorology, engineering infrastructure, water demand from other users, and regulatory constraints for environmental protection. Given this complexity, there are no established guidelines for forecasting future surface water availability for agriculture. The first, second, and third simulation scenarios use the mean future rain projection. The fourth, fifth, and sixth simulated scenarios use the wetter future rain projection.

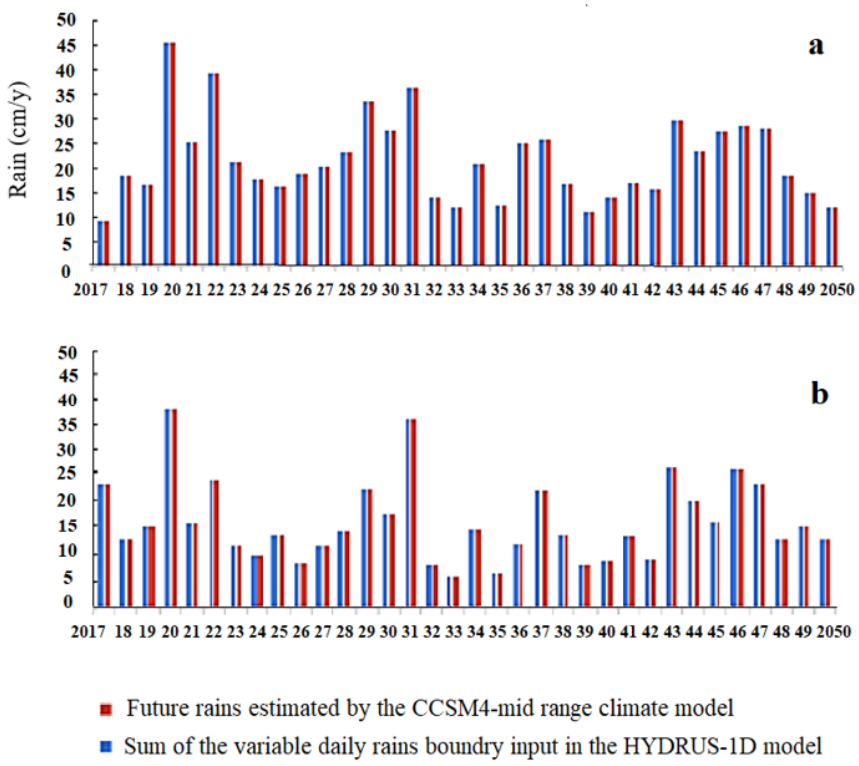

Figure 4.2 Future annual predicted rain amounts in the east (a) and west (b) of SJV during 2018- 2050, using a Mid-Average future rain scenario, according to the 4th California water assessment report suggested climate model (CCSM4).

Table 4.1. Future simulations with HYDRUS-1D and two climate models.

Future soil water and solute simulations with different future irrigations	Climate models for future rain predictions 2020 -2045	
	CCSM4 _Climate Model	**CNRM_CM5 Climate model**
HYDRUS_1D Model	1.Groundwater proportion 20% (0.2 G) and moderate rain.	4.Groundwater proportion 20% (0.2 G.) and more rain.
	2.Groundwater proportion 50% (0.5 G.), and moderate rain**.**	5.Groundwater proportion 50% (0.5 G.) and more rain.
	3.Groundwater proportion 80% (0.8 G.) and moderate rain.	6.Groundwater proportion 80% (0.8 G.) and more rain.

4.3. Results and Discussion

4.3.1. Irrigation Quality Effect on Root Zone Salinity

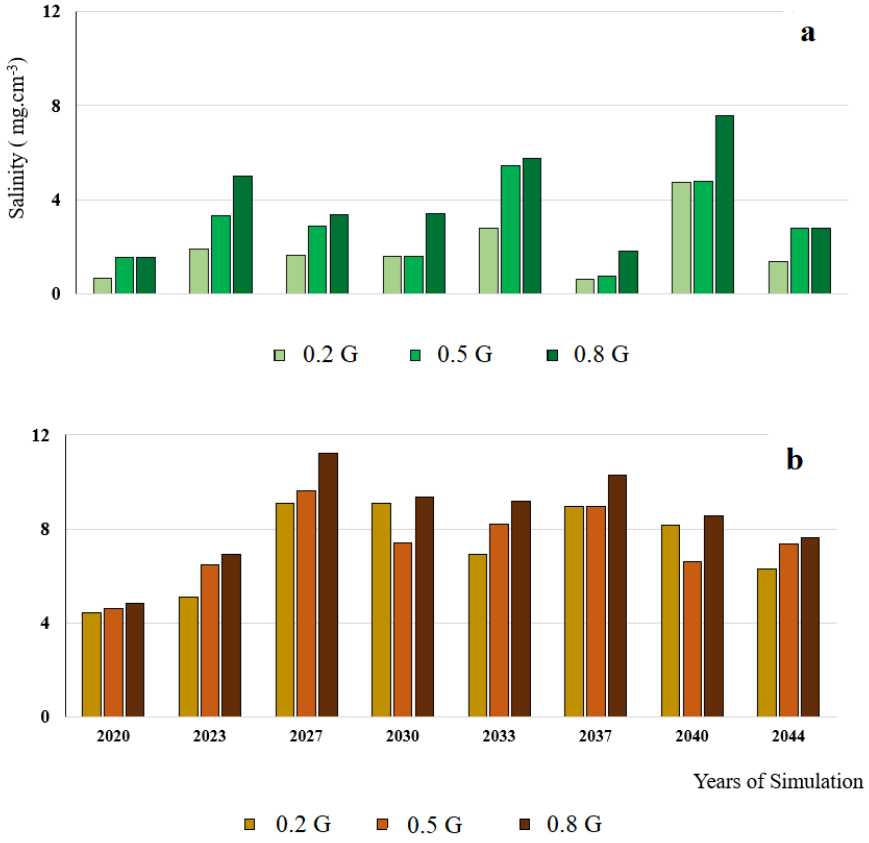

Figure 4.3. Anticipated accumulations of salinity every three years in (a) the eastern LEA site and (b) the western HWA site, using three future irrigation projections 0.2 G, 0.5 G, and 0.8 G, which indicate that 20%, 50%, and 80% of the future irrigation is groundwater.

In the results reported in Chapter 3, we concluded that the salinity early in the season (caused by the irrigation water salinity trend) has a more important impact than the winter rain. Unsurprisingly, the impact of rain on controlling salinity was greatest when the growing season had initial low root zone salinity. In this chapter, the analysis of root zone salinity will reflect both the effect of annual irrigation criteria and year rain intensity together. Root zone salinity trends were discussed at the initial time (October) of each simulated hydrological year.

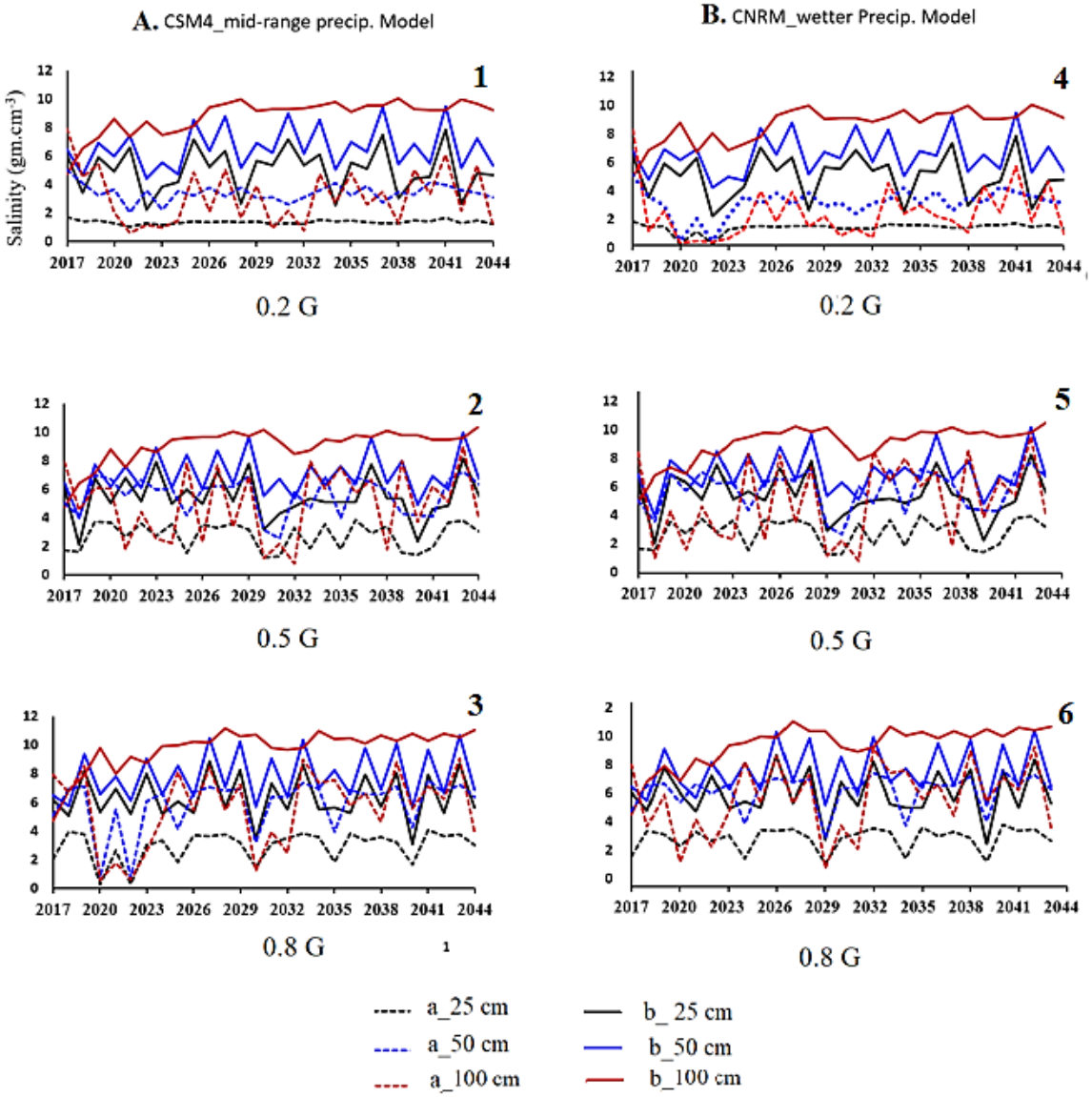

Figure 4.4. Simulated salinity using HYDRUS-1D at three root zone depths 25, 50, and 100 cm. The root zone salinity under mid-range (A) and wetter (B) future rain projections. Each rain projection was simulated for 0.2G, 0.5G, and 0.8G, which corresponds to the groundwater irrigation proportions of 20%, 50%, and 80%, respectively.

The accumulated mass of soil salinity in the three irrigation water scenarios (0.2G, 0.5G, and 0.8G) was higher as groundwater proportions of irrigation water increased to 20, 50, and 80%, as shown in the simulated rootzone salinity trends every three years (Figure 4.3). Root zone salinities during 2016-2019 were within a moderate level towards a marginally higher concentration (1.1 -2.2 dS/m and 2.2 -4.7 dS/m) in the eastern and western SJV, respectively. Whereas almond tree production decrease by 50%, based on the Maas and Hoffman (1977) threshold and slope parameters for almonds of 1.5 dS/m and 19%, respectively. The east and west of SJV represent two different hydrological and soil physical and chemical conditions.

Figure 4.4 shows salinity simulated using HYDRUS-1D at three root zone depths of 25, 50, and 100 cm for two rain scenarios A and B. Each rain projection was simulated for 0.2G, 0.5G, and 0.8G, which corresponds to the groundwater irrigation proportions of 20%, 50%, and 80%, respectively. Figures 4.4.1, 4.4.2, and 4.4.3 pertain to three simulated groundwater scenarios (0.2 G), (0.5 G), (0.8 G) for the first climate model (A). Figures 4.4.4, 4.4.5, and 4.4.6 refer to three simulated groundwater scenarios (0.2 G), (0.5 G), (0.8 G) for the second climate model (B).

The root zone average salinities in both initially low and high saline rootzones (a and b) increased when the groundwater proportion increased from 20% to 50% and 80% of the total irrigation, as shown in Figures 4.4.1 to 4.4.6. The irrigation salinity led to increased salinity in the deep layers of the root zone (Figure 4.4.1 to 4.4.6, red lines). The alternative wet and dry years in the SJV, CA, would return the root zone salinity towards a lower value every three years cycle. The pattern remains similar to the current 2017-2018 patterns for the mid-range precipitation projection A (Figures 4.4.1, 4.4.2, and 4.4.3). Also, the periodical return to initial salinity values was noticed under the wetter precipitation projection B (Figures 4.4.4, 4.4.5, and 4.4.6)

4.3.2. Irrigation Quality Effect on Almond Root Uptake

A root water uptake reduction due to the use of different irrigation waters in two different geohydrological regions of SJV during 2016- 2044 is computed as follows:

$$T_r\ (reduction) = 1 - {}^{T_S}/_{T} \tag{4.3}$$

where T_r is the fraction of simulated transpiration reduction due to salinity, T_S is the simulated transpiration (Anderson, 2016a), and T is a calculated transpiration value from the calculated evapotranspiration, $ET = ET_0{*}K_c$, and divided into transpiration and evaporation using the percentage of the soil coved fraction (SCF), $T = ET{*}SCF$, monthly almond crop factor in the studied regions (SIMIS, 2016 -2019), and reference evapotranspiration ET_0 (CIMIS, 2016 -2019).

The relation between the root zone salinity and the root water uptake reduction is shown in Figure 4.5 for the coming decades if the use of saline groundwater for irrigation increases and the current rain remains the same. The reduction in root water uptake when irrigation water salinity increases is higher in the western SJV than in the eastern SJV.

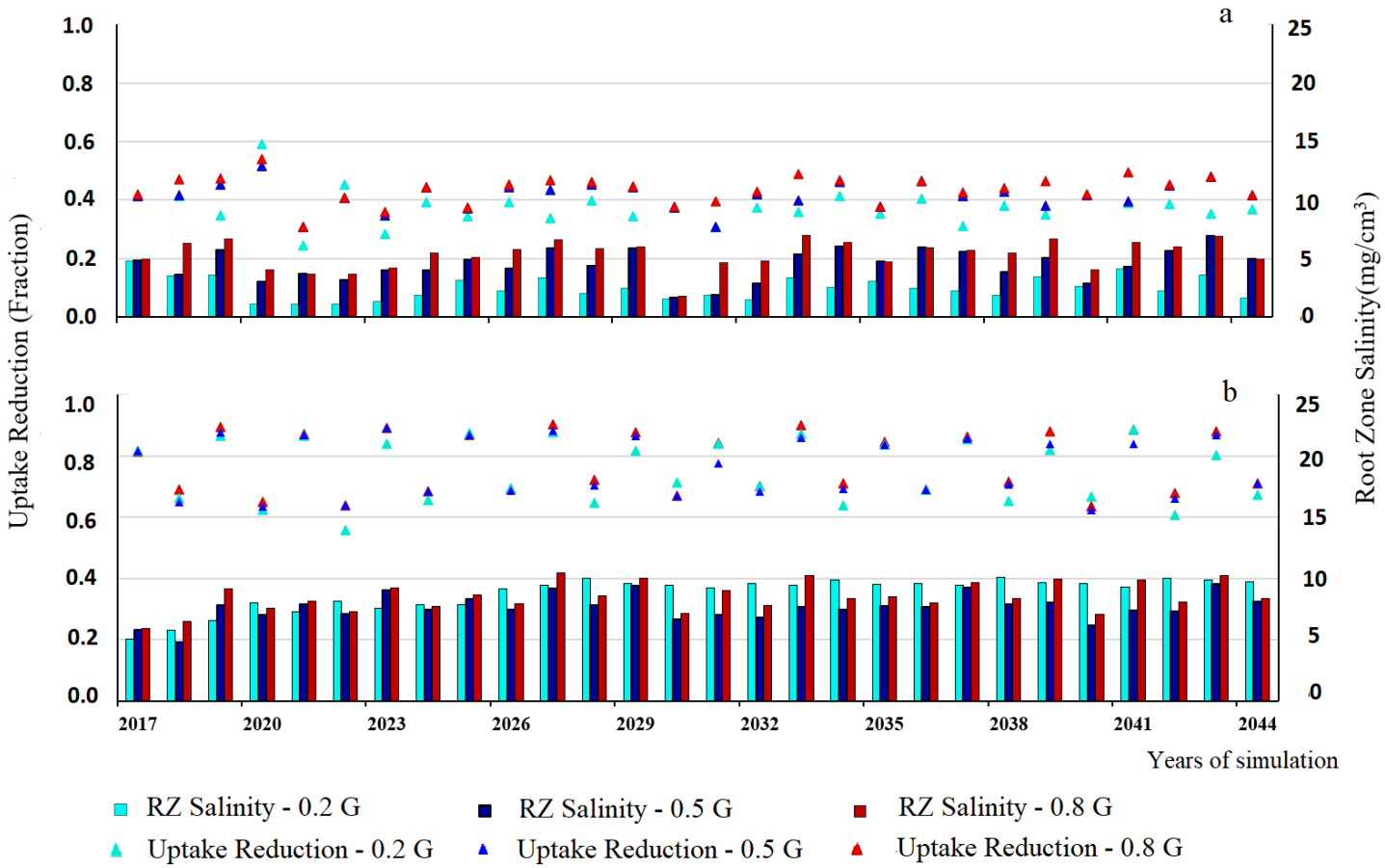

Figure 4.5. A water uptake reduction and root zone salinity at the beginning of each hydrological year (October) for three future irrigation simulations (0.2G, 0.5G, and 0.8G). The irrigation scenarios refer to 20%, 50%, and 80% of groundwater irrigation proportions. The LEA eastern site (a) and the HWA western site (b) in SJV, CA

4.3.3. Irrigation Quality Effect on Salinity leaching

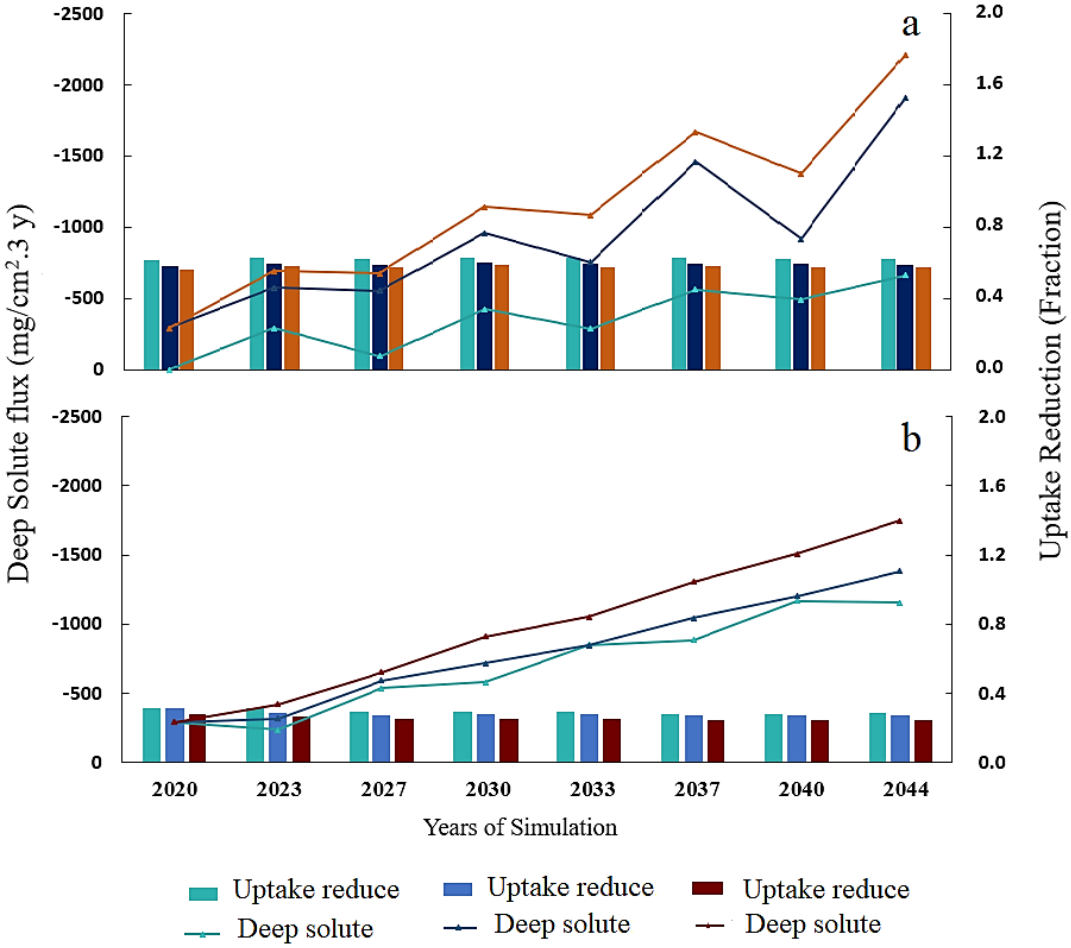

Figure 4.6. The reduction in root water uptake and cumulative soil solute fluxes at the bottom of the almond root zone for three-year periods at (a) the LEA eastern site and (b) the HWA western site, SJV. Negative values indicate the downwards movement of solutes.

However, the almonds root zone salinity had a consecutive similar effect on the root water uptake reduction, as shown in Figure 4.6, where the apparent factors that affect the water uptake reduction are the regional soil and climate variances. It was interesting to see that the bottom solute flux will increase more in the east SJV than the west SJV when the irrigation salinity increases within three water salinity alternatives (Figure 4.6).

Simulated water leaching fractions and salt leached fractions were defined in the bottom of the root zone by equations 4.1 and 4.2, respectively (Skaggs (2014).

$$WLF = {J_{LR}}/{J_0} \tag{4.1}$$

$$SLF = {Q_{LR}}/{Q_0} \tag{4.2}$$

where J_{LR} and J_0 are the seasonal cumulative water fluxes at the bottom of the root zone and the soil surface, respectively, and Q_{LR} and Q_0 are the corresponding salt mass fluxes.

Both removed soil solution and accumulated soil salinity under the simulated three water scenarios showed a logical increase for the leached salts in corresponding to the increase of the irrigation water salinity. The paradox existed when the (0.5 G and 0.8 G) irrigation scenarios with 50% and 80% of groundwater blend showed higher leaching rates in the low saline eastern site that have relatively higher rains than the eastern site. The increase of leached solute amounts was related to higher soil hydraulic conductivity and a better irrigation quantity and quantity. This emphasizes the need to prioritize the good water qualities to the orchards that are less saline in order to maintain their lower salinity status.

Both removed soil solute salts (Figure 4.4) and accumulated soil solute salts (Figure 4.6) under the simulated three water scenarios showed an increase corresponding to an increase in

irrigation water salinity. The paradox existed when the send (0.5 G) and (0.8 G) irrigation scenarios with 50% and 80% of groundwater blend showed higher leaching rates in the low saline eastern site (Figure 4.6. a) than the western site (Figure 4.6. a b) The increase of leached solute amounts was related to a better soil hydraulic conductivity and a better irrigation quantity and quantity. The relatively higher rains on a particular site would explain the tendency for more leaching. This emphasizes the need to prioritize the good water qualities to the orchards that are in a higher salinity risk, to enhance more deep soil salinity fluxes.

These results agree with the values of the leached salt amounts in both of the (0.2 G) and (0.5 G) irrigation scenarios in (Figure 4.4b), where the soil is clayey, more saline, and sodic (as described in chapter 2 of this study). Also, the irrigation scenario (0.8 G) shows lower deep solute fluxes in the high saline site (Figure 4.6b) than the deep fluxes under the same irrigation scenario in the eastern low saline site (Figure 4.6a), which explains the tendency of this site's soil to adsorbed more seasonal salinities during the irrigation seasons with slower leaching rate during the rest of the year. On the other hand, the better soil salinity, texture, and precipitation conditions in the east (Figure 4.6a) could lead to a higher risk of salinity leaching towards groundwater, which refers to the importance of lowering the proportions of saline irrigations in the eastern sites as well, if groundwater levels are high.

4.3.4. Future Rain and Irrigation Quality Effect on Almond Uptake

Figure 4.7 shows the effects of both using more saline water for irrigation and wetter future climate. The results show that the effect of more future rains is not significant in reducing the root zone salinity effect on the reduction of the root water uptake caused using more saline water.

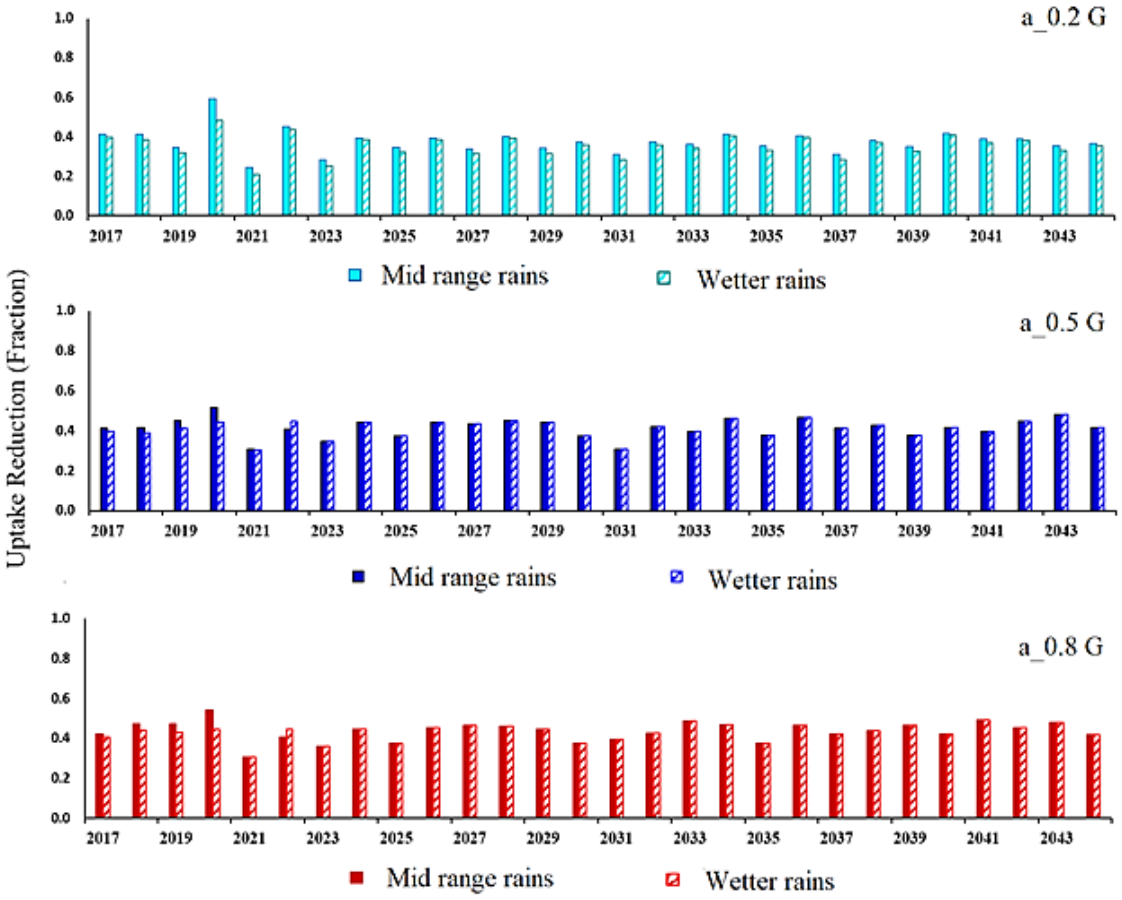

Figure 4.7. Water uptake reduction for three assumed future irrigation scenarios (0.2 G, 0.5 G, and 0.8 G), and future rain increase from a mid-range to a wetter range in the eastern region of SJV (a).

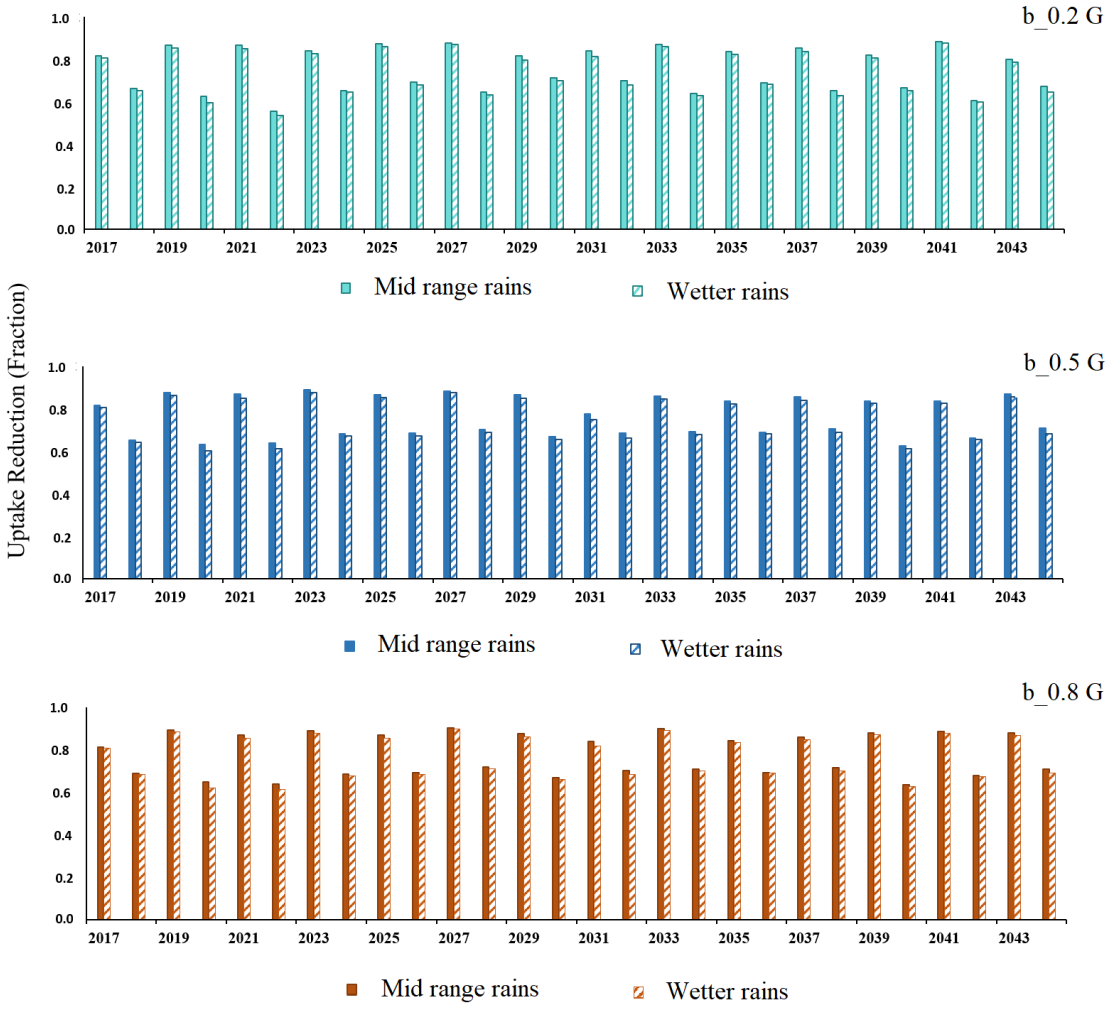

Figure 4.8. Water uptake reduction for three assumed future irrigation scenarios (0.2 G, 0.5 G, and 0.8 G), and a future rain increase from a mid-range to a wetter range in the western region of SJV (b).

As shown in Figures 4.7 and 4.8, in both east and the west of SJV, all the reductions are around an average for all irrigation scenarios. In the east use of lower saline water, the reduction is noticeably lower than the simulated uptake reduction under higher irrigation salinity in scenarios (0.5 G) and (0.8 G), as shown in figure 4.7. On the other hand, in the west, all 0.2 G low saline irrigation scenarios caused a similar reduction to the uptake reduction caused using higher proportions of groundwater in the scenarios 0.5 G and 0.8 G (Figure 4.8). Note here that the predicted wetter precipitation is only 127% of the mid-range precipitation predictions, according to California's 4th assessment climate model predictions. That would explain the close values of water uptake reduction compared under the two precipitation scenarios.

The effect of wetter future rain projections shows that water uptake reduction in the west high saline site will not be of big variances as the east SJV site (Figures 4.7., 4.8, dashed columns). In the initial low saline root zones, the higher the irrigation salinity, the more root water uptake reduction will occur, regardless of the amount of rainfall.

As shown in Figure 4.8, the roots water uptake reduction was related to the different root salinity criteria, e.g., RZ salinity is the concentration of salts (mg.cm^{-3}), removed solute is the amount of solute removed from the top and bottom rootzone (gm.cm^{-2}), and the leaching fractions of water and salts as defined in equation (4.8). Simple correlation analysis was conducted for the mentioned solute and salinity outputs of HYDRUS-1D future twelve conducted scenarios.

4.3.5. Future Rain and Irrigation Quality Effect on Future RZ Salinity

We referred to the seasonal rainfall effect on salinity by the soil water content conditions. Soil antecedent moisture affects the influence of rain on the distribution of salts in the RZ (Lai *et al.*, 2016). When the antecedent soil moisture is low, most of the rainfall is retained in the upper

part of the soil profile, and thus only a limited effect of rain on the deep percolation of soil solute is expected (Lange *et al.*, 2010). Others indicate the rain contribution to root zones' water transport regardless of salinity (e.g., Hardie, 2011), who determined how effective rains contribute to soil water flow using the change of the soil moisture content related to the total amounts of precipitation.

Figure 4.1 shows that the root zone salinity differences were minor irrespective of the water source. The salinity in the east SJV (continuous lines) is overall lower than the salinity in the west SJV (dotted lines). In Figure 4.10, a trend of the rootzone salinity at different depths shows during consecutive years an increase in the years of dry rain type with an alternative year of simulated salinity decrease when the year type is wet. Increasing the portion of the groundwater in the 2nd and 3rd water future projections showed a greater effect on the salinity of the western studied SJV site. An increase in root zone salinity was observed in the eastern SJV sites. The red lines are the deep layers where salinity tends to be higher under all studied conditions.

Projections of future precipitation are uncertain; models vary widely, and different sub-regions can exhibit different patterns. While it is difficult to discern strong trends from the full range of climate projections, one recent analysis forecasted a drying trend in California during the 21st century (Cayan *et al.*, 2009).

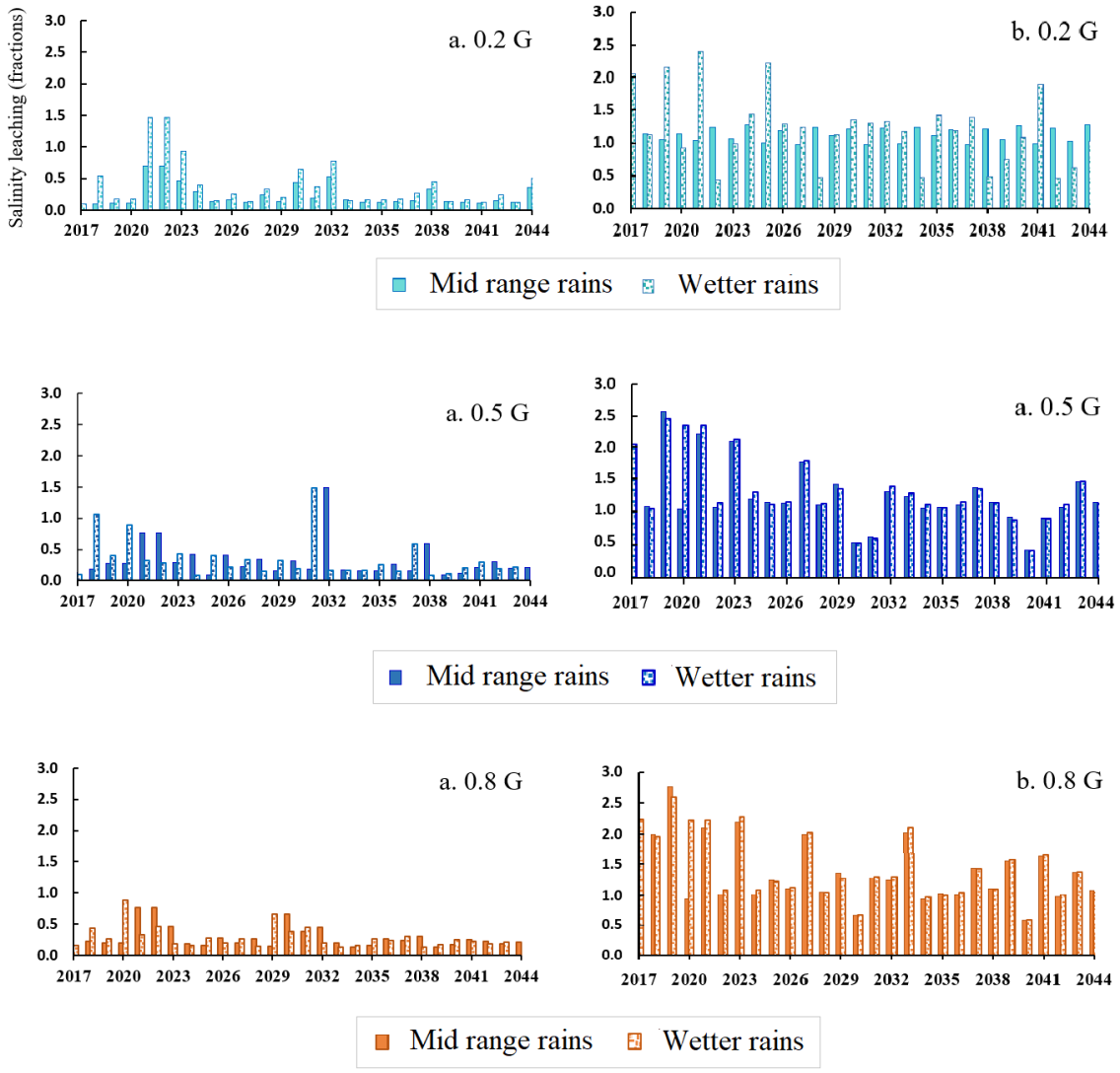

Figure 4.9. The combined effect of the use of more groundwater for irrigation in three irrigation scenarios (0.2 G, 0.5 G, and 0.8 G) and future mid-range and wetter range projection in the east (a) and west (b) regions of SJV, CA.

According to this analysis, some areas in northern California may experience higher annual rainfall amounts and potentially larger storm events, but California as a whole, particularly southern California, will be 15 to 35% drier by 2100 (Cayan *et al.,* 2009).

Models with both more and less overall precipitation for California indicate an increase in drying as measured in climatic water deficit (Micheli *et. al.*, 2012), so there is high certainty that there will be an increase in summer dryness even in years of higher-than-average precipitation. Southern California shows the potential effect of summer drought on vegetation due to limited soil moisture and primary production (Mooney 1977; Underwood *et al*., 2018). On the other site, extreme winter precipitation events may be expected. Zecca *et al.* (2018) compared two future high and low rain projections with a warmer climate for CA. They used the CMIP5 HIGH−r and CMIP5 LOW−r climate models, respectively. The authors concluded a significantly larger increase in precipitation during extreme precipitation events than an increase in the overall rain annual amounts. CA extreme precipitation would be more than double the increase in the average annual precipitation. The authors highlighted that the models that better simulate the El Nino-California precipitation teleconnection would yield larger increases in extreme precipitation. Based on a cluster analysis of seasonal changes in current precipitation, air temperature, and El Niño effects in the Pacific Southwest, 18 representative models for California and the Great Basin, Nevada, referred to the need for experimental, 'learn-as-you-go' framework in management efforts (Flint *et al*., 2015; Underwood *et al*., 2018).

The leaching fractions of water and salinity weres computed from the fraction of the leached fluxes at the bottom of the root zone to the amount that enters the top root zone. The leached fluxes, which are inversely proportional to the root zone salinity, was affected by the rainfall season and the soil's initial salinity conditions as follows. In figure 4.9 the all the future scenarios showed similar leaching fractions under the mid-average and wetter climate projections. The first scenario in west SJV had intense salt leaching events during the summer and winter of 2017 -2019. The same leaching practices were assumed to be followed in the early coming decade.

4.3.6. Future Rain and Irrigation Quality Effect on Salinity Leaching

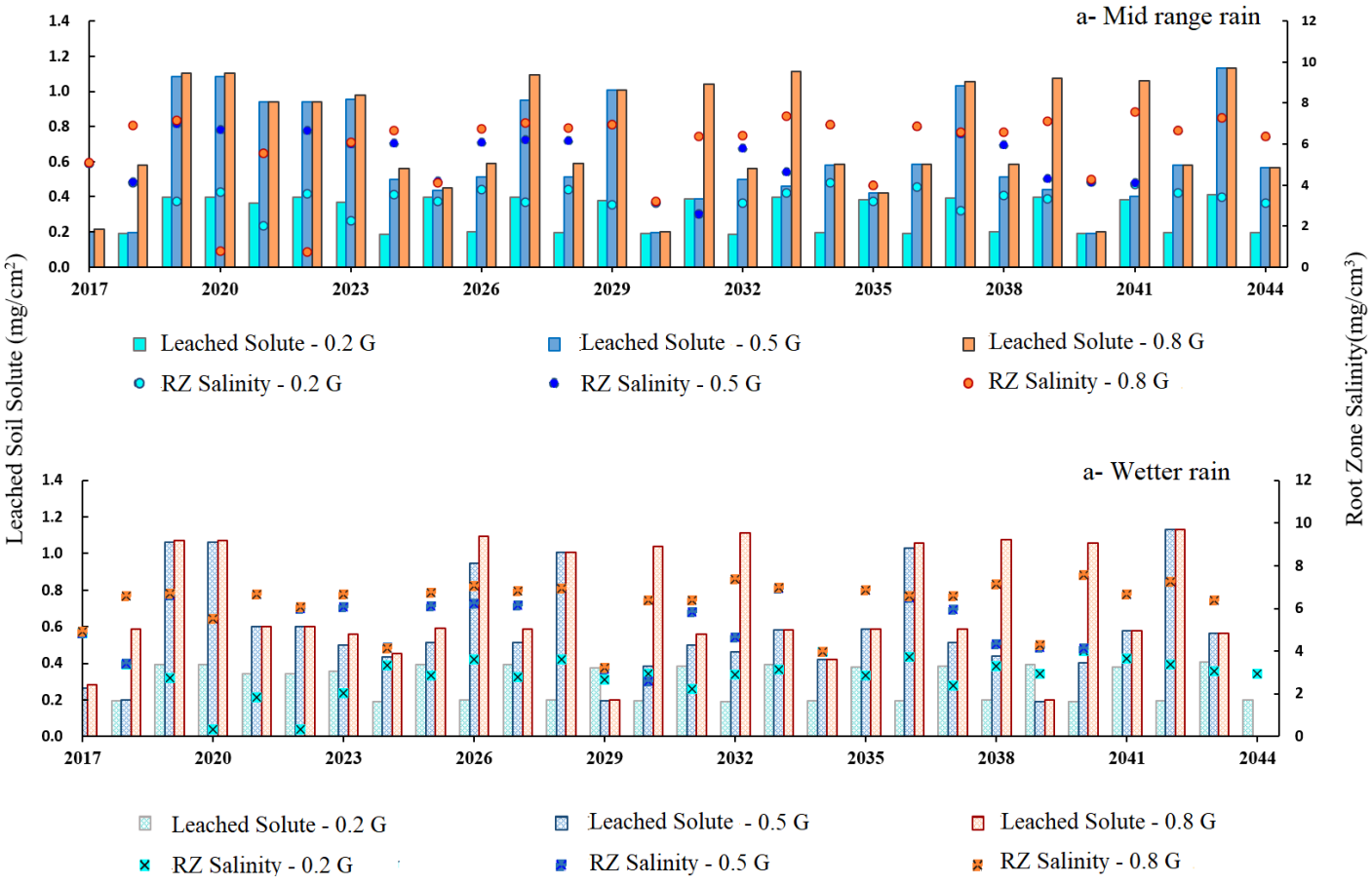

Figure 4.10. Cumulative leached salinity and average root zone salinity in October (the hydrological start of each year), in the eastern SJV under two future rain projections (top - moderate rain, bottom - higher rain).

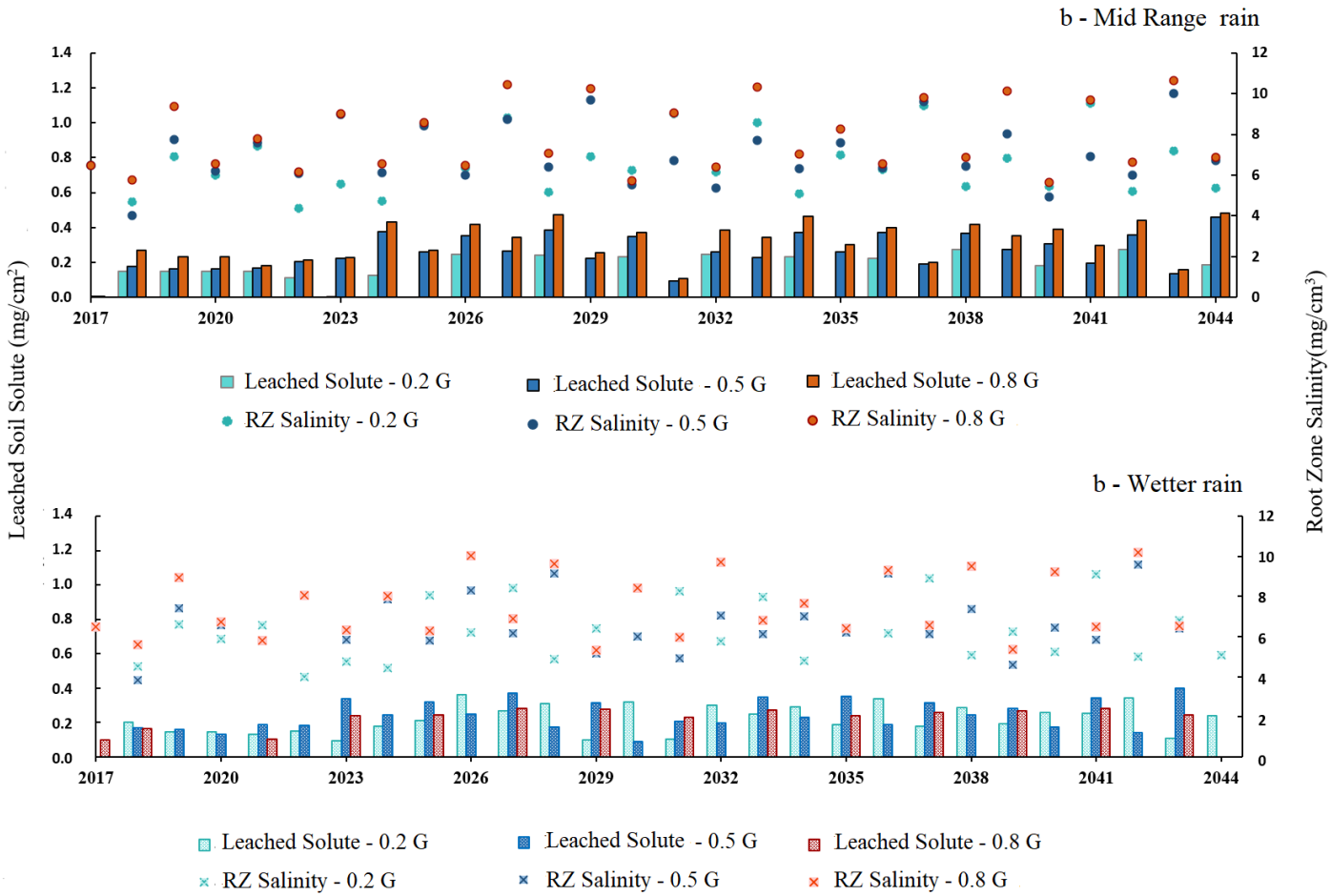

Figure 4.11. Cumulative leached salinity and average root zone salinity in October (the hydrological start of each year), in the western SJV (b) under two future rain projections (top - moderate rain, bottom - high rain).

The salinity reduction efficiency is defined as the amount of salt removed per unit depth of leaching water decreases as more leaching water is applied (Burt and Isbell 2005). The required frequency of leaching varies with the degree of salinity, evaporative demand, and salt sensitivity of the crops. The salinity of the root zone middle depths is compared for three irrigation scenarios (illustrated by dots per every three years), as shown in Figures 4.10 and 4.11. The third scenario (0.8 G) that relies on groundwater for irrigation by 80% had the greatest leaching fractions of salinity when compared to scenarios (0.2 G) and (0.5 G) that have 20% and 50% groundwater portions, during the years of 2030 and 2040. That refers to the accumulation of these added salts by irrigation to the root zone, which would have a harmful effect on groundwater salinity.

Salinity is expressed by the simulated concentration of the soil solute salts using HYDRUS-1D, and the water leaching refers to the fractions of the deep drainage water to the top applied water. The plotted salinity leaching are the fractions of the top salinity to the deep salinity of the studied rootzones. The simulated root zone water and salinity leaching trends during the next few decades responded to the increase of irrigation quality according to the regional hydrology and soil type and salinity. The more the irrigation relied on saline groundwater, the more the root zone mean salinity increased in both eastern and western regions (Figures 4.10 and 4.11). Salinity leaching fractions due to an increase in the groundwater proportion were higher in the eastern region (Figure 4.10) than the western region (Figure 4.11).

As shown in Table 4.2, the Pearson correlation coefficients between the root water uptake reductions and different salinities were investigated under three future groundwater use assumptions. The 0.2 G, 0.5 G, and 0.8 G scenarios use 20%, 50%, and 80 % of irrigation water from saline groundwater. Leaching is an important element of soil salinity management. The Pearson correlation coefficients indicated that the water leaching fraction was most related to root zone salinity in all simulations.

Table 4.2. Correlation between uptake reduction and different salinities in the eastern SJV.

Irrigation ground water proportion	**0.2 G**	**0.5 G**	**0.8 G**
Salinity in the top root zone	0.50	-0.22**	0.15
Salinity in the middle of the root zone	0.36**	-0.31**	-0.19
Salinity at the bottom of the root zone	-0.22	-0.42	-0.10
Root zone's mean salinity	-0.41	-0.38	-0.17
Solute removed from the top root zone	-0.20*	0.37*	0.08
Solute removed from the deep root zone	0.02**	0.33	0.19**
Water leaching fraction	-0.36	-0.45	-0.43
Salt leaching fraction	0.34	0.36	0.16**

Table 4.3. Correlation between uptake reduction and different salinities in the western SJV.

Irrigation ground water proportion	**0.2 G**	**0.5 G**	**0.8 G**
Salinity in the top root zone	0.69**	0.65**	0.86**
Salinity in the middle of the root zone	0.81**	0.74**	0.89**
Salinity at the bottom of the root zone	0.85**	0.86**	0.91**
Root zone's mean Salinity	0.85**	0.82**	0.92**
Solute removed from the top root zone	-0.36	0.45*	0.48**
Solute removed from the deep root zone	-0.76**	-0.46*	-0.48**
Water leaching fraction	-0.72**	-0.74**	-0.82**
Salt leaching fraction	-0.86**	0.59**	0.68**

** Correlation is significant at the 0.01 level (2-tailed).

* Correlation is significant at the 0.05 level (2-tailed).

The correlations of the water uptake reduction and the root zone's salinity were positive for all measurement depths (Table 4.2). The correlation between the water leaching fraction and the removed solute amounts was irreversible with the root zone salinity increase. Salinities at all depths of RZ show an effect on the reduction of root water uptake. On the other hand, in the root zone of lower initial soil salinity (Table 4.3), the criteria that increased root water uptake (which means decreased the uptake reduction due to salinity) was the water leaching fraction. Under both high and low root zone salinity conditions, the Pearson correlation coefficient was (negative), indicating a decrease in the water uptake reduction, but the root zone salinity at the top and bottom soil layers, which was effectively correlated with the water uptake reduction, not the averages. In western SJV, the correlation between the reduction in the root water uptake was significant at the 0.01 level with most of the simulated rootzone soil salinity criteria (Table 4.3). Whereas in the eastern SJV, the observed root water uptake reductions didn't show a significant correlation with most of the salinity analyzed criteria in (Table 4.1). Maheshwari *et al*. (2015) stated that other factors as evapotranspiration and rainfall should be considered to represent a correlation between the RZ salinity accumulation and leaching.

4.4. Conclusion

If we are going into more saline irrigation water projections in the future, then rain will be increasingly insufficient for salinity leaching. The results of the coming early decade simulations (2020-2045) showed that predicted more rain amounts would dilute the rootzone salinity only if combined with low saline irrigation water. Previously accumulated salinity in the rootzone hinders the effect of rain from reducing the root zone salinity. Future three water salinity alternatives were compared. Results show that the leached soil solute will increase in the eastern SJV than the western SJV. The contribution of seasonal winter rainfall on root zone salinity was to return the state of the rootzone to its initial salinity every cycle of wet/dry year. The results of twelve HYDRUS-1D

future scenarios showed that the effect of the increased irrigation water salinity proved to be a predominant influencer over the effect of rain on leaching. The use of more saline groundwater for irrigation increased the root zone accumulated salinity in the western SJV more than in the eastern SJV. Salinity risk will increase in the east SJV only when 50% or 80% of saline groundwater is used for irrigation. The simulated root water uptake reduction was consistent. Cumulative reductions of root water uptake and cumulative root zone salinity build discussed previously showed that the more severe effects for the higher irrigation salinity, that stay on a top-level for the eastern and western SJV regions, even with the effect of seasonal rains in returning the rootzone to previous initial low salinity after a dry season increase. The results of the simulated cumulative water and salt leaching versus the root water uptake could be used as a guide to provide some RZ salinity management strategies for almond trees. Future research questions should examine how to maintain the root zone salinity in a suitable range for Almond (*Prunus dulcis*) trees. One approach would be to direct future water management scenarios to optimize the use of groundwater in the western SJV to have adequate water leaching fractions. We do not recommend the use of more groundwater proportions in the eastern SJV as well, least it would increase the salinity of deep depths. In the western SJV, root water uptake reductions are similar for all irrigation scenarios. In the eastern SJV, the root water uptake reduction was noticeably lower when using 20% groundwater than when using 50% and 80% groundwater.

4.5. References

AghaKouchak, A., Cheng, L., Mazdiyasni, O., and Farahmand, A., 2014. Global warming and changes in risk of concurrent climate extremes: Insights from the 2014 California drought. Geophysical Research Letters, 41(24), 8847–8852.

Allen, R.J., Anderson, R.G., 2018. 21st century California drought risk linked to model fidelity of the El Niño teleconnection. npj Clim Atmos Sci 1, 21.

Bellvert, J., Adeline, K., Baram, S., Pierce, L., Sanden, B.L., and Smart, D.R., 2018. Monitoring crop evapotranspiration and crop coefficients over an almond and pistachio orchard throughout remote sensing. Remote Sens, 10, 2001; doi:10.3390.

Cal-Adapt., 2018. Data: Extended Drought Scenarios, LOCA Downscaled Climate Projections, VIC generated climate variables forced by LOCA (Scripps Institution of Oceanography), Gridded Historical Observed Meteorological and Hydrological Data (University of Colorado, Boulder).https://caladapt.org/tools/extendeddrought/#year=wateryear&lat=36.15625&lng=-120.21875&boundary=locagrid&scenario=late_century&units=imperial.

Cayan, D., Tyree, M., Dettinger, M., Hidalgo, H., Das, T., Maurer, E., Bromirski, P., Graham, N., and Flick, R., 2009. Climate Change Scenarios and Sea Level Rise Estimates for the California 2009 Climate Change Scenarios Assessment. California Energy Commission. Retrieved from http://www.energy.ca.gov/2009publications/CEC-500-2009-014/CEC-500-2009-...(link is external)

Coles, S., 2001. An introduction to statistical modeling of extreme values. London: Springer-Verlag. ISBN: 1-85233-459-2.

Cook, B.I., Smerdon, J.E., Seager, R., and Coats,S., 2014. Global warming and 21st century drying. Clim. Dyn. 43, 2607–2627.

CVP-OCAP, 1992. Long-Term Central Valley Project Operations Criteria and Plan, 1992. U.S. Department of the interior bureau of Reclamation, Mid Pacific Region, Sacramento, CA. Water Resources Center Archives, UC Berkeley.

Dettinger, M., 2011. Climate change, atmospheric rivers, and floods in California - a multi-model analysis of storm frequency and magnitude changes. Journal of the American Water Resources Association, 47(3), 514–523.

Flint, L.E., Flint, A.L., Thorne, J.H., Weiss, S.B., Boynton, R., and R., Curtis, A.J., 2015. Basin Characterization Model of the Great Basin: a dataset of historical and future hydrologic response to climate change. (https://ca.water.usgs.gov/projects/reg_hydro/projects/dataset.html)

Gilleland, E., 2015. Introduction to Extreme Value Theorem Analysis. National Center for Atmospheric Research.

Hardie, B.M., 2011. Effect of antecedent soil moisture on infiltration and preferential flow in texture contrast soils. Ph.D. dissertation, School of Agricultural Science, The University of Tasmania.

Hoover, D.J., Odigie, K.O., Swarzenski, P.W., and Barnard, P., 2017. Sea-level rise and coastal groundwater inundation and shoaling at select sites in California, USA. *Journal of Hydrology: Regional Studies*, *11*(January), 234–249.

Isidoro, D., and Grattan, S.R., 2011. Predicting soil salinity in response to different irrigation practices, soil types and rainfall scenarios. *Irrig. Sci.,* 29, 197–211.

Jury, W.A., Or, D., Pachepsky, Y., Vereecken, H., and Hopmans, J.W., 2011. Kirkham's legacy and contemporary challenges in soil physics research. *Soil Science Society of America Journal*, *75*(5), 1589–1601.

Lobell, D.B., and Marshall, B.B., 2010. On the use of statistical models to predict crop yield responses to climate change. J. of Agricultural and Forest Meteorology, 150, 1443 – 1452.

Maas E.V., and Hoffman, G.J. 1977. Crop salt tolerance - current assessment. J. Irrig. And Drainage Div., ASCE 103 (IR2), 115-134.

Minhas, P.S., Ramos, T.B., Ben-Gal, A., and Pereira, L.S., 2020. Coping with salinity in irrigated agriculture: Crop evapotranspiration and water management issues. Agricultural Water Management, 227, 105832.

Mooney, H.A., 1977. The carbon cycle in Mediterranean-climate evergreen scrub communities Presented at the Symp. on Environ. and Fuel Manage. Consequences of Fire in Mediterranean Ecosyst. Palo Alto, CA.

Pierce, D.W., Cayan, D.R., and Dehann, L., 2016. Creating Climate Projections to Support the 4th California Climate Assessment. La Jolla, CA: Division of Climate, Atmospheric Sciences, and Physical Oceanography, Scripps Institution of Oceanography. http://water.ca.gov/climatechange/docs/2015/Perspectives_Guidance_Climate_Change_Analysis.pdf.

Rasouli, F., Pouya, A.K., Šimůnek, J., 2013. Modeling the effects of saline water use in wheat-cultivated lands using the UNSATCHEM model. Irrig. Sci. 31, 1009–1024.

Sandberg, J., and Manza, P., 1991. Evaluation of central Valley project water supply and delivery systems. Ch3: Simulation Models and Climate Change Scenarios. Global Climate Change Response Program United States Department of the Interior Bureau of Reclamation Mid-Pacific Regional Office, Sacramento, California. Water resources center archives, University of California Berkeley. pp.2,3,19.

Sanden, B.L., Ferguson, L., Reyes, H.C., and Grattan, S.C., 2004. Effect of Salinity on Evaporation and yield of San Joaquin Valley Pistachios. Proceedings of IVth International Symposium on Irrigation of Horticultural Crops, *Acta Horticulturae* 664:583 – 589.

Scudiero, E., Corwin, D., Anderson, R., Yemoto, K., Clary, W., Wang, Z., and Skaggs, T., 2017. Remote sensing is a viable tool for mapping soil salinity in agricultural lands. *Calif. Agr.* 71(4):231-238.

Scudiero, E., Corwin, D.L., and Skaggs, T.H., 2015. Regional-scale soil salinity assessment using landsat ETM+ canopy reflectance. *Remote Sens. Environ.* 169, 335–343.

Sillmann, J., Thorarinsdottir, T., Keenlyside, N. Schaller, N., Alexander, L.V., Hegerl, G., Seneviratne, S.I., Vautard, R., Zhang, X., and Zwiers, F.W., 2017. Understanding Modeling and predicting weather and climate extremes: Challenges and opportunities. Weather and Climate Extremes, 65 -74.

Šimůnek, J., van Genuchten, M.Th., and Šejna, M., 2016. Recent developments and applications of the HYDRUS computer software packages, Vadose Zone Journal, 15(7), pp. 25, doi: 10.2136/vzj2016.04.0033, 2016.

Snyder, R., Geng, S., Orange, M, and Sarreshteh, S., 2012. Calculation and Simulation of Evapotranspiration of Applied Water. *J. Integrative Agriculture* 11(3), 489 – 501.

Thiery, W., Davin, E.L., Seneviratne, S.I., Bedka, K., Lhermitte, S., and van Lipzig, N.P., 2016. Hazardous thunderstorm intensification over Lake Victoria. Nat. Communication, 7.

USGS NWIS, 2018. USGS National Water Information System (NWIS), Water Quality for California, last log in 2018.https://www.usgs.gov/media/images/usgs-nwis-water-quality-data-california

Underwood, E.C., Hollander, A.D., Flint, L.E., Flint, A.L., and Safford, H.D., 2018. Climate change impacts on hydrological services in southern California. *Environ. Res. Lett.,* 13 (2), 124019.

UN-Water, 2014. Water for life decade. Water Scarcity, United Nations Water report 11/24/2014. https://www.un.org/waterforlifedecade/scarcity.shtml.

UN-Water, 2018. Sustainable Development Goal (SDG) 6 Synthesis Report on water and sanitation. https://www.unwater.org/publication_categories/sdg-6-synthesis-report-2018-on-water-and-sanitation/

Wilks, D., 2011. Statistical methods in the atmospheric sciences (3rd ed.). Oxford; Waltham, MA: Academic Press.

Wilson, P., Wheeler, D., and Kennedy, D., 1998. Management of the California State Water Project, Appendix E, 1993 Water Operations in the Sacramento-San Joaquin Delta, Bulletin 132-94.

Zecca, K., Allen, R.J., and Anderson, R.G., 2018. Importance of the El Niño Teleconnection to the 21st Century California Wintertime Extreme Precipitation Increase. Geophysical Research Letters 45(19): 10,648-10,655.

Appendix 4. Historical and Future Water Resources

Table A4.1. Three projections of the used water resources in eastern and western SJV, CA.

Year of simulation	GW storage condition	Max. T East SJV	Rain East SJV (cm/y)	Max. T West SJV	Rain West SJV (cm/y)	Year Type	1st Irrig. *	2nd Irrig. **	3rd Irrig. ***
2020	Low	51.43	16.67	80.28	45.45	Wet (W)	SW	SW	GW
2021	Enough	51.47	45.45	81.05	25.21	Critical(C)	SW	GW	GW
2022	Low	50.00	25.21	80.22	39.32	Wet (W)	SW	GW	GW
2023	Enough	50.38	39.32	80.82	21.15	Dry (D)	SW	GW- SW	GW
2024	Medium	49.54	21.15	81.12	17.75	Dry (D)	SW	SW-	SW
2025	Low	50.64	17.75	83.25	16.19	Critical(C)	SW	SW-GW	GW
2026	Low	49.53	16.19	81.65	18.91	Dry (D)	SW	SW-GW	GW
2027	Low	50.83	18.91	82.66	20.25	Dry (D)	SW	SW-GW	GW
2028	Critical	51.92	20.25	82.25	23.31	Critical(C)	SW	GW	GW
2029	Low	52.44	23.31	81.33	33.51	Wet (W)	SW	SW	SW
2030	enough	52.64	33.51	83.43	27.65	Critical(C)	SW	SW	GW
2031	Medium	52.66	27.65	82.48	36.30	Very Wet (W)	SW	SW- GW	GW
2032	Medium	50.84	36.30	83.89	14.08	Dry (D)	SW	SW	GW
2033	Low	50.80	14.08	82.63	12.01	Dry (D)	SW	GW	GW
2034	Low	52.77	12.01	84.82	20.82	Critical(C)	SW	GW	SW
2035	Low	51.43	20.82	83.55	12.33	Dry (D)	SW	GW	GW
2036	Low	52.32	12.33	83.66	25.10	Critical	SW	GW	GW
2037	Low	52.54	25.10	82.74	25.80	Wet (W)	SW	SW- GW	GW
2038	enough	52.82	25.80	83.25	16.79	Critical(C)	SW	SW	GW
2039	Low	52.04	16.79	84.63	11.04	Dry (D)	SW	SW	SW
2040	Low	52.36	11.04	85.51	14.02	Dry (D)	SW	SW	GW
2041	Low	52.80	14.02	84.71	17.09	Critical(C)	SW	SW- GW	GW
2042	Low	53.49	17.09	85.07	15.70	Dry (D)	SW	GW	GW
2043	Low	51.87	15.70	82.80	29.64	Above normal	SW	GW	GW
2044	enough	55.06	29.64	85.91	23.36	Critical(C)	SW	SW	SW
2045	Low	52.85	23.36	82.77	27.43	Dry (D)	SW	SW	GW
2046	Low	52.64	27.43	83.28	28.51	Wet (W)	SW	GW	GW
2047	enough	79.04	28.51	51.01	19.847	Critical(C)	SW	SW	GW
2048	Medium	78.28		52.62	15.931	Dry (D)	SW	SW- GW	GW
2049	Low	79.05		52.12	25.621	Wet (W)	SW	GW	SW
2050	enough	78.22		50.97	13.971	Dry (D)	SW	SW	GW

Projected three water resources use scenarios.

* Enough CVP surface water Supply ** Water Scarcity scenario(M-WS)

***Worse water scenario: High Groundwater demand

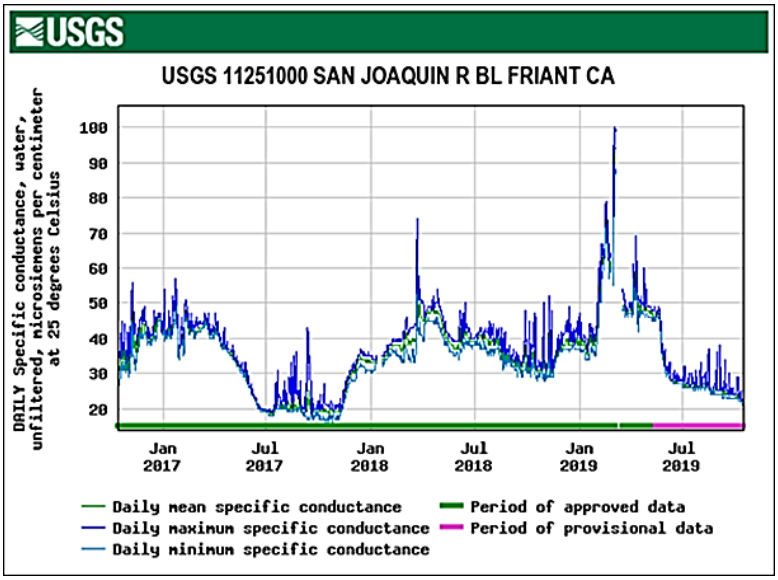

Figure A4.12. Surface water quality for the future scenarios of precipitation. Annual average surface water electrical conductivity (0.44 dS/m) (USGS NWIS data, 2018).

Chapter 5 Summary and Conclusions

The overall goal of this doctoral thesis was to investigate the current and long-term effects of the use of more saline water resources for irrigation in the SJV almond and pistachio orchards. The use of saline water for irrigation represents one of many important agricultural problems. The field monitoring of root zone salinity in different depths under different environmental (e.g., different climates and soil types) and management (e.g., different irrigation techniques and crops) conditions require extensive experimental efforts and costs. Numerical models can overcome these problems and become efficient alternative tools to examine and optimize different management practices for various objectives, such as removing salts from the root zone and designing the best management practices for drip-irrigated orchards in arid zones.

Chapter 2 describes extensive experimental datasets collected in almond and pistachio salt-affected orchards in two different geological regions of the San Joaquin Valley, CA. Particular regions and orchards were chosen to examine the seasonal accumulation of soil salinity in the root zones of almond and pistachio trees with a wide range of initial (i.e., the initial salinity) and boundary (i.e., rainfall and salinity of irrigation water) conditions. Long-term, continuous volumetric soil water contents and bulk electrical conductivity measurements were conducted at four rootzone depths of 25, 50, 75, and 100 cm. Actual evapotranspiration measurements were used to estimate the tree's water uptake reduction due to salinity, and the results were related to three factors: a) the temporal distribution of rains and irrigation events, including the effects of salinity of the irrigation water, b) the soil chemistry, including the effects of the initial *Sodium Adsorption Ratio* (*SAR)* and the root zone soil solute electrical conductivity (*EC*) at each depth and location, and c) soil physical properties, such as soil type and hydraulic conductivity, bulk density, and porosity. Inter-seasonal and annual water budgets were used to analyze the soil measured salinities of the almond and pistachio rootzones.

In Chapter 3, model simulations are proposed as an alternative to onsite measurements. Many geological and technical problems could be addressed by obtaining and evaluating continuous dynamic trends of water contents and salinities under different environmental and management conditions. However, before numerical models can be used for such a purpose, they need to be calibrated and validated for evaluated conditions. The popular HYDRUS-1D code was used to simulate water flow and transport of salts at the experimental sites described in Chapter 2. The model was calibrated and validated using data collected during the 2017-2019 years. The model was successfully calibrated to describe flow and transport processes at two experimental sites (the LEA site in the east SJV and the HWA site in the west SJV). The model was less successful in describing flow and transport processes at the other sites due to various reasons (e.g., the presence of a low permeability duripan at one site or the effects of the high Na content on soil hydraulic properties at another site). The root zone salt dynamics (at sites with successful simulations) was assessed using simulated salt concentrations at different depths, and water and solute leaching fluxes. Salinities were assessed during different parts of the season, such as during an "early" season when winter rains were the predominant factor and during a "late" season when irrigation water with higher salinity was the dominant factor. The numerical model provided continuous estimates of water contents, salinities, as well as water and solute fluxes at different depths. Such information for different environmental conditions and management scenarios can be used to optimize root zone salinity management practices or to predict future trends under changing climate conditions.

In Chapter 4, the HYDRUS-1D code was used to simulates the future anticipated root zone salinity problems for various soil, irrigation, and rainfall scenarios. Two general climate scenarios commonly found in climate ensemble modeling were used to generate future climate trends of the early century (2020-2050). The first scenario predicts moderate temperature and rain increases,

while the second assumes a warmer future climate projection with a more significant increase in rains. The two Global Climate Models (CCSM 4 and CNRM-CM5) were used to predict future precipitation. Three different scenarios, assuming different fractions of irrigation water come from saline groundwater (20, 50, and 80% denoted as 0.2G, 0.5G, and 0.8G, respectively), were evaluated to account for expected limited surface water resources in the future. The results of the three simulated scenarios showed, in general, expected trends with increased amounts of leached salts for a corresponding increase in irrigation water salinity. Unexpected results were obtained for the second and third irrigation scenarios (with the 50 and 80% groundwater blend), which showed higher leaching rates at the low salinity eastern site with relatively higher rains than at the western site. We related these increases to preferable soil hydraulic properties. Root water uptake (and thus yield) reductions at both eastern and western sites of SJV were similar to those reported in Chapter 3 for all irrigation scenarios. The uptake reduction is noticeably lower at the eastern site when lower salinity irrigation water (0.2G) is used than when higher salinity irrigation water (i.e., 0.5G and 0.8G) is used. On the other hand, all irrigation scenarios (0.2., 0.5, and 0.8 G) caused a similar reduction in transpiration at the western site.

The results of these future soil salinity analyses could be used to guide policy and management makers. However, it should be emphasized that the study findings are specific for evaluated sites and specified initial and boundary conditions. Similar studies would be needed for different sites and different irrigation scenarios. Soil characteristics restoration is the main resource for root zone salinity management. It showed the primary role in salinity accumulation, leaching, and almonds and pistachios evapotranspiration, with a less significant impact of seasonal rains. The soil solution's effect on soil hydraulic properties (e.g., a reduction in K_s due to high Na content) was not considered in our simulations. Thus, future simulations that would consider the soil salinity effects on soil hydraulic properties are suggested.